

**COMPARISON OF POLYELECTROLYTE COMPLEX FORMATION IN
BULK AND AT INTERFACES**

**Ph.D. Thesis by
Nejla ÇİNİ**

Department : Chemistry

Programme : Chemistry

SEPTEMBER 2010

**COMPARISON OF POLYELECTROLYTE COMPLEX FORMATION IN
BULK AND AT INTERFACES**

**Ph.D. Thesis by
Nejla ÇİNİ
(509032204)**

Date of submission : 16 August 2010

Date of defence examination: 21 September 2010

Supervisor (Chairman): Prof. Dr. Tülay TULUN (ITU)

Co-supervisor: Prof. Dr. Gero DECHER (UdS)

Members of the Examining Committee : Prof. Dr. Süleyman AKMAN (ITU)

Prof. Dr. Reşat APAK (IU)

Prof. Dr. Vincent BALL (UdS)

Prof. Dr. Micheal GRUNZE (U.H)

Prof. Dr. Figen KADIRGAN (ITU)

SEPTEMBER 2010

**ÇÖZELTİ VE ARA YÜZEYLERDE POLİELEKTROLİT KOMPLEKS
OLUŞUMUNUN KARŞILAŞTIRILMASI**

DOKTORA TEZİ
Nejla ÇİNİ
(509032204)

Tezin Enstitüye Verildiği Tarih : 20 Ağustos 2010

Tezin Savunulduğu Tarih : 21 Eylül 2010

Tez Danışmanı: Prof. Dr. Tülay TULUN (İTÜ)
Eş Danışman : Prof. Dr. Gero DECHER (UdS)
Diğer Jüri Üyeleri : Prof. Dr. Süleyman AKMAN (İTÜ)
Prof. Dr. Reşat APAK (İÜ)
Prof. Dr. Vincent BALL (UdS)
Prof. Dr. Micheal GRUNZE (U.H)
Prof. Dr. Figen KADIRGAN (İTÜ)

EYLÜL 2010

“Taking the life as the most fascinating and complex property of matter, nature clearly shows that the minimum size of life form is of nanoscopic to macroscopic dimension.”

Gero Decher

FOREWORD

I would like to, sincerely, thank and appreciate Prof. Dr. Tülay TULUN, who brought such interesting subject of “sodium(polyphosphate) based polyelectrolyte complexes in aqueous solution” to my interest, for her constructive and fruitful scientific discussions, valuable helps, and for her guidance throughout my PhD research, and for her encouraging me to apply for the scholarship of French Government of which is titled Co-tutelle program, and provides me to get two PhD diplomas from Technical University of Istanbul and University of Strasbourg.

I would like to, sincerely, thank and appreciate Prof. Dr. Gero DECHER for giving me opportunity to work with him and learn Layer-by-Layer method which is discovered and developed by him, and to learn the methods on characterisation of surfaces, and enlarging my scientific point of view with his productive scientific discussions, and for his deep interest and kind helps on my PhD thesis work.

I am very much indebted Prof. Dr. Vincent BALL for his valuable contribution and discussions on the bulk properties of polyelectrolyte complexes, and permitting me to work in his laboratory and making the facilities of his lab available for me in order to perform some important experiments.

I would like to thank to Dr. Olivier FELIX for his scientific help in laboratories and for his correspondence with me in any official requirements.

I would like to thank Prof. Dr Figen KADIRGAN for giving permission to use her laboratory and to her research colleague, Mrs. Sibel SARI ÖZENLER who helped me in obtaining FTIR spectra.

I very much thank Mr. Cristophe CONTAL for his help in taking AFM images, and my friend, Mrs. Francine VALENGA, for her kind help in a surface zeta potential measurement during my absence in France.

I would like to thank for the Administration of ITU, Faculty of Science and Letters and Graduate School of Engineering and Technology for giving me permission to be abroad with a duration of 16 months, and to my colleagues in Analytical Chemistry Department of ITU and in Institut Charles Sadron for their friendly supports.

I gratefully acknowledge the financial support of Research Foundation of Graduate School of Engineering and Technology in ITU (Project Nr: 31835) and the French Government (Bourse Government Français, Grant Nr: 20075088).

I am very much appreciated to my family for their invaluable and continuous morale support during my growing up and education life.

August 2010

Nejla Çini

M. Sci.

TABLE OF CONTENTS

| | <u>Page</u> |
|--|--------------|
| FOREWORD | vii |
| TABLE OF CONTENTS | ix |
| ABBREVIATIONS | xi |
| LIST OF TABLES | xiii |
| LIST OF FIGURES | xv |
| SUMMARY | xxi |
| ÖZET | xxxii |
| 1.INTRODUCTION | 1 |
| 2.LITERATURE REVIEW | 3 |
| 2.1 Polyelectrolyte Complex Formation | 3 |
| 2.1.1 Application Areas of PECs | 8 |
| 2.2 Polyelectrolyte Multilayer Thin Films | 9 |
| 2.2.1 Langmuir-Blodgett (LB) technique..... | 9 |
| 2.2.2 Self-assembled monolayers (SAMs)..... | 11 |
| 2.2.3 LbL (Layer by Layer) deposition technique | 13 |
| 2.2.4 The zone model For Polyelectrolyte Multilayer Thin Films..... | 21 |
| 2.2.5 Growth Process in Polyelectrolyte Multilayer Thin Films | 22 |
| 2.3 Polyphosphates..... | 26 |
| 3.EXPERIMENTAL PART | 29 |
| 3.1 Materials..... | 29 |
| 3.2 Methods..... | 29 |
| 3.2.1 Characterization of PSP and PAH..... | 29 |
| 3.2.1.1 Determination of molecular weight of PSP by end group titration..... | 29 |
| 3.2.1.2 Determination of molecular weight of PSP by viscometry..... | 31 |
| 3.2.1.3 Determination of molecular weight of PAH by viscometry | 32 |
| 3.2.1.4 Determination of equivalent weight of PSP and PAH | 32 |
| 3.2.1.5 Determination of the Dissociation Constants of PSP and PAH..... | 33 |
| 3.2.2 Preparation of polyion solutions | 35 |
| 3.2.3 Investigation of PSP/PAH complex formation in bulk..... | 35 |
| 3.2.3.1 Determination of PSP/PAH stoichiometry by conductometric titration..... | 35 |
| 3.2.3.2 Determination of PSP/PAH stoichiometry by viscometry..... | 36 |
| 3.2.3.3 Kinetic Investigation of PSP/PAH complex formation by Isothermal Titration Calorimetry, ITC | 37 |
| 3.2.3.4 Kinetic investigation of PSP/PAH complex formation by conductometry and viscometry..... | 41 |
| 3.2.3.5 Analysis of Supernatant Liquids by Vicsometry | 41 |
| 3.2.3.6 Analysis of Supernatant Liquids by FTIR Spectroscopy | 42 |
| 3.2.3.7 Dynamic Light Scattering | 44 |
| 3.2.3.8 Measurement of Zeta Potential | 46 |

| | | |
|-----------|--|------------|
| 3.2.4 | PSP/PAH complex formation and characterization at interfaces..... | 48 |
| 3.2.4.1 | Cleaning Procedure | 48 |
| 3.2.4.2 | Deposition of PEI-(PSP-PAH) _n multilayers..... | 48 |
| 3.2.4.3 | Ellipsometry Measurements | 49 |
| 3.2.4.4 | Characterization of PEI-(PSP-PAH) _n multilayer by Atomic force microscopy | 50 |
| 3.2.4.5 | Grain Size Analysis of the AFM topographies | 52 |
| 3.2.4.6 | Optical Microscopy Experiment | 52 |
| 3.2.4.7 | Zeta potential measurement of PEI-(PSP-PAH) _n multilayers on glass substrate | 53 |
| 4. | RESULTS AND DISCUSSION..... | 55 |
| 4.1 | Characterization of PSP and PAH..... | 55 |
| 4.1.1 | Determination of molecular weight of PSP and PAH..... | 55 |
| 4.1.2 | Determination of equivalent weight of PSP and PAH | 55 |
| 4.2 | Investigation of PSP/PAH complex formation in bulk | 55 |
| 4.2.1 | Determination of PSP/PAH stoichiometry by conductometric titration | 55 |
| 4.2.2 | Determination of PSP/PAH stoichiometry by viscometry | 59 |
| 4.2.3 | Kinetic investigation of PSP/PAH complex formation by conductometry and viscometry | 61 |
| 4.2.4 | Analysis of Supernatant Liquids by Viscometry..... | 62 |
| 4.2.5 | Analysis of Supernatant Liquids by FTIR Spectroscopy | 64 |
| 4.2.6 | Isothermal Titration Microcalorimetry, ITC, Measurements | 66 |
| 4.2.7 | Dynamic Light Scattering (DLS) and Zeta Potential Measurements..... | 70 |
| 4.3 | PSP/PAH complex formation and characterization at interfaces..... | 72 |
| 4.3.1 | Ellipsometry measurements | 72 |
| 4.3.2 | Characterization of PEI-(PSP-PAH) _n multilayer by Atomic force microscopy, AFM, and Grain Size Analysis..... | 78 |
| 4.3.2.1 | Decomposition of PSP/PAH deposits..... | 84 |
| 4.3.2.2 | Optical Microscopy Experiments..... | 85 |
| 4.3.3 | Zeta potential measurement of PEI-(PSP-PAH) _n multilayers on glass substrate..... | 86 |
| 5. | CONCLUSIONS..... | 91 |
| 5.1 | Future Perspectives..... | 95 |
| | REFERENCES | 97 |
| | APPENDICES | 109 |
| | APPENDIX A : French Summary | 109 |
| | APPENDIX A : French Summary | 111 |
| | Résumé de Thèse..... | 111 |
| | CURRICULUM VITAE..... | 121 |

ABBREVIATIONS

| | |
|--------------------------------------|------------------------------------|
| PEC | : Polyelectrolyte complex |
| LbL | : layer-by-layer |
| PSP | : poly (sodium phosphate) |
| PAH | : poly (allylamine hydrochloride) |
| PEI | : poly(ethyleneimine) |
| P4VPC | : poly(4-vinylpyridinium chloride) |
| PABCI | : 4-amino benzoic acid |
| PC | : polycation |
| PA | : polyanion |
| LB | : Langmuir-Blodgett |
| SAM | : self-assembled monolayer |
| PSS | : poly (styrenesulphonate) |
| PEM | : polyelectrolyte multilayer |
| HA | : hyaluronic acid |
| CHI | : chitosan |
| PGA | : poly(L-glutamic acid) |
| PLL | : poly(L-lysine) PLL |
| PAHOH | : basic form of PAH |
| (HPO₃)_n | : acidic form of PSP |
| FITC | : fluorescein isothiocyanate |

LIST OF TABLES

| | <u>Page</u> |
|---|-------------|
| Table 4.1: The results of end group titration..... | 55 |
| Table 4.2: Stoichiometry of PSP/PAH complex determined at pH:6.70. | 57 |
| Table 4.3: The stoichiometry of PSP/PAH complexes by viscometry and direct conductometry..... | 58 |
| Table 4.4 : Stoichiometry of PSP/PAH complex determined at pH:5 and 8. | 58 |
| Table 4.5: Supernatant liquid and control sample specific viscosities for solution PSP/PAH mixtures. | 63 |

LIST OF FIGURES

| | <u>Page</u> |
|--|-------------|
| Figure 2.1: Illustration of integral and pendant type of polyelectrolytes [3]. | 4 |
| Figure 2.2: Schematic representation of polyelectrolyte complex formation [3]. | 7 |
| Figure 2.3: a) A nanomembrane [43] b) an image of a multilayer Light Emitting Diode [45], c) the package of a contact lens from CIBA-Vision that has a layerbylayer based coating on its surface. Photo courtesy of L. Winterton of CIBA-Vision: it was presented at the 223rd, ACS National meeting on April 7–11, 2002 in Orlando. Focus® Excelens™, a contact lens, Copyright CIBA-Vision [1]. | 9 |
| Figure 2.4: Surfactant molecules arranged on an air-water interface. | 10 |
| Figure 2.5: Representation of a SAM structure. | 11 |
| Figure 2.6: (a) A simplified schematic of the principle for the first two adsorption steps in film deposition as starting with a positively charged substrate. (b) Schematic representation of film deposition by LbL-Spraying. (c) Schematic representation of film deposition process by LbL-Dipping. Steps 1 and 3 represent the adsorption of a polyanion and polycation respectively, and steps 2 and 4 are washing steps. Counterions are omitted for clarity. The polyion conformation and layer interpenetration are an idealization of the surface charge reversal with each adsorption step. The four steps are the basic buildup sequence for the simplest film architecture (A/B) _n where n is the number of deposition cycles. The construction of more complex film architectures requires only additional deposition cycles and a different sequence [1]. | 14 |
| Figure 2.7: Experimental setup for multilayer film deposition by spraying [47]. | 15 |
| Figure 2.8: Scheme of the standard procedure used in the layer by layer spray deposition [47]. | 17 |
| Figure 2.9: Illustration of three possible situations arise depending on the charge density of the cationic polymer: (a) When this charge density is low no complexation occurs. (b) At a higher polymer charge density complexation at the surface occurs, followed by (partial) desorption of the complexes. (c) When both polymers are highly charged, the complex remains strongly bound to the substrate; stable multilayers can be formed [142]. | 18 |
| Figure 2.10: Evolution of the ζ -potential for alternated HA and PLL deposition during 20 deposition cycles. Positive (open symbols) values correspond to PLL addition followed by rinsing, and negative values (closed symbols) correspond to HA addition after rinsing [86]. | 19 |

| | |
|---|----|
| Figure 2.11: Fabrication of LbL multilayer film by hydrogen bonding between carboxylic acid groups and pyridine groups [50]. | 20 |
| Figure 2.12: The zone model for polyelectrolyte multilayers. Zone I is adjacent to the substrate, Zone II forms the “bulk” of the multilayer and Zone III is adjacent to the film/solution or film/air interface [1]. | 21 |
| Figure 2.13: Polyelectrolyte multilayer film thickness as a function of layer numbers a) an example for a linear growth regime of ○: PSS, ×: PAH given in literature [44] b) an example of exponential (supralinear) growth obtained by poly(acrylic acid) (PAA) and poly(ethyleneglycol) (PEG) given in literature [43]. | 23 |
| Figure 2.14: Molecular Structures of Linear polyphosphates. | 26 |
| Figure 3.1: Chemical structures of PSP and PAH. | 29 |
| Figure 3.2: Schematic illustration for the set up of isothermal titration calorimeter [128]. | 37 |
| Figure 3.3: Infrared region of the electromagnetic spectrum. | 43 |
| Figure 3.4: Schematic of Zeta potential Measurement [154]. | 47 |
| Figure 3.5: Standard procedure for LbL-Spray PSP/PAH deposition. | 49 |
| Figure 3.6: Schematic representation of an ellipsometry set up [157]. | 49 |
| Figure 3.7: Principle of AFM [132]. | 51 |
| Figure 3.8: Schematic illustration of the layerbylayer-spraying setup for 2 vertically hold glass surfaces. | 54 |
| Figure 4.1: Conductometric titration curves of PSP with PAH at pH:6.7 in salt free solution. PSP and PAH are in equimolar concentration (Red: $1 \times 10^{-2} \text{M}$, Green: $1 \times 10^{-3} \text{M}$, Blue: $1 \times 10^{-4} \text{M}$, Black: $1 \times 10^{-5} \text{M}$ PSP and PAH). The error in these data is of the order of 0.2 μS . | 56 |
| Figure 4.2: Conductometric titration curves of PSP with PAH at pH:6.7 in 0.15M NaCl. PSP and PAH are in equimolar concentration (Red: $1 \times 10^{-2} \text{M}$, Green: $1 \times 10^{-3} \text{M}$, Blue: $1 \times 10^{-4} \text{M}$, Black: $1 \times 10^{-5} \text{M}$ PSP and PAH). The error in these data is of the order of 0.2 μS . | 56 |
| Figure 4.3: Conductometric titration curves of PAH with PSP at pH:6.70 in salt free solution. PSP and PAH are in equimolar concentration (Red: $1 \times 10^{-2} \text{M}$, Blue: $1 \times 10^{-4} \text{M}$ PSP and PAH). The error in these data is of the order of 0.2 μS . | 56 |
| Figure 4.4: Conductometric titration curves of PAH with PSP at pH:6.7 in 0.15M NaCl. PSP and PAH are in equimolar concentration (Red: $1 \times 10^{-2} \text{M}$, Blue: $1 \times 10^{-4} \text{M}$). The error in these data is of the order of 0.2 μS . | 57 |
| Figure 4.5: Conductometric titration curves of $1 \times 10^{-4} \text{M}$ PSP and PAH in A: I=0.15 M NaCl, B: I=0.5M NaCl, Red:PSP titrant, Blue:PAH titrant at pH; ○: 5, ■: 6, □: 7, and ●: 8. The error in these data is of the order of 0.2 μS . | 59 |
| Figure 4.6: Reduced viscosity of PSP/PAH complex as a function of (left): mol ratio and ionic strength, (right): pH and ionic strength. ($C_{\text{PSP}}=1 \times 10^{-3} \text{g/dl}$, PSP and PAH are prepared in equimolar concentration, ○— : 0.01M NaCl, -■- - -: 0.15M NaCl, □... : I=0.5M NaCl). The error in these data is of the order of 10.3 dl/g. | 59 |

| | |
|--|----|
| Figure 4.7: Dependence of reduced viscosity of PSP/PAH complex as a function of ionic strength and pH. ($C_{PSP}=1 \times 10^{-3}$ g/dl, PSP and PAH are prepared in equimolar concentration, pH; \blacklozenge : 3, \boxplus : 4, \circ : 5, \blacksquare : 6, \square : 7, \bullet : 8, \triangle : 10, \blacktriangle : original pH). The error in these data is of the order of 6.3 dl/g. | 60 |
| Figure 4.8: Reduced viscosity and specific conductivity change as a function of mol ratio ($C_{PSP}=0.01$ g/dl, PSP and PAH are prepared in equimolar concentration in salt free solution, Blue: viscosity data, Red: Conductivity data). The error in these data is of the order of 6.3 dl/g and 0.2 μ S respectively..... | 61 |
| Figure 4.9: Time dependency of specific conductivity, specific viscosity of PSP/PAH complex prepared at $I=0.15$ M NaCl, pH:6.70 (Red: 1×10^{-2} M, Green: 1×10^{-3} M, Blue: 1×10^{-4} M, Black: 1×10^{-5} M PSP and PAH). | 62 |
| Figure 4.10: FTIR spectra of PSP prepared by different procedures..... | 64 |
| Figure 4.11: FTIR spectrum of solid PSP and PAH, and PSP/PAH complex prepared by 1:1 mol ratio at 1×10^{-2} M polyelectrolyte concentration, $I=0.15$ M NaCl at pH 6.70..... | 65 |
| Figure 4.12: FTIR spectrum of the solid PSP/PAH complex samples obtained from the supernatant liquids by drying..... | 66 |
| Figure 4.13: Experimental heat flow obtained at 25°C in the presence of a 0.15M NaCl at pH 6.7 for 21 stepwise injection of 8 μ L, 5×10^{-2} M PSP into 2×10^{-4} M PAH with a stirring rotation at 310 rpm. Consecutive injections were separated by a resting period of 200s. | 67 |
| Figure 4.14: Experimental heat flow obtained at 25 °C in the presence of a 0.15M NaCl at pH 6.70 for a single injection of stepwise injection of 7.5 μ L, 2×10^{-2} M PSP into 1×10^{-4} M PAH with a stirring rotation at 310 rpm. The reference cell was filled with 0.15M NaCl at a pH of 6.70. | 68 |
| Figure 4.15: a) Experimental heat flow obtained at 25°C in the presence of a 0.15M NaCl at pH 6.70 for 4 stepwise injection of 5 μ L, 2×10^{-2} M PSP into 1×10^{-4} M PAH with a stirring rotation at 310 rpm. The reference cell was filled with 0.15M NaCl at a pH of 6.70. b) Experimental heat flow obtained at the same conditions and parameters for the dilution step. | 69 |
| Figure 4.16 : Time dependency of zeta potential of PSP/PAH complex particles prepared in unit mol ratio at pH:6.7, Left: $I=0.15$ M NaCl, Right: $I=1$ M NaCl; \blacksquare : PSP added, \square : PAH added, PSP and PAH: 1×10^{-4} M. | 70 |
| Figure 4.17: Time dependency of hydrodynamic radius of PSP/PAH complex particles prepared in unit mol ratio at pH:6.7, Left: $I=0.15$ M NaCl, Right: $I=1$ M NaCl; \blacksquare : PSP added, \square : PAH added, PSP and PAH: 1×10^{-4} M. | 71 |
| Figure 4.18: Evolution of the thickness of a PEI-(PSP/PAH) $_n$ deposits with the layer numbers showing the effect of ionic strength at pH:6.70 for 1×10^{-3} M, (left) and for 1×10^{-4} M polyelectrolyte concentration (right), \bullet : salt free, \circ : $I=0.05$ M NaCl, \blacksquare : $I=0.15$ M NaCl, \square : $I=0.5$ M NaCl, \diamond : $I=1$ M NaCl..... | 73 |

| | | |
|---------------------|--|----|
| Figure 4.19: | Evolution of the thickness of a PEI-(PSP/PAH) _n deposits with the layer numbers showing effect of polyelectrolyte concentration at pH 6.70, I=0.15M NaCl, Red: 1x10 ⁻² M, Green:1x10 ⁻³ M, Blue:1x10 ⁻⁴ M Black:1x10 ⁻⁵ M PSP and PAH. | 74 |
| Figure 4.20: | Left: represent the variation of linear fit slope values as a function of polyelectrolyte concentration, Right: represent the variation of linear fit slope values as a function of ionic strength for 1x10 ⁻⁴ M PSP/PAH deposits at pH 6.70..... | 75 |
| Figure 4.21: | Change in the average slope of linear growths of PSP/PAH deposits at equimolar of ■:1x10 ⁻² M, □: 1x10 ⁻³ M, ●: 1x10 ⁻⁴ M, ○:1x10 ⁻⁵ M PSP and PAH as a function of polyanion and polycation concentration at I=0.15M NaCl and pH:6.70. | 75 |
| Figure 4.22: | Evolution of the thickness of a PEI-(PSP/PAH) _n deposits with the number of layer numbers at pH:6.70, I=0.15M NaCl, for 1x10 ⁻⁴ M PSP/PAH. The insets shows the photographic image of a deposit obtained after 150 deposition steps (left), and after 30, 40, 60, 80 100 and 120 deposition steps (right). Different symbols correspond to different experiments carried out independent from each other. | 76 |
| Figure 4.23: | Evolution of the thickness of a PEI-(PSP/PAH) _n deposits with the layer numbers at 1x10 ⁻⁴ M in the presence of 0.15M NaCl at pH 6.70 for spraying time per deposition step: ■: 5s, ▲ :10s..... | 77 |
| Figure 4.24: | Evolution of the thickness of a PEI-(PSP/PAH) _n deposits with the layer numbers at 1x10 ⁻⁴ M in the presence of 0.15 M NaCl at pH 6.7 obtained by different spraying conditions given above. (Green: S mode 1,Blue: S mode 2, Red: S Mode 3). | 78 |
| Figure 4.25: | (Left) AFM height images, (right) AFM phase images of the surface of PSP/PAH deposits prepared at 1x10 ⁻⁴ M polyelectrolyte concentrations, I= 0.15 M NaCl, pH:6.7. m represents deposited the number of layers.. The image size is 2x2 μm ² . The z scales ranges from 0 to 250 nm. | 79 |
| Figure 4.26: | (Left) AFM height images, (right) AFM phase images of the surface of PSP/PAH deposits prepared at 1x10 ⁻³ M polyelectrolyte concentrations, I= 0.15 M NaCl, pH:6.70. m represents deposited number of layers. The image sizes are 2x2 μm ² . The z scales ranges from 0 to 20 nm. | 79 |
| Figure 4.27: | Evolution of the RMS roughness determined from the AFM topographies as a function of layer number: (left): 1x10 ⁻⁴ M; (right):1x10 ⁻³ M polyelectrolyte concentrations at I=0.15M NaCl and pH:6.70. | 80 |
| Figure 4.28: | Evolution of the average grain size (determined from AFM topographies in Figure 4.26) with the thickness and number of layers given in Figure 4.22. The error bars corresponds to the standard deviation for the size of more than 100 grains measured in each individual image. | 81 |

| | |
|---|----|
| Figure 4.29: (above) AFM height images (below) AFM phase images of the surface of PSP/PAH deposits prepared at 1×10^{-4} M polyelectrolyte concentrations, $I= 1$ M NaCl, pH:6.70. m represents deposited number of layers. The image size is $2 \times 2 \mu\text{m}^2$. The z scales ranges from 0 to 100 nm. | 82 |
| Figure 4.30: (Left) Evolution of the thickness of a PEI - (PSP/PAH) $_n$ deposits with the layer numbers (right) evolution of the RMS roughness (determined from the AFM topographies) as a function of deposition step. PSP and PAH are prepared at 1×10^{-4} M, $I=1$ M NaCl and pH:6.70. | 82 |
| Figure 4.31: Chemical Structure of Lumapin. | 83 |
| Figure 4.32: AFM height images for the 20 th layer of PSP/PAH and PSP/Lupamin deposits prepared at 1×10^{-4} M polyelectrolyte concentrations, $I= 0.15$ M NaCl, pH:6.70. The image size is $5 \times 5 \mu\text{m}^2$. The z scales ranges from 0 to 30 nm. | 83 |
| Figure 4.33: Evolution of the average thickness of ■:PEI-(PSP/PAH) $_n$ and □:PEI-(PSP/Lupamin) $_n$ at 1×10^{-4} M polyelectrolyte concentrations, $I= 0.15$ M NaCl, pH:6.70. | 84 |
| Figure 4.34: AFM height (above) AFM phase images (below) for the surface of PSP/PAH deposits prepared at 1×10^{-4} M polyelectrolyte concentrations, $I= 0.15$ M NaCl, pH:6.70. (A) PSP/PAH deposited up to layer number of 120 and (B) after dipping of the 120 layered deposited sample into 0.15 M NaCl for 1 and (C) 2 hours. The image size is $2 \times 2 \mu\text{m}^2$. The z scales ranges from 0 to 200 nm. | 85 |
| Figure 4.35: (left) AFM images, (right) Optical microscop images for the PSP/PAH complex adsorbed on a silicon wafer after 1:1 mol ratio of PSP/PAH complex prepared and PEI coated wafer was dipped for 24 hours into 0.15 M NaCl solution. Total Thickness: (51.70 ± 0.17) A. | 86 |
| Figure 4.36: Evolution of the ζ potential (mV) during the alternated deposition of PSP and PAH layers at $I= 0.15$ M NaCl, pH:6.70 as a function of the layer number (left): for 1×10^{-4} M, (right): 1×10^{-3} M PSP/PAH concentration. Red: correspondes to PSP last layer, Blue corresponds to PAH ended last layer. | 87 |
| Figure 4.37: AFM image obtained after layer PEI - (PSP/PAH) $_{40}$. For both images, the dimensions are $5 \times 5 \mu\text{m}^2$. (left:height, right:phase mode images). | 88 |
| Figure 5.1: Proposed build - up mechanism of PEI - (PSP - PAH) $_n$ deposits prepared by alternated spray deposition. The arrows are aimed to represent quasi 2D diffusion of the polyelectrolyte chains. | 95 |

COMPARISON OF POLYELECTROLYTE COMPLEX FORMATION IN BULK AND AT INTERFACE

SUMMARY

Polyelectrolytes are polymers which contain ionic groups in their repeat units and therefore exhibit electrolyte properties [1-6]. Polyelectrolyte complexes (PECs) are formed by the interaction between polyanions and polycations through which small counterions are released. PECs play an important role in environmental technologies and in biological systems. Research on the fundamentals of PEC formation is getting increasingly important because of versatility in numerous applications (e.g., pharmaceutical, cosmetic and food industries, papermaking, drug delivery and gene therapy, rheological properties of suspensions, multilayer films etc...).

PEC formation can take place in bulk or at interfaces, the latter phenomenon has led to the development of a new form of nanostructured hybrid materials in the form of thin films (G. Decher et al. Ongoing development since 1990) [39-45].

The deposition of polymer-based films via layer-by-layer (LbL) assembly has become a popular surface functionalization method because of its versatility, ease of preparation, and the fact that it can be applied not only to oppositely charged polyelectrolytes but to many types of polymers carrying mutually complementary functionalities (e.g., hydrogen-bond donors and acceptors). Consequently, such hybrid films offer a wealth of potential applications in materials science [36, 41, 46, 49, 108, 150-153].

Multilayer structures composed of polyions, other charged molecular, or colloidal objects (or both) are fabricated as schematically outlined below.

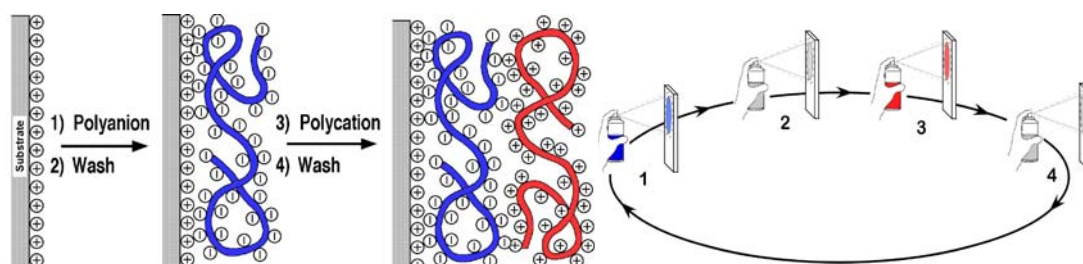


Figure 1: (Left) A simplified schematic of the principle for the first two adsorption steps in film deposition as starting with a positively charged substrate. (Right) Schematic representation of LbL-Spray deposition. Steps 1 and 3 represent the adsorption of a polyanion and polycation respectively, and steps 2 and 4 are washing steps. Counterions are omitted for clarity. The polyion conformation and layer interpenetration are an idealization of the surface charge reversal with each adsorption step. The four steps are the basic buildup sequence for the simplest film architecture $(A/B)_n$ where n is the number of deposition cycles. The construction of more complex film architectures requires only additional spray cycles and a different deposition sequence [1].

The predominant driving force in PEC formation is electrostatic interaction between the oppositely charged macromolecules. However, hydrophobic interaction, van der Waals forces and hydrogen bonding can play a role in increasing complex stability. The formation and the properties of PECs depend on various factors including the nature and position of the ionic groups, charge density and concentration, proportion of opposite charges, molecular weight of the macromolecules and physicochemical environment [16-19]. An important point in describing PECs is their stoichiometry, i.e. the molar ratio of cationic to anionic groups within the complex.

The aim of this study is to compare the properties of a classic PEC in bulk with those of a PEC formed at close-to-identical conditions at an interface (multilayer film) in order to work out the fundamental differences and similarities between such systems. For such a study it is advantageous to select a pair of polyelectrolytes whose interaction can easily be controlled by parameters such as concentration, stoichiometry, pH, and ionic strength. In the present study, Poly (sodium phosphate) (PSP, Molecular Mass = 2900 g/mol) and poly(allylamine hydrochloride) (PAH, Molecular Mass = 56000 g/mol) were chosen as polyanion and polycation, respectively. Both polyions were water soluble, and PSP is one of the few anionic, inorganic polyelectrolytes with its unique properties. Complexation of PSP with other polycations in the bulk solution was given elsewhere previously [20-24], but PSP /PAH complex formation in bulk and at interface of multilayers has been given for the first time.

The complex formation between PSP and PAH in bulk was investigated by conductometry, viscosimetry, spectroscopy, dynamic light scattering, isothermal titration microcalorimetry and zeta potential determination methods depending on different parameters, such as: concentration, ionic strength and pH. PSP/PAH complex formation at interface was carried out mostly by LbL-spray deposition with the identical parameters as in the bulk studies, and the behavior of the complex at interfaces is examined by ellipsometry, AFM and zeta potential measurements.

The PSP and PAH were dissolved in a solution of $I=0.15M$ NaCl. The pH of each solution was adjusted to 6.70 which corresponds to the average pK_a value of PSP and PAH so that the degree of dissociation for both polyelectrolytes was maintained identical.

Table 1: The stoichiometry of PSP/PAH complexes by Conductometry.

| Results by Conductometry | | | |
|---------------------------------|--------------------------|--------------------|---------------------|
| Titrant | Solution | PSP:PAH mol ratio | |
| | | Salt Free Solution | $I=0.15$ mol/L NaCl |
| 1×10^{-2} M PAH | 1×10^{-2} M PSP | 0.91:1 | 0.77:1 |
| 1×10^{-3} M PAH | 1×10^{-3} M PSP | 1:1.40 | 1:1 |
| 1×10^{-4} M PAH | 1×10^{-4} M PSP | 0.77:1 | 1.25:1 |
| 1×10^{-5} M PAH | 1×10^{-5} M PSP | 1.61:1 | 1.25:1 |
| 1×10^{-2} M PSP | 1×10^{-2} M PAH | 1:1.67 | 1:1 |
| 1×10^{-4} M PSP | 1×10^{-4} M PAH | 1.61:1 | 0.91:1 |

Table 2: The stoichiometry of PSP/PAH complexes by viscometry and direct conductometry.

| Methods | PSP | PAH | PSP:PAH mol ratio |
|----------------------|------------------------|------------------------|-------------------|
| Viscometry | 9.8×10^{-4} M | 9.8×10^{-4} M | 1:1 |
| Direct Conductometry | 1×10^{-3} M | 1×10^{-3} M | 1:1.47 |

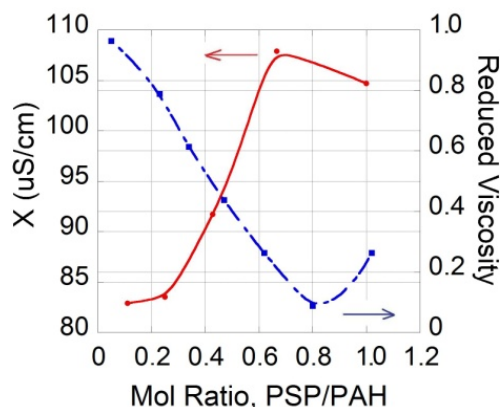


Figure 2: Reduced viscosity and specific conductivity change as a function of mol ratio ($C_{\text{PSP}}=0,01\text{g/dl}$, PSP and PAH are prepared in equimolar concentration in salt free solution, Blue: viscosity data, Red: conductivity data). The error in these data is of the order of 6.3 dl/g and $0.2\mu\text{S}$ respectively.

The stoichiometry of PSP/PAH complexes in bulk was found to be close to 1:1 by conductometry, viscometry, and supernatant analysis.

Table 3: Results of Supernatant Analysis.

| Complex Composition | Control Sample | η_{SP} (supernatant) | η_{SP} (control) | $\eta_{\text{SP}(\text{control})} / \eta_{\text{SP}}$ |
|--|----------------------------|----------------------------------|------------------------------|---|
| 1×10^{-4} M PSP-PAH (1:1 mol ratio, allowed to sediment and then PSP added) | 3.3×10^{-3} M PSP | 0.063 | 0.069 | 1.10 |
| 1×10^{-4} M PSP-PAH (1:1 mol ratio, allowed to sediment and then PAH added) | 3.3×10^{-3} M PAH | 0.068 | 0.079 | 1.16 |
| 1×10^{-4} M PSP-PAH (1.5:1 mol ratio) | 2.0×10^{-5} M PSP | 0.102 | 0.110 | 1.08 |
| 1×10^{-4} M PSP-PAH (1:1.5 mol ratio) | 2.0×10^{-5} M PAH | 0.113 | 0.127 | 1.12 |

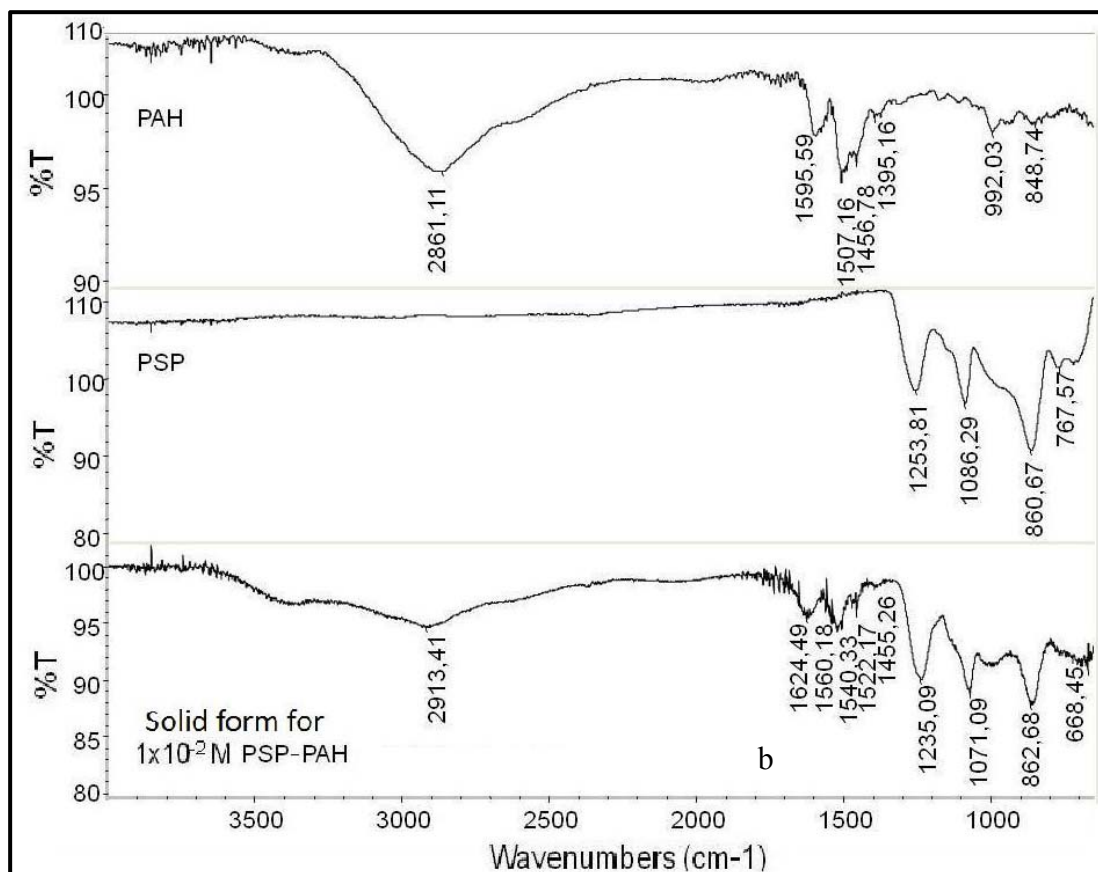


Figure 3: FTIR spectrum of solid PSP and PAH, and PSP/PAH complex prepared by 1:1 mol ratio at 1x10⁻² M polyelectrolyte concentration, I=0.15M NaCl at pH 6.70.

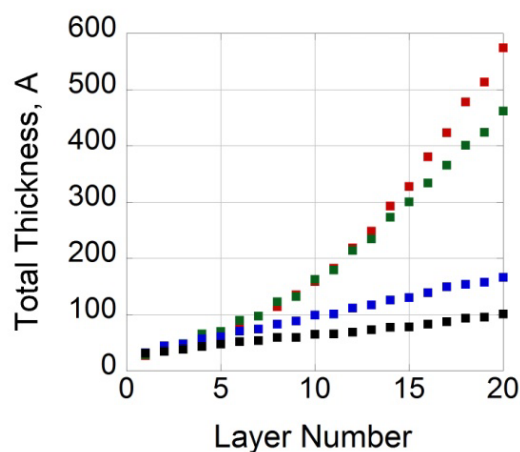


Figure 4: Evolution of the thickness of a PEI-(PSP/PAH)_n deposits with the layer numbers showing effect of polyelectrolyte concentration at pH 6.70, I=0.15M NaCl, Red: 1x10⁻² M, Green: 1x10⁻³ M Blue: 1x10⁻⁴ M Black: 1x10⁻⁵ M PSP and PAH.

The result of multilayer studies showed that the growth regime depends strongly on the concentration of PSP and PAH. It was observed that the film growth *seems* to be linear at the lowest concentrations (1x10⁻⁵ and 1x10⁻⁴ M) and can be fitted by an exponential growth at 1x10⁻³ M; the combination of an exponential growth followed by a linear one has been observed at 1x10⁻² M.

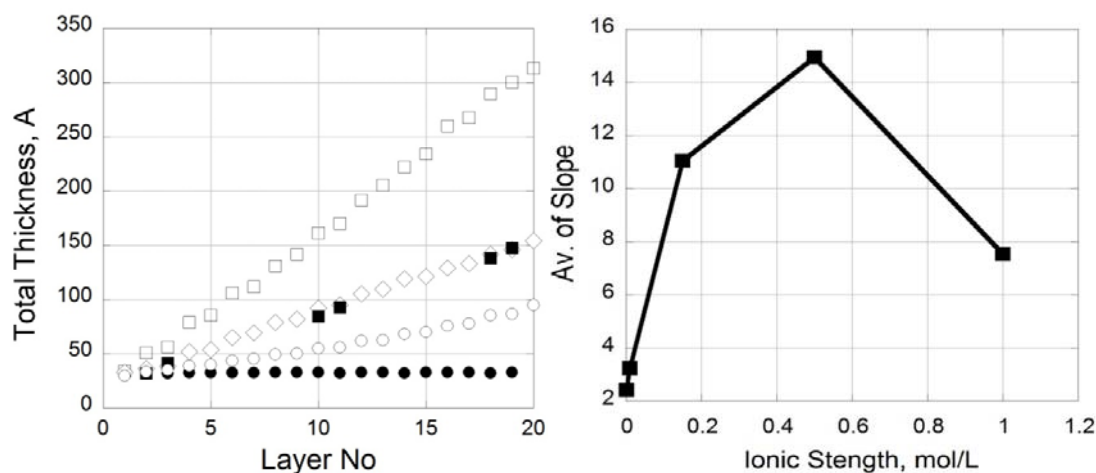


Figure 5: (Left) Evolution of the thickness of a PEI-(PSP/PAH) n deposits with layer numbers showing the effect of ionic strength at pH:6.70 for 1×10^{-4} M polyelectrolyte concentration, \bullet : salt free, \circ : I=0.05M NaCl, \blacksquare : I=0.15M NaCl, \square : I=0.5M NaCl, \diamond : I=1M NaCl. (Right) Evaluation of the variation of linear fit slope values as a function of ionic strength for 1×10^{-4} M PSP/PAH deposits at pH 6.70.

Despite of the appearance of optical interference colors, AFM topographies show that the deposits obtained at 1×10^{-4} M are islandlike and that the islands increase in size up to a layer number of at least 150. On the other hand, at 1×10^{-3} M, the deposits have the morphology of smooth films. Analysis of the root-mean-square (RMS) roughness of the deposits as a function of the number of deposition steps showed a markedly different behavior. While the roughness decreased from ~ 5 to ~ 1 nm at 1×10^{-3} M, it increased from ~ 5 to ~ 75 nm at 1×10^{-4} M.

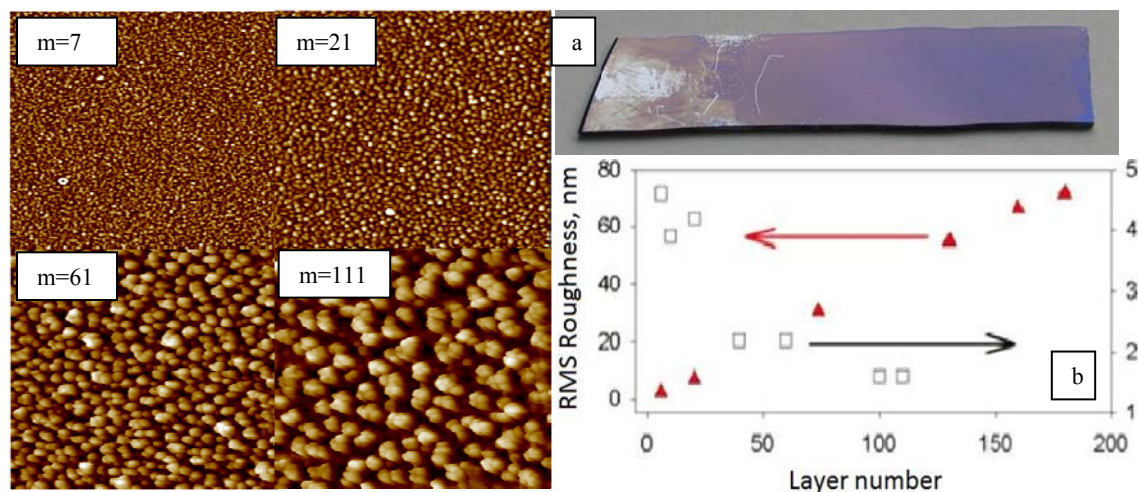


Figure 6: (Left) Representative surface topographies ($2 \mu\text{m} \times 2 \mu\text{m}$) of deposits prepared by spray deposition each at 1×10^{-4} M polyelectrolyte each in the presence of 0.15 M NaCl at pH 6.7 with $m =$ layers number s , (Right) a) Photographic image of a deposit obtained after 150 deposition steps (the marks on the left side of the sample are due to handling), b) Evolution of the RMS roughness (determined from the AFM topographies) with m : (\blacktriangle , lefthand axis) 1×10^{-4} M; (\square , right-hand axis) 1×10^{-3} M.

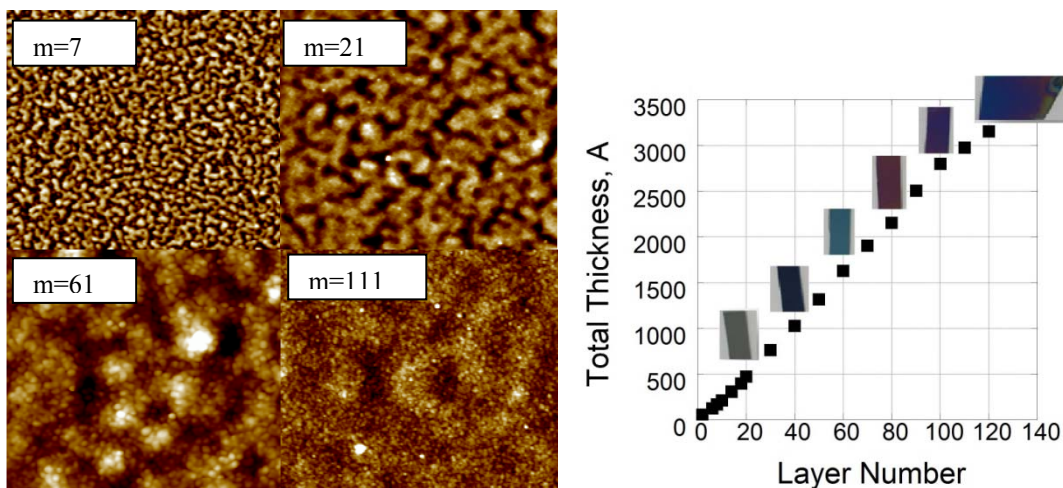


Figure 7: (Left) Representative surface topographies ($2\mu\text{m} \times 2\mu\text{m}$) of deposits prepared by spray deposition each at 1×10^{-3} M polyelectrolyte concentration in the presence of 0.15 M NaCl at pH 6.7 with $m =$ layers numbers, (Right) Evolution of the thickness of a PEI-(PSP/PAH) n deposits with the layer numbers at pH:6.70 for 1×10^{-4} M polyelectrolyte concentration, insets shows the photographic image of a deposit obtained after 30, 40, 60, 80, 100 and 120 deposition steps respectively.

The effect of PSP and PAH addition to the PSP/PAH complex after it is equilibrated is negligible in terms of thermodynamic properties, but the equilibrium is dynamic. This result is also in good agreement with dynamic light scattering studies. Time dependent conductometry, viscosimetry, and dynamic light scattering studies showed that kinetics of PSP/PAH complexation in bulk and at interfaces are on the same scale.

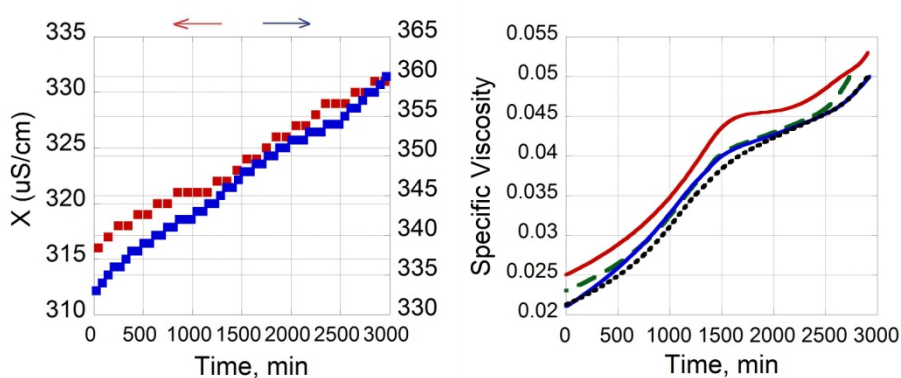


Figure 8: Time dependency of specific conductivity and specific viscosity of PSP/PAH complex prepared at $I=0.15\text{M}$ NaCl, pH:6.70 (Red: 1×10^{-2} M, Green: 1×10^{-3} M, Blue: 1×10^{-4} M, Black: 1×10^{-5} M PSP and PAH).

Counter ion release proceeds over extended time, and seems not to be finished even if the complexes reach a steady diameter (Figure 8). This result points to a very slow structural rearrangement of the complexes. The viscosimetry data point to the same assumption.

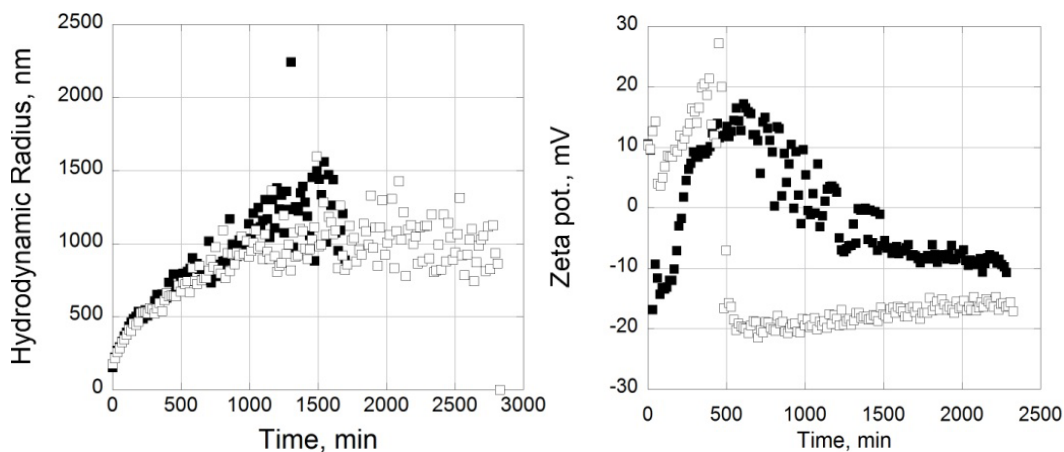


Figure 9: (A) Time dependency of hydrodynamic radius, (B) Time dependency of zeta potential of PSP/PAH complex particles prepared in unit mol ratio at pH:6.7, $I=0.15$ M NaCl for 1×10^{-4} M PSP and PAH, ■: PSP added, □:PAH added.

The complexes formed in solution upon mixing PSP and PAH in 1/1 molar ratio at the same conditions display a slow increase in their size (up to $2.5 \mu\text{m}$ 24 h after the PSP mixing with PAH) and a reversal in their zeta potential from a positive to a negative value which is around -20 mV (Figure 9).

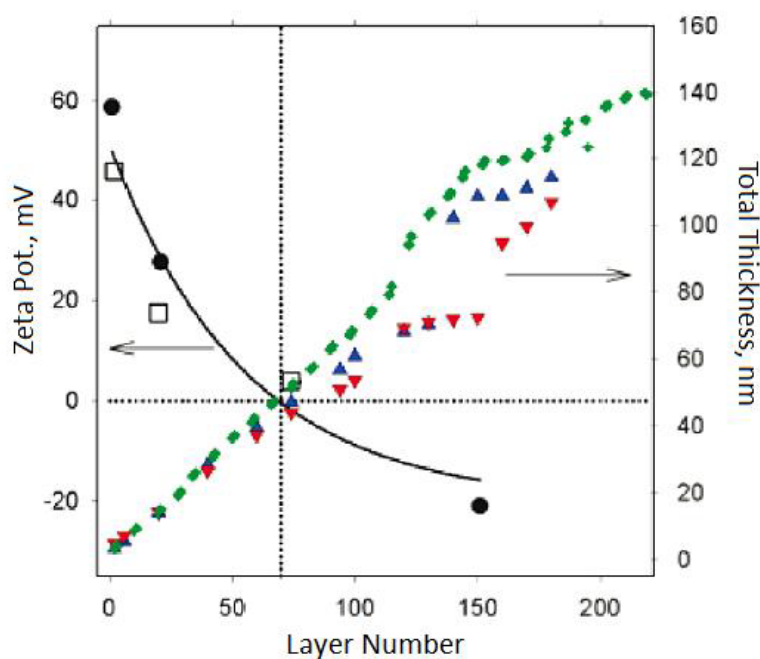


Figure 10: (left-hand scale) Evolution of the macroscopic ζ potential (the error bars correspond to one standard deviation over five measurements and are smaller than the symbols) of deposits obtained by alternately spraying of PSP and PAH at pH:6.7, $I=0.15$ M NaCl for 1×10^{-4} M PSP and PAH onto PEI-coated glass slides as a function of m : even values of m corresponds to the last sprayed layer of anionic PSP; odd values of m corresponds to the last sprayed layer of cationic PAH. The dotted horizontal line corresponds to $\zeta=0$ mV and the vertical one to $m=75$. (right-hand scale) Evolution of the average film thickness as a function of m . Different symbols correspond to different experiments carried out independent from each other.

Another observation is related to the ζ potential, whose sign is normally expected to correspond to the sign of the charge of the polyelectrolyte adsorbed as the last layer [73, 109]. However, it was observed the ζ potential did not alternate between positive and negative values upon the deposition of PSP and PAH (Figure 10). As long as the ζ potential was positive (i.e., for $m=75$), the ζ potential continuously decreased with increasing m . When the ζ potential approached zero, an instability occurred with respect to the previously regular film growth. Some samples temporarily showed slightly sublinear growth while others temporarily showed slightly superlinear growth. After ζ reached a plateau value of about -20 mV after 150-200 deposition steps, the film growth continued with approximately the same slope as observed at small layer numbers. Even exponentially growing films, which exhibited island-like growth for very small layer numbers ($m < 15$) showed an alternating ζ potential [93].

Interestingly, the growing of particle size and alteration of ζ potential occurs in the same range both in bulk and in LbL deposition in which the complexation process can even be interrupted by drying and the kinetically trapped states can be investigated.

As a result, both used polyelectrolytes, PSP and PAH, were carefully characterized. It was demonstrated that an increase in PSP and PAH concentration allowed for a progressive transition from linear growth to a supralinear.

It is found that PSP/PAH deposition is an interesting example of a film growth process in which the nanoscale roughness increases linearly with the film thickness while the macroscopic film homogeneity is remarkable. It is highly surprising that chains of the PAH can adsorb onto a surface with a macroscopically positive ζ potential and that the polyelectrolyte complex formation at the interface leads to the development of islands with a rather small polydispersity with the growing sizes of more than 300 nm without coalescing into a continuous film.

These results also indicate that interactions other than electrostatic ones might contribute the build up of the multilayer deposit so that dynamic structural changes occur in the polyelectrolyte complexes on the surface.

The complex formation between PAH and PSP in bulk is indeed dynamic. The order of polycation/polyanion addition in complex formation and the effect of PSP and PAH addition to the complex are very negligible in terms of thermodynamic properties. It is interesting to observe that the particle size grows in the same range both in bulk and in LbL deposition.

These findings led us to propose a model in which the deposit is builded by progressive aggregation of PSP and PAH accompanied by their lateral diffusion to form complexes.

The present study led to the discovery of a new growth regime of deposits by simple spray deposition from aqueous solution: the growth by the deposition of islands that do not coalesce up to $m=150$ deposition steps.

In this study self-patterning polyelectrolyte multilayers were obtained and described for the first time. The dimensions of the nanoscale pattern are a function of the number of deposition cycles.

The kind of observed progressive increase in grain size and the apparent existence of different scales of roughness could have very interesting applications; such as, superhydrophobic coatings [150-152], bio-active surfaces (transfection, bio-sensors,

separation of proteins), bio-remediation surfaces, and polyphosphate functions in living organisms [36, 41, 46, 49, 108, 110, 121, 123, 153].

Besides, the results of PSP/PAH system in the bulk solution might be a model system for the reactions between the natural polyions in the eukaryote and prokaryote organisms.

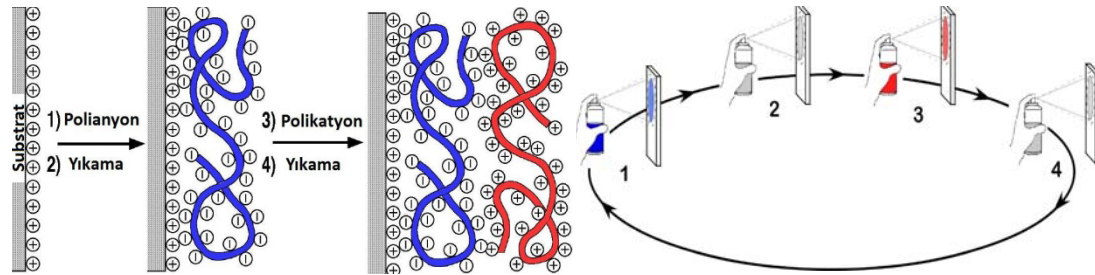
Moreover, it will be more interesting to use PSP/PAH system as a model system in order to demonstrate the core/shell structure which goes under rearrangement during complexation leading to the charge reversal on particles [27].

ÇÖZELTİ VE ARA YÜZEYLERDE POLİELEKTROLİT KOMPLEKS OLUŞUMUNUN KARŞILAŞTIRILMASI

ÖZET

Polielektrolitler tekrarlanan birimlerinde iyonik gruplar içeren ve elektrolit özellikleri taşıyan polimerlerdir [1-6]. Polielektrolit kompleksler (PEC) polianyon ve polikasyonlar arasındaki etkileşim ve karşı iyonların ayrılmasıyla oluşur. PEC, çevre teknolojileri ve biyolojik sistemlerde önemli rol oynarlar. Kullanım alanlarının çeşitliliği sebebi ile (örneğin, eczacılık, kozmetik ve gıda endüstrisi, kağıt yapımı, ilaç salınımı ve gen terapisi, süspansiyonların reolojik özellikleri, çoktabakalı filmler vs...) PEC oluşumu üzerine yapılan çalışmalar son yıllarda artan bir önem kazanmaktadır.

PEC oluşumu çözelti ve arayüzelerde meydana gelebilir, arayüzelerdeki PEC oluşumu yeni nanoyapılar olarak ince filmler halinde hibrid malzemelerin gelişmesini sağlar (G. Decher ve çalışma grubu 1990'lı yıllardan itibaren bu gelişmeleri sürdürmektedir) [39-45]. Polimer tabanlı filmlerin tabaka tabaka (LbL) metodu ile hazırlanması, işlem kolaylığı ve çeşitliliği, sadece zıt yüklü polielektrolitlere değil aynı zamanda birbirini tamamlayan ortak fonksiyonlu gruplar içeren (örneğin, hidrojen bağı alan ve veren) bir çok polimer tipine de uygulanabilmesi sebebi ile yaygın olarak kullanılan yüzey hazırlama tekniğidir. Sonuç olarak, bu hibrid filmler malzeme biliminde çok geniş uygulama alanı sunmaktadır [36, 41, 46, 49, 108, 150-153]. Poliiyonlardan veya yüklü diğer moleküllerden ya da kolloidlerden (veya her ikisinden) meydana gelen çok tabakalı yapıların hazırlanışı aşağıda şematik olarak gösterilmiştir.



Şekil 1: (Solda) Pozitif yüklü substrat üzerinde film yapımının ilk iki adsorpsiyon basamağını gösteren basit şema (Sağda) LbL-Sprey: 1 ve 3, sırasıyla, polianyon ve polikasyonun adsorpsiyonunu; 2 ve 4 yıkama basamaklarını göstermektedir. Karşı iyonlar ihmal edilmiştir. Her adsorpsiyon basamağında, yüzey yükünün değişimi poliiyon konformasyonu ve tabaka interpenetrasyonu ile sağlanır. 1-4 basamakları, (A/B)_n (n: tabaka sayısı) basit film yapısı için temel basamaklardır. Daha kompleks filmlerin yapımı farklı sıra ve ek spreyci basamaklarını gerektirmektedir [1].

PEC oluşumunda en baskın etken zıt yüklü makromoleküller arasındaki elektrostatik etkileşimdir. Bununla beraber; hidrofobik etkileşim, Van der Waals kuvvetleri ve hidrojen bağı da kompleks stabilitesini artırarak bu etkileşimde rol oynar.

PEC'lerin özellikleri ve oluşumu iyonik grupların yapısı ve konumu, yük yoğunluğu ve konsantrasyonu, zıt yüklerin oranı, makromoleküllerin molekül ağırlığı ve fiziksel çevresi gibi çeşitli faktörlere bağlıdır [16-19]. PEC'leri tanımlayan en önemli özellik, kompleksin içinde katyonik ve anyonik grupların molar oranı, yani komplekslerin stokiometrisidir.

Bu çalışmanın amacı, çözeltideki PEC özelliklerinin aynı koşullarda çok tabakalı filmlerin arayüzeyinde oluşturulan PEC özellikleri ile karşılaştırılarak, çözelti ve arayüzeydeki kompleks oluşumunun temel benzerlik ve farklılıklarının araştırılmasıdır. Bu amaçla konsantrasyon, stokiometri, pH ve iyonik şiddet gibi parametreler ile etkileşimi kontrol edilebilen bir çift polielektrolit olarak Poli (sodyum fosfat) (PSP, $M_A = 2900/\text{mol}$) ve poli(allilamin hidroklorür) (PAH, $M_A = 56000 \text{ g/mol}$) seçilmiştir.

PSP benzersiz özellikleri olan, suda çözünen, enteresan bir inorganik polielektrolittir [20-24].

Çözeltideki PSP/PAH kompleks oluşumu; konsantrasyon, iyonik şiddet, pH gibi farklı parametrelere bağlı olarak iletkenlik, viskozimetri, spektroskopi, dinamik ışık saçınımı, zeta potansiyel tayini ve izotermal mikroklorimetrik titrasyon metodları ile araştırılmıştır. Arayüzeyde PSP/PAH kompleks oluşumu bulk çözeltideki aynı koşullarda, daha çok LbL sprej tekniği ile yapılmış ve arayüzeydeki kompleks davranışı elipsometri, AFM ve zeta potansiyel ölçümleri ile incelenmiştir.

PSP ve PAH $I=0,15\text{M}$ NaCl çözeltisi içinde hazırlanmıştır. Her bir çözeltinin pH'ı PSP ve PAH'ın ortalama pK_a değerine karşılık gelen 6,70'e ayarlanarak her iki polielektrolitin dissosiasyon derecelerinin aynı kalması sağlanmıştır.

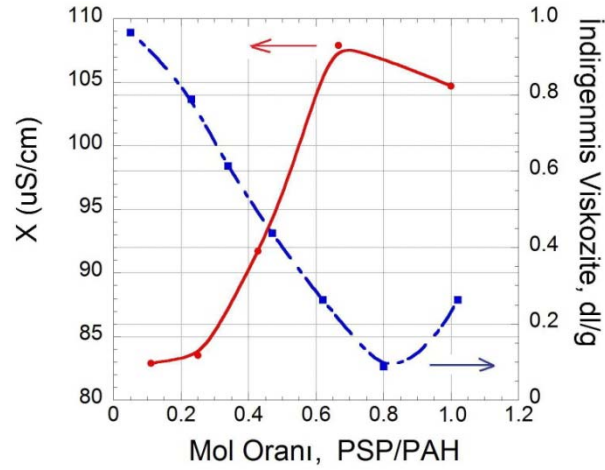
Çözeltideki PSP/PAH kompleks stokiometrisi iletkenlik, viskozimetri ve supernatant analizleri ile 1:1'e yakın bulunmuştur.

Çizelge 1: PSP/PAH kompleks stokiometrisi (İletkenlik Sonuçları).

| İletkenlik Sonuçları | | | |
|----------------------------------|----------------------------------|-------------------|-----------------------------|
| Titrant | Çözelti | PSP:PAH mol oranı | |
| | | Tuzsuz Çözelti | $I=0.15 \text{ mol/L NaCl}$ |
| $1 \times 10^{-2} \text{ M PAH}$ | $1 \times 10^{-2} \text{ M PSP}$ | 0.91:1 | 0.77:1 |
| $1 \times 10^{-3} \text{ M PAH}$ | $1 \times 10^{-3} \text{ M PSP}$ | 1:1.40 | 1:1 |
| $1 \times 10^{-4} \text{ M PAH}$ | $1 \times 10^{-4} \text{ M PSP}$ | 0.77:1 | 1.25:1 |
| $1 \times 10^{-5} \text{ M PAH}$ | $1 \times 10^{-5} \text{ M PSP}$ | 1.61:1 | 1.25:1 |
| $1 \times 10^{-2} \text{ M PSP}$ | $1 \times 10^{-2} \text{ M PAH}$ | 1:1.67 | 1:1 |
| $1 \times 10^{-4} \text{ M PSP}$ | $1 \times 10^{-4} \text{ M PAH}$ | 1.61:1 | 0.91:1 |

Çizelge 2: PSP/PAH kompleks stokiyometrisi (Viskozimetri Sonuçları).

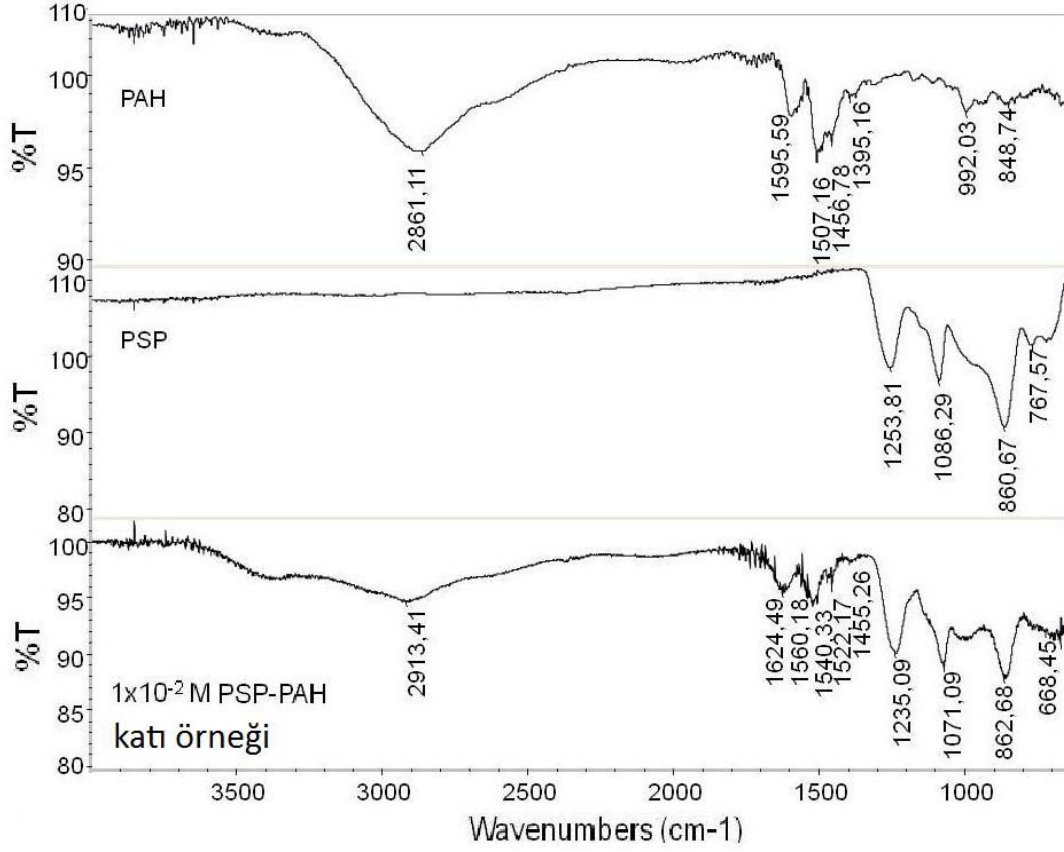
| Metodlar | PSP | PAH | PSP:PAH mol oranı |
|---------------------|------------------------|------------------------|-------------------|
| Viskozimetri | 9.8×10^{-4} M | 9.8×10^{-4} M | 1:1 |
| Doğrudan iletkenlik | 1×10^{-3} M | 1×10^{-3} M | 1:1.47 |



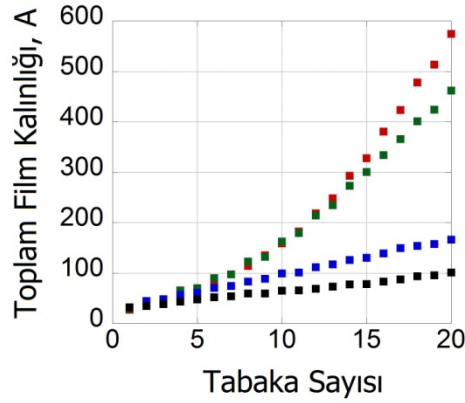
Şekil 2: Mol oranının fonksiyonu olarak indirgenmiş viskozite ve spesifik iletkenlik değişimi ($C_{PSP}=0,01$ g/dl, PSP ve PAH eşit molar konsantrasyonda tuzsuz çözeltide hazırlanmıştır. Mavi: viskozite verileri, Kırmızı:iletkenlik verileri. Verilerdeki standard hata sırasıyla 6.3 dl/g ve $0.2 \mu S'$ dir.).

Çizelge 3: Süpernetant Analizleri.

| Kompleks Bileşimi | Kontrol Çözelti | η_{SP} (supernetant) | η_{SP} (kontrol) | $\eta_{SP}(\text{kontrol}) / \eta_{SP}$ |
|---|----------------------------|---------------------------|-----------------------|---|
| 1×10^{-4} M PSP-PAH (1:1 mol oranı, çökme sağlandı ve PSP eklendi) | 3.3×10^{-3} M PSP | 0.063 | 0.069 | 1.10 |
| 1×10^{-4} M PSP-PAH (1:1 mol oranı, çökme sağlandı ve PAH eklendi) | 3.3×10^{-3} M PAH | 0.068 | 0.079 | 1.16 |
| 1×10^{-4} M PSP-PAH (1.5:1 mol oranı) | 2×10^{-5} M PSP | 0.102 | 0.110 | 1.08 |
| 1×10^{-4} M PSP-PAH (1:1.5 mol oranı) | 2×10^{-5} M PAH | 0.113 | 0.127 | 1.12 |

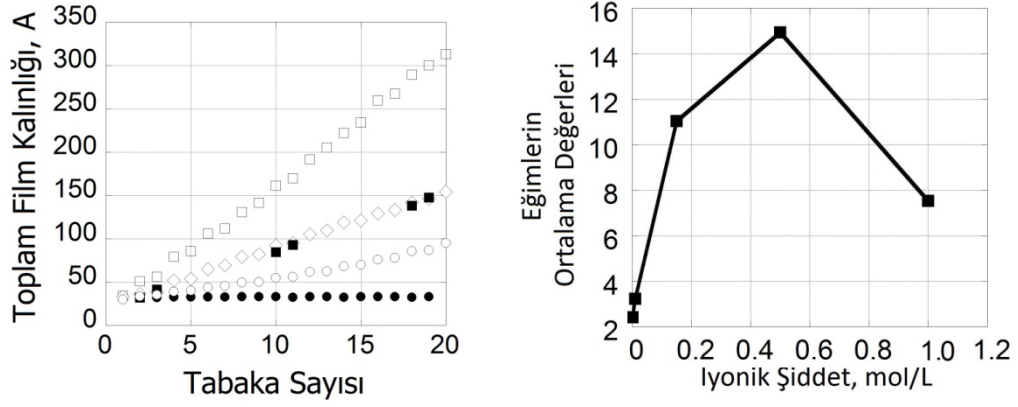


Şekil 3: Katı PSP ve PAH, ve 1:1 mol oranında, 1×10^{-2} M polielektrolit konsantrasyonu, $I=0.15$ M NaCl, pH 6.70 de hazırlanmış PSP /PAH kompleksine ait FTIR spektrumları.



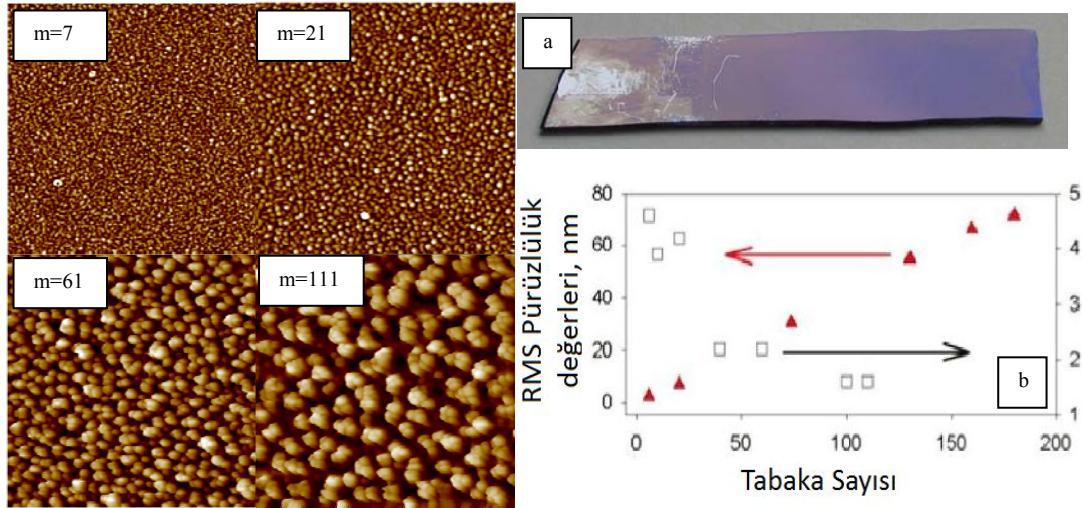
Şekil 4: PEI-(PSP/PAH) n depositlerinin tabaka sayısına göre kalınlık değerleri ve polielektrolit konsantrasyonunun sabit iyonik şiddet, $I=0.15$ M NaCl, ve pH:6.70 da PEI-(PSP/PAH) n depositlerinin kalınlığındaki değişime etkisi; Kırmızı: 1×10^{-2} M, Yeşil: 1×10^{-3} M Mavi: 1×10^{-4} M, Siyah: 1×10^{-5} M PSP ve PAH.

Çokluta baka sonuçları, film gelişiminin PSP ve PAH konsantrasyonuna oldukça bağlı olduğunu göstermiştir. Düşük konsantrasyonlarda film gelişiminin lineer olduğu (1×10^{-4} ve 1×10^{-5} M), 1×10^{-3} M' da üstel büyümeye uyduğu ve 1×10^{-2} M' da ise üstel büyümeyi takiben lineer gelişim olduğu gözlenmiştir.

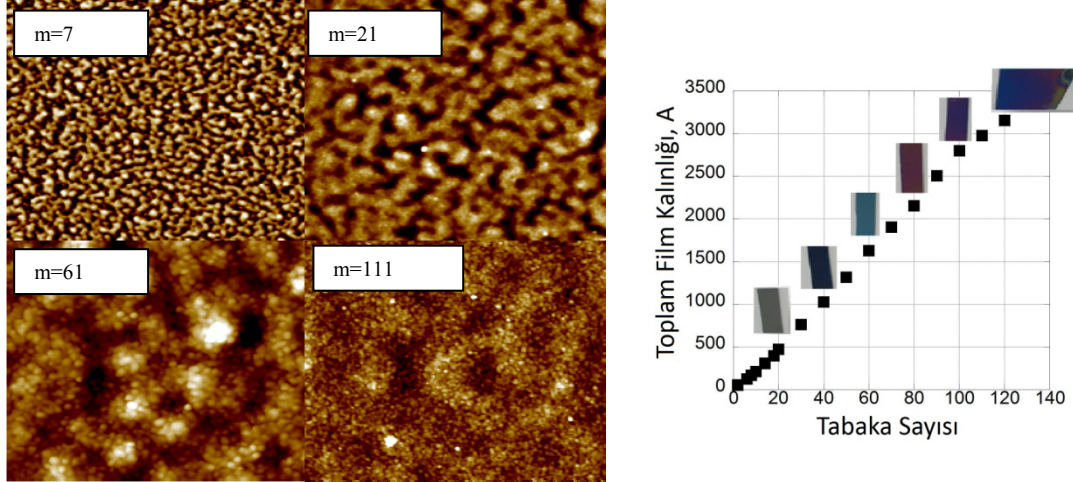


Şekil 5: PEI-(PSP/PAH) n depositlerinin tabaka sayısına göre kalınlık değerleri. (Sol) 1×10^{-4} M polielektrolit konsantrasyonunda ve pH:6.70 da iyonik şiddetin PEI-(PSP/PAH) n depositlerinin kalınlığındaki değişime etkisi ●: tuzsuz, ○: I=0.05M NaCl, ■: I=0.15M NaCl, □: I=0.5M NaCl, ◇: I=1M NaCl. (Sağ) 1×10^{-4} M PSP/PAH ve pH: 6.70 da lineer film gelişim eğimlerinin iyonik şiddetin fonksiyonu olarak değişimi.

Optik interferans renkli görüntülerine rağmen, AFM topografileri 1×10^{-4} M poliyon konsantrasyonunda yüzeyde ada-benzer yapıda birikimlerin olduğunu ve ada boyutlarının en az 150 tabaka sayısına kadar büyüdüğünü (şekil alt, sol) göstermiştir. Ayrıca, 1×10^{-3} M'daki depolanma düz film morfolojisine sahiptir (şekil alt, sağ). Tabaka sayısının fonksiyonu olarak yüzey pürüzlülük analizleri, (root-mean-square, RMS), yüzeyde klasik çoklu tabaka filmlerinden farklı davranışlar bulunduğu işaret etmiştir. Yüzey pürüzlülüğü, 1×10^{-3} M poliyon konsantrasyonunda ~5 ile ~1 nm arasında azalmış, 1×10^{-4} M poliyon konsantrasyonunda ise ~5 ile ~75 nm arasında artmıştır.

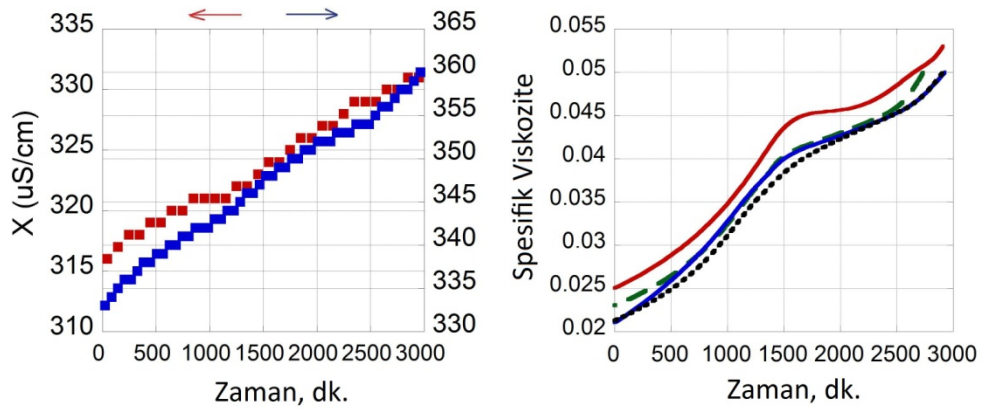


Şekil 6: (Sol) 1×10^{-4} M, I=0,15 M NaCl , pH=6,7 koşullarında sprej metodu ile hazırlanmış depositlerin farklı tabaka sayılarına ait ($2 \mu\text{m} \times 2 \mu\text{m}$) yüzey topografileri. (Sağ), a: 150 tabaka sayısından sonra elde edilen yüzey görüntüsü (numunenin sol taraftaki çizgiler tutuşdan dolayıdır) (b) AFM topografilerinden elde edilen RMS pürüzlülük değerleri, 1×10^{-4} M (▲, sol eksen) ; 1×10^{-3} M (□, sağ eksen).



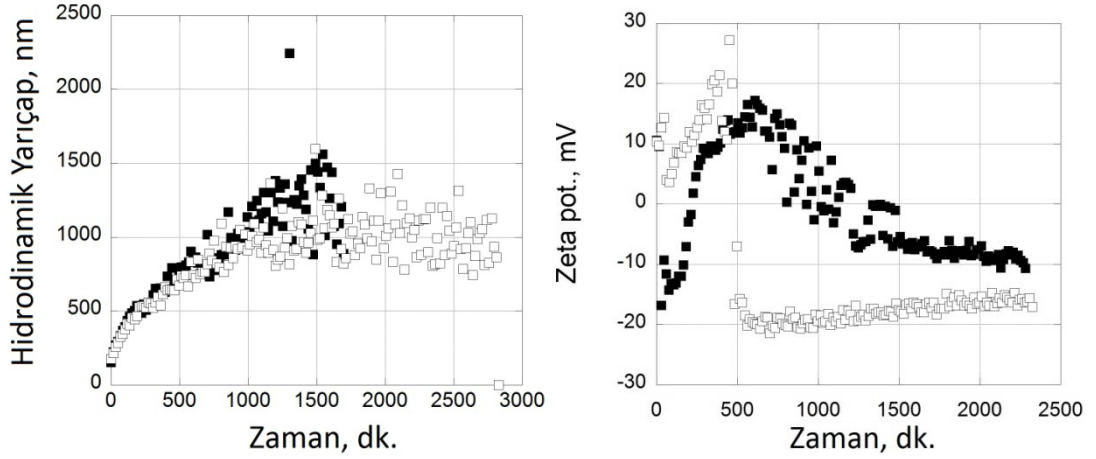
Şekil 7: (Sol) 1×10^{-3} M, $I=0.15$ M NaCl, $pH=6.7$ koşullarında sprej metodu ile hazırlanmış depositlerin farklı tabaka sayılarına ait ($2 \mu m \times 2 \mu m$) yüzey topografileri. (Sağ) 1×10^{-3} M polielektrolit konsantrasyonunda ve $pH:6.70$ koşullarında sprej metodu ile hazırlanmış PEI-(PSP/PAH) n depositlerinin tabaka sayısına göre kalınlık değerleri, iç resimler sırası ile 30, 40, 60, 80 100 ve 120 tabaka sayısından sonra elde edilen yüzey görüntülerini göstermektedir.

PSP-PAH kompleksleşmesi çok yavaş ve dinamik olmakla birlikte, PSP/PAH kompleksi dengeye geldikten sonra kompleks üzerine PSP veya PAH eklenmesinin termodinamik özellikler bakımından ihmal edilebilir düzeyde olduğu bulunmuştur. Bu sonuç dinamik ışık saçılması çalışmaları ile iyi bir şekilde uyumludur.



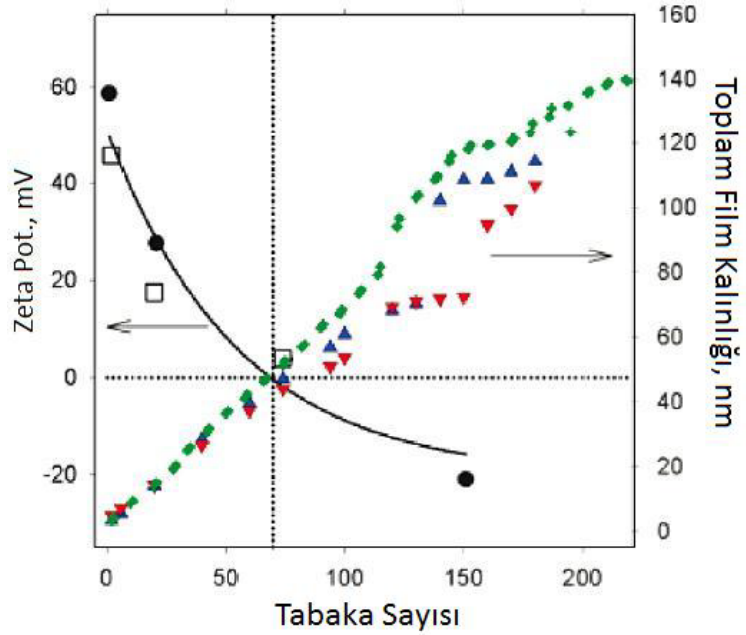
Şekil 8: 1:1 mol oranı, $I=0.15$ M NaCl ve $pH:6.70$ da hazırlanmış PSP/PAH kompleksinin (sol) spesifik iletkenlik ve (sağ) viskozite değerlerinin zamana bağlı değişimi. Kırmızı: 1×10^{-2} M, Yeşil: 1×10^{-3} M, Mavi: 1×10^{-4} M, Siyah: 1×10^{-5} M PSP ve PAH.

Zamana bağlı iletkenlik, viskozite ve dinamik ışık saçılması çalışmaları sonuçları, PSP-PAH kompleksleşme kinetiğinin çözelti ve arayüzeyde benzer ölçekte olduğunu göstermiştir.



Şekil 9: 1:1 mol oranı, $I=0.15M$ NaCl ve $pH:6.70$ da hazırlanmış PSP/PAH kompleksinin (sol) partikül büyüklüğü ve (sağ) zeta potansiyel değerlerinin zamana bağlı değişimi. ■: PSP eklemesi, □:PAH eklemesi.

Çözeltide, PSP ve PAH'ın 1:1 mol oranında aynı koşullarda karıştırılmasıyla oluşan komplekslerde partiküllerin yavaşça büyümekte (PSP ve PAH karıştırıldıktan 24 saat sonra $2,5 \mu m$ 'ye kadar) ve zeta potansiyel değişimi pozitif den yaklaşık $-20mV$ negatif değere değişmektedir (Şekil 9).



Şekil 10: (sol eksen) 1×10^{-4} M poliyon konsantrasyonu, $I=0,15$ M NaCl $pH=6,7$ koşullarında PEI kaplı cam yüzey üzerine LbL spray tekniği ile hazırlanmış PSP/PAH deposit yüzeylerinin tabaka sayısının fonksiyonu olarak makroskopik ζ potansiyel değerleri (hata çubukları 5 ölçüm değeri için hesaplanan standard sapma değerlerine karşılık gelmektedir ve simgelerden küçüktür), çift ve tek m sayıları sırası ile anyonik PSP ve katyonik PAH son spray tabakalarına karşılık gelmektedir. Kesikli yatay çizgi $\zeta=0$ mV, düşey çizgi $m=75$ değerlerine karşılık gelmektedir. (sağ eksen) tabaka sayısı (m) fonksiyonu olarak ortalama film kalınlığı değerleri. Farklı semboller, birbirinden bağımsız olarak tekrarlanmış farklı deneylere karşılık gelmektedir.

Diğer ilginç bir sonuç ise son tabakada adsorplanan polielektrolitin yük işaretine karşılık gelen yüzey zeta potansiyel değeri ile ilgilidir [73, 109]. Bununla beraber, zeta potansiyel işaretinin PSP ve PAH tabakaları birikimi ile değişmediği görülmüştür. Zeta potansiyeli pozitif olduğu sürece (örneğin, m:75 için) zeta potansiyeli tabaka sayısının artması ile sürekli olarak azalmıştır (Şekil 9). Zeta potansiyeli sıfır olduğunda, daha önce regular olarak büyüyen filme göre kararsızlık olmuş, bazı örnekler geçici olarak bu aralıkta sublineer bazıları ise superlineer gelişim göstermiştir. Zeta potansiyeli 150-200 tabaka sayısından sonra yaklaşık -20 mV değerinde sabit kalmış ancak film gelişiminin daha düşük sayıdaki tabakalarda elde edilen aynı eğimle devam ettiği görülmüştür. Düşük tabaka sayılarında bile ada-benzer yapı gösteren eksponensiyel filmler ($m < 15$), zeta potansiyel işaretleri pozitif ve negatif değerler almaktadır [93].

Kompleksleşmenin kurutma aşamasında kesilmesine ve kinetik olarak engellenmesine rağmen çözeltide ve LbL depolanmasının her ikisinde de partikül büyümesi ve zeta potansiyel değişiminin aynı ölçekte olması enteresandır.

Sonuç olarak, kullanılan polielektrolitler, PSP ve PAH, karakterize edilmiştir. PSP ve PAH konsantrasyonunun artması lineer film gelişiminden supralineer film gelişimine geçişe imkan vermektedir.

Makroskopik film homojenliği dikkate değer iken, nano ölçekte pürüzlülüğün film kalınlığı ile lineer olarak artması PSP/PAH kompleksinin ilginç bir film gelişim örneği olduğunu göstermiştir. PAH zincirlerinin makroskopik olarak pozitif zeta potansiyele sahip bir yüzeye adsorbe olabilmesi oldukça şaşırtıcıdır. Arayüzeydeki kompleks oluşumu sürekli bir film olarak birleşmeksizin 300 nm den daha büyük partiküllü, küçük polidispersiteye sahip ada yapısına yol açmaktadır.

Bu sonuçlar, elektrostatik etkileşimden başka diğer etkileşimlerin de çok tabakalı film yapısına katkısının olabileceğini ve böylece yüzeydeki polielektrolit komplekslerde dinamik yapısal değişikliklerin meydana gelebileceğini işaret etmektedir.

PSP ve PAH arasında çözeltide oluşan kompleksleşme dinamiktir. Polianyon/polikasyon ekleme sırasının ve PSP/PAH kompleksi dengeye geldikten sonra kompleks üzerine PSP veya PAH eklenmesinin kompleksleşmeye etkisi termodinamik özellikler bakımından ihmal edilebilir düzeydedir. Partikül boyutu büyümesinin çözelti ve LbL arayüzeyde benzer ölçekte olması enteresandır.

Bu sonuçlar, kompleks oluşumu için her iki poliyonun lateral difüzyonu ile birlikte ona eşlik eden PSP ve PAH agregasyonun da olduğu bir kompleksleşme modelinin önerilmesine katkı sağlamaktadır.

Bu çalışma, sulu çözeltiden basit püskürtme ile 150 tabaka basamağına kadar birleşme olmadan ada oluşumunun meydana geldiği yeni bir film gelişimini ortaya çıkarmıştır.

Bu çalışmada, kendi kendine düzenlenen polielektrolit çoklu tabakaları elde edilmiş ve ilk kez tanımlanmıştır. Nano ölçekteki düzenin boyutları tabaka sayısının bir fonksiyonudur.

Çalışmada saptanan partikül boyutu büyümesi ve farklı derecelerdeki pürüzlülük değerlerinin varlığı, geleneksel LbL yaklaşımı kullanılarak üretilen kaplamalara tamamlayıcı olarak superhidrofobik yüzeyler gibi çok ilginç uygulama alanlarında kullanılabilir [36, 41, 46, 49, 108,150-153].

1. INTRODUCTION

Polyelectrolytes are polyions which contain ionic groups in their repeat units and therefore exhibit electrolyte properties. Polyelectrolyte complexes (PEC) are formed by mixing solutions of polyanions and polycations with the release of the counterions. Complex formation between anionic and cationic polyelectrolytes has been a well-known phenomenon for more than 90 years [1- 10].

PEC formation can take place in bulk or at interfaces, the latter phenomenon has led to the development of a new form of nanostructured hybrid materials in the form of thin films (G. Decher et al. Ongoing development since 1990). The deposition of polymer-based films via layer-by-layer (LbL) assembly has become a popular surface functionalization method because of its versatility and ease of preparation. PEC formation is important on the basis of industrial processes, such as flocculation and also hybrid films obtained by LbL assembly offer a wealth of potential applications in material science [36-38, 46, 49, 51, 150-153]

Several variables affect the formation mechanisms and the stability of polyelectrolyte complexes formed both in bulk and at interface; such as the molar ratio of cationic to anionic groups, polyelectrolyte concentration, pH, ionic strength, temperature, etc. In addition, chain rigidity/flexibility, topography, charge density, and molecular weight of the polyelectrolytes also play an important role on defining the structure of the PECs.

Most of the polyanions as charged moieties used in polyelectrolyte multilayer films up to now were carboxylates, sulfates or sulfonates, but to our knowledge, no investigations have been done on with polyphosphates, which display interesting behavior due to being an interesting water soluble, integral type of inorganic polyelectrolyte with some unique properties concerning its interactions with charged species. Hence, in this study, poly (sodium phosphate), PSP, with a degree of polymerization, $n=24$ and poly (allylamine hydrochloride), PAH, having a higher molecular weight (56000 g/mol) than PSP were chosen as polyanion and polycation, respectively.

The aim of this study is to compare the properties of a classic PEC in bulk with those of a PEC formed at close-to-identical conditions at an interface (multilayer film) in order to work out the fundamental differences and similarities between such systems using the same parameters such as concentration, stoichiometry, pH, and ionic strength.

In the manuscripts, fundamental information about polyelectrolyte complexes and the review of studies on polyelectrolyte complex formation in bulk and at interface are given in Chapter 2. The materials and experimental methods utilized throughout the study are described in Chapter 3. The evolution and discussions on the results are presented in Chapter 4. Conclusions from results and discussions are briefly summarized, and future perspectives are proposed in Chapter 5.

2. LITERATURE REVIEW

In this chapter, some literatures were reviewed related with the fundamental concept of polyelectrolyte complex formation. The literatures referred in this study were, particularly, chosen depending on the used parameters and types of polyelectrolytes. The literatures were considered to be referred in which the polyelectrolytes, are water soluble linear chain polyions and, basically, similar and/or same parameters were used.

2.1 Polyelectrolyte Complex Formation

Polyelectrolytes are polyions which contain ionic groups in their repeat units and therefore exhibit electrolyte properties. Polyelectrolyte complexes (PECs) are formed by mixing solutions of polyanions and polycations with the release of the counterions. Complex formation between anionic and cationic polyelectrolytes has been a well-known phenomenon for more than 90 years [1-10].

The review surveys of the thermodynamic, kinetics and reaction mechanism of oppositely charged polyelectrolytes in aqueous solution gives two different types of polyelectrolyte complexes such as, soluble nonstoichiometric PECs which form stable, optically transparent solutions, and insoluble stoichiometric PECs, which either precipitate in water or exist as homogeneous turbid colloidal systems without phase separation [4-13]. If there is an excess of polyelectrolyte of one sign in solution, nonstoichiometric complexes yielded. As opposed to nonstoichiometric PECs, stoichiometric PECs contain equal amounts of oppositely charged groups, so that their charge is zero and complexation, generally, results in macroscopical phase separation. Besides, it is known that PECs containing weak polyelectrolytes show lower degree of aggregation in comparison with the PECs containing strong polyelectrolytes.

Several variables affect the formation mechanisms and the stability of polyelectrolyte complexes formed both in bulk and at interface; such as the molar ratio of cationic to anionic groups, polyelectrolyte concentration, pH, ionic strength,

temperature, etc. In addition, chain rigidity/flexibility, topography, charge density, and molecular weight of the polyelectrolytes also play an important role on defining the structure of the PECs. For instance, it has been reported that the increase in ionic strength in a system containing at least one weakly charged polyelectrolyte leads to phase separation [13-35].

Studies on polyelectrolyte complexes date back to 1896 when the precipitated egg albumin with protamine was investigated by Kossel [6]. Fuoss and Sadek in 1949 described the turbidimetric titration of poly(vinyl-N-n-butyl pyridinium bromide) with sodium(polyacrylate) and sodium poly(styrene sulfonate), which yielded non-stoichiometric PEC [5]. Complexes between synthetic polyelectrolytes with high charge density (poly(4-vinylbenzyltrimethylammonium chloride) associates with poly(sodiumstyrenesulfonate)) were first investigated in 1961 by Michaels [4].

In this aspect, the accessibility of the functional groups is of special interest. Therefore, polyelectrolytes were classified according to the position of the functional groups which are called pendant or integral type. In pendant-type polyions, the charges have placed at the side groups, whereas in integral-type, the charges have placed on backbone of polyions (Figure 2.2) [3].

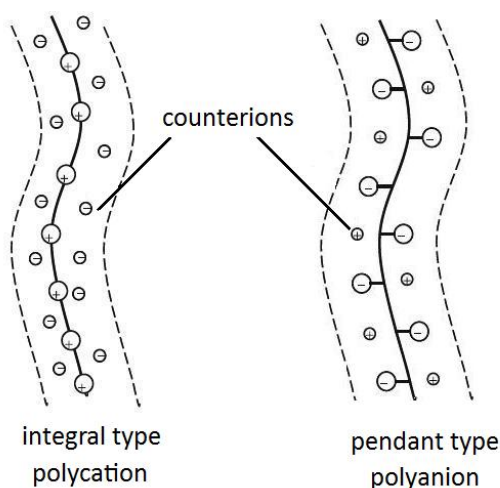


Figure 2.1: Illustration of an integral type and a pendant type of polyelectrolytes [3].

Tsuchida and coworkers have studied with polycarboxylicacids; such as poly(acrylicacid) and its derivatives, poly(ethyleneoxide), and investigated non-stoichiometric PECs in aqueous and nonaqueous media. The effect of temperature, chain length, molecular weight of the polyions were considered as the dominated

parameters on polyelectrolyte complexation. In their work, it was reported that the stability of PECs increase with the degree of polymerization of polyanion. They have reported that the increasing the chain length of the polycation results in increase in the complex stability and strong hydrogen bonding [7-9].

Kabanov and coworkers investigated the formation and structure of water soluble PECs and the influence of pH, molar mass of polycations and polyanions on the complex stability, as well as the condition of polyelectrolyte complex formation. They examined the mechanism of rearrangement of complexes between tri(polyphosphate), poly(sodiummetacrylate) and poly(ethyl-4-vinylpyridiniumbromide) depending on molar mass of polycations and polyanions on the complex stability by turbidimetry and conductometry. In their work, they have synthesized the polyphosphate by condensation polymerization of sodiumdihydrogenphosphate. They have proposed a novel model for PEC formation in which two thermodynamical conditions has to be fulfilled together. These conditions were is the sticking of a globule to an open linear chain (cooperative coupling) and the strong positive interaction between the globules [16-19].

Tulun and coworkers used poly(sodiumphosphahate), PSP, and poly(4-vinylpyridinium chloride), P4VPC, which are both linear and water soluble, but they are integral type of inorganic, anionic and organic, cationic polyions respectively. They have investigated the complexation and swelling of PSP and P4VPC depending on the concentrations of polyions, ionic strenght, pH and various low molecular weight salts. It was reported that the complex stoichiometry exceeds from unity and the composition of the complex was independent of the order of addition. It was found that the efficient pairing of active groups on the polyanion and polycation chains are interrupted at high ionic strenght. Therefore, rearrangement of polyions occurs with the coiling of polyion chains; thus the stoichiometry exceeds the unity. The resultant complex showed swelling property in different solvent mixtures. A maximum degree of swelling was obtained in the solvent mixture of NaBr + water and NaBr + water + acetone. It was reported that the sorption of salts increased with increasing salt concentration [20]. Complexation and dissolution properties of the PSP and P4VPC in dilute solution depending on the range of the composition were also investigated in a different work of Tulun and coworkers [21]. In this work, they have determined the stoichiometry of PSP and P4VPC complex from the weights of

isolated PSP/P4VPC complexes as well as the analysis of the supernatant liquid in conjunction with the weights of initial components and complex. It is found that reaction stoichiometry is very close to 1:1 and dissolution of the complex required a certain minimum hydrogen ion concentration. They have investigated the stoichiometry of complex formed by PSP and 4-amino benzoic acid, PABCl, in ethanol solution and reported that decreasing of pH depresses the complexation of PABCl with PSP at high ionic strength [22]. The interaction between polyelectrolyte complex formed by PSP and PABCl and Cu (II) ions after dissolution of the complex in nonaqueous solvents was also studied [23], and DMF, DMSO and ethanol were used for the dissolution PEC. The interaction between PEC small molecules and Cu (II) ions was demonstrated by potentiometric titration and the stability constant of PEC-Cu (II) complex was found to be 1.59×10^3 . They also investigated the complexation and swelling properties of alkylated tripolyphosphate and P4VPC. In this work, polyphosphate chain was alkylated leading to increase in the chain length in order to provide a reduce of hydrolytic degradation. It was observed the formed polyelectrolyte complex was ionically crosslinked and shows highly swelling behavior in the presence of low molecular salts [24].

Similarly, Philipp et al. have used turbidimetry, potentiometry and conductometry to investigate the influence of charge density and molecular geometry on PEC composition [25]. They have suggested that deviations from 1:1 stoichiometry could be due to structural features of the polyelectrolyte components, as well as the process of PEC formation. In addition, it was reported that the deviation within the range may be tolerated upto a certain limit in reproducibility of preparation and characterization of PEC [25].

Dautzenberg investigated the structure and the characteristics of strong polyelectrolyte complexes formed by sodium poly(styrenesulfonate) and poly(diallyldimethylammonium chloride) and their acrylamide copolymers. In their work it was shown that the presence of small amount of salt during complex formation causes much lower values of the degree of aggregation. They have also reported that PEC formed by mixing polycation (PC) and polyanion (PA) solutions, mostly consists of three components: (i) small soluble PCs and PAs, (ii) dispersed colloidal particles of aggregated PC and PA complexes, and (iii) larger insoluble precipitate particles [12, 13].

Besides, it is reported that the final structure of the complex aggregates can be either in a ladder structure with fixed ionic cross-links or a scrambled-egg structure with a statistical charge compensation (Figure 2.2) [3].

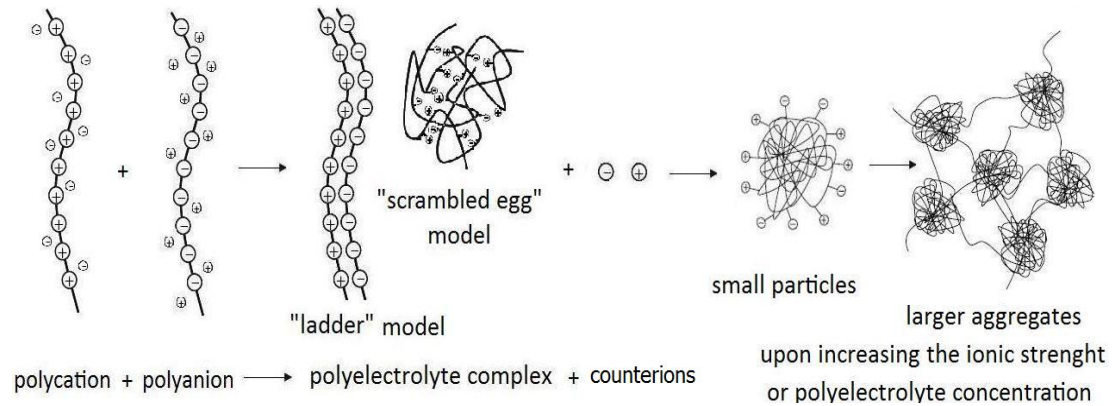


Figure 2.2: Schematic representation of polyelectrolyte complex formation [3].

The driving force for the formation of PECs is the strong Coulombic interactions between oppositely charged polyelectrolytes, which leads to interpolymer ionic condensation.

In addition, inter-macromolecular interactions are involved in the formation of PEC structures such as hydrogen bonding, Van der Waals forces, hydrophobic and dipole interactions. It is known that the process of complex formation is also entropy driven because of the release of counterions that are no longer restricted to the polymer backbone chain. Overbeek and Voorn [14] have tried to theoretically explain the experimental results obtained by Bungenberg de Jong and Kruyt [15] using the Debye- Huckel theory, and they determined the electrostatic energy and the entropy of mixing for two-component (polyelectrolytes and solvent) and three-component (polyelectrolytes, solvent and inert electrolyte) system.

It is reported that pH is significant factor in controlling the stability of polyelectrolyte complexes if a polymer capable of hydrogen bonding is used. In an acidic medium, weak polyacid predominantly is found in the nondissociated form, therefore interaction is more likely occur by intermolecular hydrogen bonding. In the neutral region, both a weak polyacid and a weak polybase are partially charged. In this circumstance, formation of the polyelectrolyte complex is favorable. On the other hand, the weak polyacid is fully ionized and the weak polybase is not charged in an alkaline medium, therefore, the interaction between the components are not favorable in these conditions [25, 27].

Dissociation of PEC can be achieved by appropriate choice of experimental conditions such as; pH and/or ionic strength. The addition of a low molecular mass salt leads to the shielding of electrostatic interactions and dissociation of PECs. The charge screening of the components by added salt leads to a decrease in the number of interpolyelectrolyte salt bonds within PEC followed by dissociation of PEC to the initial polyions [28, 29]. On the other hand, shielding of electrostatic interactions between the oppositely charged core and the shell of the interpolymer complex particle may promote stabilization of complexes in solution. It has been reported that once a certain critical concentration of the salt is reached, the the increase in the dimensions of the complex is so high. This is due to increment of the tendency for monomer units to leave from the shell. To minimize losses of such a redistribution, the volume of macroions increases sharply but they do not separate as a whole since they should adsorb a large amount of counterions inside them for charge compensation.

2.1.1 Application Areas of PECs

PEC formation can take place in bulk or at interfaces. Research on the fundamentals of PEC formation is getting increasingly important because of innumerable applications.

They can be used as membranes, coating films and fibers, microcapsules and implants. Because of their high degree of hydrophilicity, biocompatibility and permeability they are of special interest in the field of biological systems. PEC based materials can be used in artificial kidneys, prosthetic materials for body repair, coatings and components of heart valves and artificial hearts, or as contact lenses [41, 49, 108].

Another field of growing interests are DNA complexes with synthetic or natural polycations because of their application for the cell transfection [36, 153]. The process of encapsulation at the micron scale of the PE or PECs in gene delivery systems also gained much interests [36, 46]. Biomaterials themselves, for instance, can be formed by films called “polyelectrolyte multilayers” made by an alternate deposition of polyanions and polycations on a charged surface (Figure 2.3). These films were discovered by Decher et al., [39-45].

The deposition of polymer-based films via layer-by-layer (LbL) assembly has become a popular surface functionalization method because of its versatility, ease of preparation, and the fact that it can be applied not only to oppositely charged polyelectrolytes but to many types of polymers carrying mutually complementary functionalities (e.g., hydrogen-bond donors and acceptors) [1].

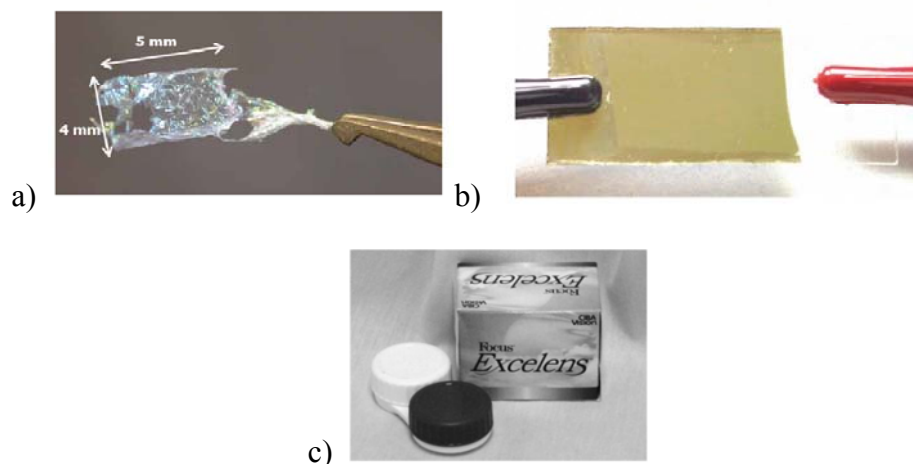


Figure 2.3: a) A nanomembrane [43] b) an image of a multilayer Light Emitting Diode [45], c) the package of a contact lens from CIBA-Vision that has a layerbylayer based coating on its surface. Photo courtesy of L. Winterton of CIBA-Vision: it was presented at the 223rd, ACS National meeting on April 7–11, 2002 in Orlando. Focus® Excelsens™, a contact lens, Copyright CIBA-Vision [1].

2.2 Polyelectrolyte Multilayer Thin Films

There are several techniques for preparation of ultrathin film such as the Langmuir-Blodgett (LB) technique and self-assembled monolayer (SAM) method [52-55]. Langmuir–Blodgett deposition, invented by Langmuir and Blodgett, and the SAM technique, developed by Nuzzo and Allara [56].

2.2.1 Langmuir-Blodgett (LB) technique

Monolayers are formed on a water surface and subsequently transferred onto a solid support in Langmuir-Blodgett (LB) technique, invented by Irving Langmuir and Katharine B. Blodgett.

A Langmuir–Blodgett film contains one or more monolayers of an organic material, deposited from the surface of a liquid onto a solid by immersing (or emersing) the solid substrate into (or from) the liquid. A monolayer is adsorbed homogeneously with each immersion or emersion step, thus films with very accurate thickness can be

formed. This thickness is accurate because the thickness of each monolayer is known and can be added to find the total thickness of a Langmuir-Blodgett Film. The monolayers are assembled vertically and are usually composed of amphiphilic molecules with a hydrophilic head and a hydrophobic tail such as surfactants.

When surfactant concentration is less than critical micellar concentration, the surfactant molecules arrange themselves as shown in Figure 2.4.

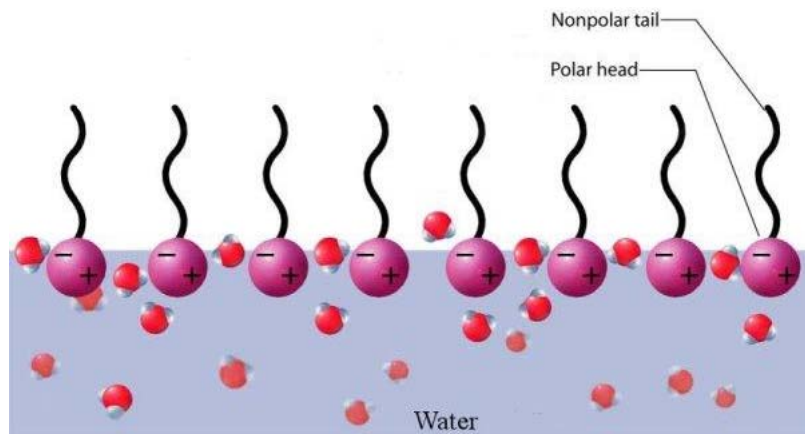


Figure 2.4: Surfactant molecules arranged on an air-water interface.

This tendency can be explained by surface-energy considerations. Since the tails are hydrophobic, their exposure to air is favoured over that to water. Similarly, since the heads are hydrophilic, the head-water interaction is more favourable than air-water interaction. The overall effect is reduction in the surface energy (or equivalently, surface tension of water). LB films are formed when amphiphilic molecules like surfactants interact with air at an air-water interface.

Many possible applications have been suggested over years for Langmuir–Blodgett films. These films have different optical, electrical and biological properties which are composed of some specific organic compounds. Organic compounds usually have more positive responses than inorganic materials for outside factors (pressure, temperature or gas change).

- LB films can be used as passive layers in MIS (metal-insulator-semiconductor) which have more open structure than silicon oxide, and they allow gases to penetrate to the interface more easily and have obvious effects.
- LB films also can be used as biological membranes. Lipid molecules with the fatty and polar regions have got extended attention because of being adequately suited to the Langmuir method. This kind of biological

membranes can be investigated in the mode of drug action, the chemistry of biologically active molecules, and the modelling of biological system.

- Also, it is possible to propose field effect device for observing the immunological response and enzyme-substrate reactions by collecting biological molecules such as antibodies and enzymes in insulating LB films.
- Application to glass and make antireflecting but at the same time allowing 99% of visible light to pass through.
- UV resist LB films and UV light and conductivity of a LB film.

Pioneering work on synthetic nanoscale multicomposites of organic molecules in the late 1960s was carried out by Kuhn and colleagues using this technique [54]. In their work, donor and acceptor dyes in different layers of LB films were the first nanomanipulations used for mechanical handling of individual molecular layers for separation and contact formation with angstrom precision. Unfortunately, the LB technique is not always useful for practical application because of the requirement for rather expensive instruments and not being applicable for many kinds of material. This technique requires the assembly components to be amphiphilic. In addition, weak physical attraction inside the films leads to the considerable instability of biomolecules. Besides, the molecules are not trapped firmly and frequently rearrange after or even during LB deposition.

2.2.2 Self-assembled monolayers (SAMs)

A self assembled monolayer (SAM) is an organized layer of amphiphilic molecules in which one end of the molecule, the “head group” shows a special affinity for a substrate. SAMs also consist of a tail with a functional group at the terminal end as seen in Figure 2.5.

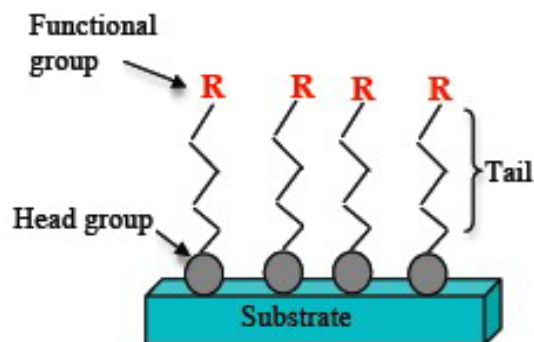


Figure 2.5: Representation of a SAM structure.

SAMs are created by the chemisorption of hydrophilic “head groups” onto a substrate from either the vapor or liquid phase followed by a slow two-dimensional organization of hydrophobic “tail groups”. Initially, adsorbate molecules form either a disordered mass of molecules or form a “lying down phase”, and over a period of hours, begin to form crystalline or semicrystalline structures on the substrate surface. The hydrophilic “head groups” assemble together on the substrate, while the hydrophobic tail groups assemble far from the substrate. Areas of close-packed molecules nucleate and grow until the surface of the substrate is covered in a single monolayer. Adsorbate molecules adsorb readily because they lower the surface energy of the substrate and are stable due to the strong chemisorption of the “head groups.” These bonds create monolayers that are more stable than the physisorbed bonds of Langmuir–Blodgett films.

SAM films formation occurs in two steps, an initial fast step of adsorption and a second slower step of monolayer organization. Adsorption occurs at the liquid-liquid, liquid-vapor, and liquid-solid interfaces. The transport of molecules to the surface occurs due to a combination of diffusion and convective transport.

Once the molecules are at the surface, the self organization occurs in three phases:

1. A low density phase with random dispersion of molecules on the surface.
2. An intermediate density phase with conformational disordered molecules or molecules lying flat on the surface.
3. A high density phase with close packed order and molecules standing normal to the substrate's surface.

The nature in which the tail groups organize themselves into a straight ordered monolayer is dependent on the inter-molecular attraction, or Van der Waals forces, between the alkyl and tail groups. To minimize the free energy of the organic layer the molecules adopt conformations that allow high degree of Van der Waals forces with some hydrogen bonding.

Many of the SAM properties, such as thickness, are determined in the first few minutes. However, it may take hours for defects to be eliminated via annealing and for final SAM properties to be determined. The exact kinetics of SAM formation depends on the adsorbate, solvent and substrate properties. In general, however, the kinetics are dependent on both preparations conditions and material properties of the

solvent, adsorbate and substrate. Specifically, kinetics for adsorption from a liquid solution are dependent on:

- Temperature – room temperature preparation improves kinetics and reduces defects.
- Concentration of adsorbate in the solution – low concentrations require longer immersion times and often create highly crystalline domains.
- Purity of the adsorbate – impurities can affect the final physical properties of the SAM.
- Dirt or contamination on the substrate – imperfections can cause defects in the SAM.

SAMs are an inexpensive and can be used in applications of biology, electrochemistry and electronics, nanoelectromechanical systems (NEMS) and microelectromechanical systems (MEMS), and everyday household goods. They can serve as models for studying membrane properties of cells and organelles and cell attachment on surfaces. These monolayers can also be used to modify the surface properties of electrodes for electrochemistry. However, SAMs are only deposited by the adsorption of thiols onto noble metal surfaces or by silanes onto silica surfaces. The stability of the deposited films depends on the preparation ambient and physical conditions. Therefore final structure of the SAM is dependent on the chain length and the structure of both the adsorbate and the substrate. SAM method has also the disadvantages of being applied to a limited number of substrate types although it can be applied to a wider range of substances.

2.2.3 LbL (Layer by Layer) deposition technique

The history and the principle of multilayer deposition was first described by Iler [57]. Later on, multilayered films are gained considerable interest in the scientific community. The films called “LbL polyelectrolyte multilayers” made by an alternate deposition of polyanions and polycations on a charged surface were first realized and demonstrated by Decher et al [39-45, 49]. In the last eight years, the concept of LbL technique has been reviewed on and a great number of publications concerning LbL films preparation have been reported. Compared to LB and SAM traditional techniques, LbL deposition technique is an easy, simple and inexpensive, environmental friendly method for multilayer formation with nanoscale precision by

consecutive adsorptions of positively and negatively charged species from their aqueous solutions onto substrates of almost any size and shape. It takes about 20 minutes to reach equilibrium adsorption in every step, so several hours are needed to build up a multilayer of hundreds of nanometers in thickness. It allows different types of materials to be incorporated in the film structures. Multilayer structures composed of polyions or other charged molecular or colloidal objects (or both) are fabricated by LbL technique schematically illustrated in Figure 2.6.

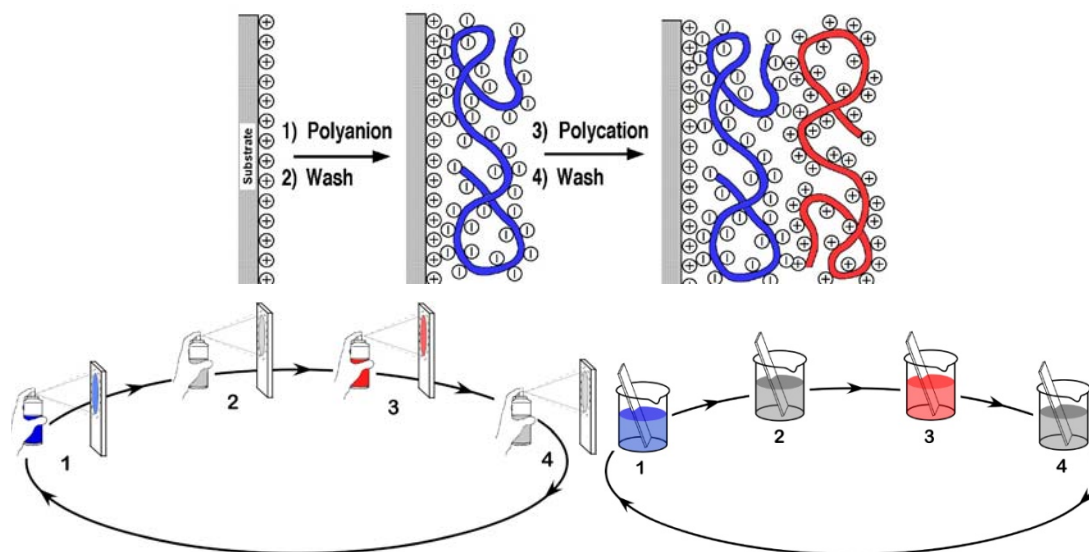


Figure 2.6: (a) A simplified schematic of the principle for the first two adsorption steps in film deposition as starting with a positively charged substrate. (b) Schematic representation of film deposition by LbL-Spraying. (c) Schematic representation of film deposition process by LbL-Dipping. Steps 1 and 3 represent the adsorption of a polyanion and polycation respectively, and steps 2 and 4 are washing steps. Counterions are omitted for clarity. The polyanion conformation and layer interpenetration are an idealization of the surface charge reversal with each adsorption step. The four steps are the basic buildup sequence for the simplest film architecture $(A/B)_n$ where n is the number of deposition cycles. The construction of more complex film architectures requires only additional deposition cycles and a different sequence [1].

In LbL technique, the substrate is brought alternatively in contact with a polyanion and a polycation solution either by dipping or by spraying the solutions over the surface to be coated for a given time.

The repeated spray/rinsing or dip/rinsing cycles during the adsorption of each individual layer increase the layer thickness in each case, as a result of structural rearrangements leading to the exposure of more anchoring sites on the surface.

The pioneering studies on spray-LbL were carried out by Winterton and co-workers [58] and followed by Schlenoff [59]. They found that such a film had a composition and thickness similar to those of a multilayer film constructed by the conventional deposition method in solution. The comparison of the fundamental differences between spraying and dipping methods was investigated in more detail by Izquierdo et al. [47].

In LbL dipping deposition, in general, the substrate is immersed into solutions of anionic and cationic polyelectrolytes, followed by rinsing of the layers with pure water or salt solution. The layer is dried before being reimmersed into the each solution.

In Figure 2.7 [47], schematic experimental set up for LbL-spray deposition is given. In this Figure, A shows the perpendicular spray of polyelectrolytes on a vertically oriented substrate indicating the spray cone. The distance between the nozzle and the receiving surface, and the direction of the draining liquid. B illustrates the spray on a sheet of paper that changes its color as a function of the quantity of water delivered. This allows distinguishing two regions: a central zone (zone 1) surrounded by a ring (zone 2). Zone 1, the central core, is perfectly wet while the surrounding ring (zone 2) is sparsely covered by fine droplets. In C, fluorescent images of a multilayer film with the deposition sequence PEI(PSS/PAH)₂PSS/PAH-FITC were given for the areas of zone D and ring d.

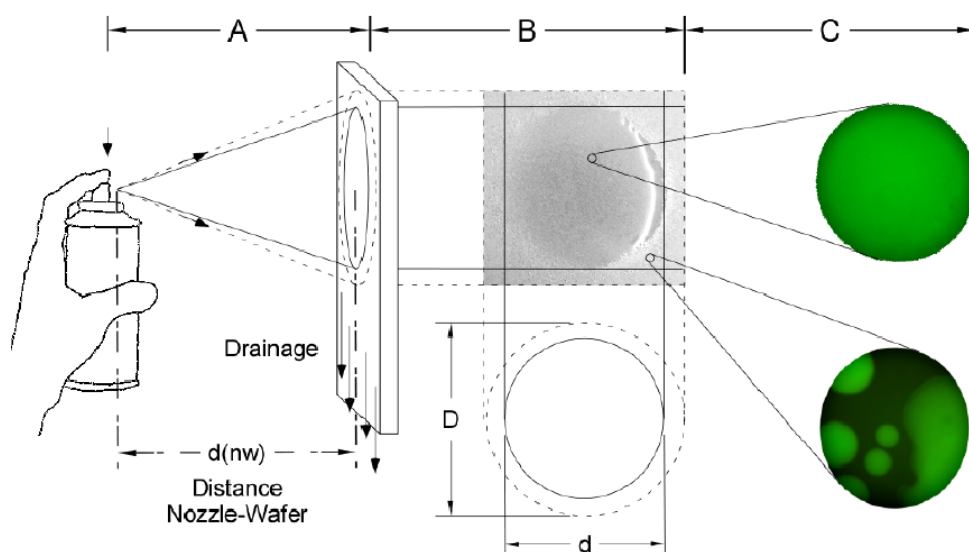


Figure 2.7: Experimental setup for multilayer film deposition by spraying [47].

It was reported by Izquedo et al. [47] that all liquid being applied does not accumulate on the surface but flows away quickly, driven by gravity, and only a thin film of liquid remain on the surface and then typically dry within minutes. Thus, this setup provides for mild but permanent agitation as driven by the draining solution. Because the thickness of the adhering solution is very thin, it is to be expected that any spray droplet arriving at the surface immediately fuse with the liquid film and replace liquid draining off. Therefore, it is assumed that the concentrations of the adsorbing species in the adhering liquid film and in the reservoir in the spray tanks are always identical, even in the close vicinity of the receiving surface. As a consequence, the depletion zone formed close to the deposition surface and the diffusion of the adsorbing species through this zone should only play a minor role, if any. This is in contrast to the dipping method. It also suggested that contact times of the polyelectrolyte solutions with the film could be very short so that the time interval between two consecutive deposition steps can be significantly reduced, compared to the deposition by dipping. Thus the spraying method allows us to change the contact times in a very precise way and polyelectrolyte multilayer deposition can be simplified and sped up enormously by spraying rather than by dipping. Moreover, because drainage constantly removes a certain quantity of the excess material arriving at the surface, the rinsing step can be skipped so that the whole buildup process can be speed up even further. In addition, only small amounts of liquids are needed to coat a large surface areas by spraying.

Standard procedure used in the LbL Spray deposition is illustrated in Figure 2.8. In this Figure, t_0 , t_1 , t_2 , t_3 , and t_4 are the spraying times given in seconds. Grey zones correspond to periods in which the spray is suspended; however, drainage and evaporation of water continue. At time t_0 , the deposition of each layer starts, and at t_1 a polyelectrolyte (polyanion or polycation) is applied by spraying. t_2 is the period in which spraying is suspended but drainage and evaporation of water continue. t_3 is the time during which the film is spray-rinsed with water (or salt solution). t_4 is the period of time as in the case of t_2 during which spray rinsing is suspended but drainage and evaporation of water continue. The total deposition time per layer (t_{layer}) is, thus, equal to $t_{\text{layer}} = t_1 + t_2 + t_3 + t_4$. Film deposition is followed by repeating the sequence defined above for each polyanion and each polycation layer.

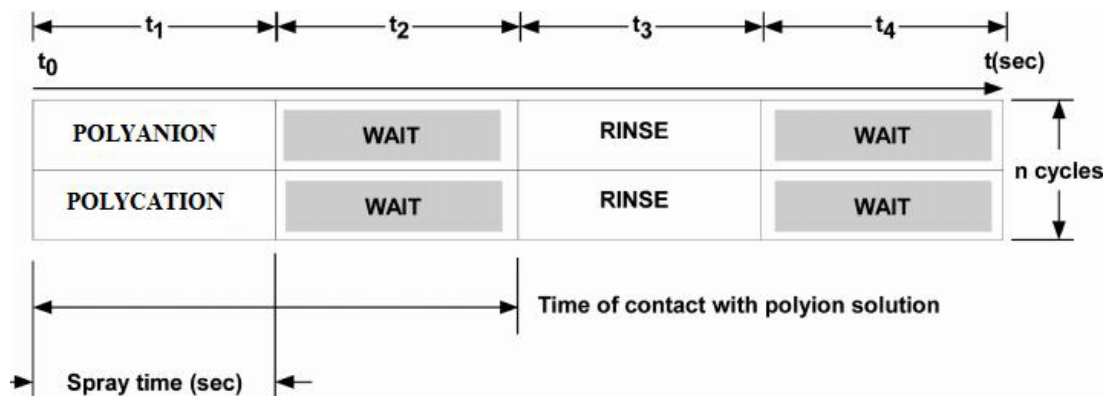


Figure 2.8: Scheme of the standard procedure used in the LbL Spray deposition [47].

Characteristic binding forces of LbL method, in general, can be categorized as i-Coulombic forces, ii-Hydrogen bond, iii-van der Waals forces, iv-Charge-transfer interaction, v-Exchange repulsion, and vi-Hydrophobic interaction. In some authors papers the driven forces of conventional LbL methods are given donor/acceptor interaction, adsorption/drying cycles, covalent bonds, stereo-complex formation or specific recognition [60-68].

The electrostatic interaction is the main driving force for LbL assembly. In this interaction, the multilayers are required to be water-soluble and multi-charged species, such as polyelectrolytes, proteins and enzymes, colloid particles, and oligo charged organic compounds. Therefore, it does not require an exact positional matching of the charged groups in the process of multilayer deposition.

An electrostatic complex for the fabrication of LbL films can be described as follows: first, polyelectrolytes were mixed with counter-charged molecules in aqueous solution to form electrostatic complexes; second, the complexes were deposited alternatively with counter-polyelectrolytes to form LbL films.

Multilayered films based on electrostatic interaction tend to be affected by the environmental conditions. Therefore, a controlled formation of such polymeric films requires a throughout knowledge of the structure, shape and charge of the polyelectrolytes in relation to its molecular weight together with the bulk properties, such as pH, ionic strength and concentration of the polyelectrolytes in solutions. It was reported that, these characteristic variables and electrostatic interaction are strongly correlated in terms of multilayers stability [26, 32, 69-72, 142]. For instance,

the effect of the polymer charge on the multilayer formation leads to three circumstances as illustrated in Figure 2.9.

One of the three possibilities is that, at a very low charge density (<5%) the attraction between the polyions becomes too weak for complex formation at the surface (Figure 2.9a). On the other hand, at a higher charge density (5%-20%) complex formation takes place. During complexation, the polyelectrolyte complex can adjust itself somewhat leading to change in its conformation for the next outer layer. Because of this adjustment, some ionic polyelectrolyte-surface bonds might be broken, as indicated by the arrows in Figure 2.9b and c. Besides, if the charge density is low, only a few bonds remain to keep the complex attached to the substrate so that desorption of the complex can take place (Figure 2.9b). If this is the case no, or instable, multilayers are formed. In contrast, at high charge density (>20%) both the bond to the newly adsorbing molecule and that to the underlying polyelectrolyte complex layer are strong. Therefore, stable multilayers are formed (Figure 9c). Within stable multilayers the mobility of polyelectrolyte molecules will be strongly limited, since they are strongly bound both to lower and higher layers [142].

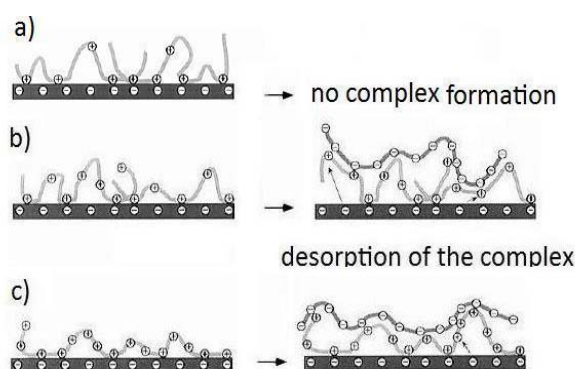


Figure 2.9: Illustration of three possible situations arise depending on the charge density of the cationic polymer: (a) When this charge density is low no complexation occurs. (b) At a higher polymer charge density complexation at the surface occurs, followed by (partial) desorption of the complexes. (c) When both polymers are highly charged, the complex remains strongly bound to the substrate; stable multilayers can be formed [142].

Moreover, when the both polyelectrolyte components are strongly charged, the increase in ionic strength results in larger thickness and stronger roughness of multilayers [74]. On the other hand, the type of salt and its concentration play a more crucial role for the systems containing at least one weakly charged component, leading even to the adsorption/desolution process.

Overcompensation of the surface charge by adsorbing polyelectrolyte allows the subsequent adsorption of oppositely charged polyelectrolyte to form the next layer, thus a change in the ζ potential [74, 86, 87, 93]. An example of evolution of the ζ -potential for alternated HA and PLL deposition during 20 deposition cycles is presented in Figure 2.10.

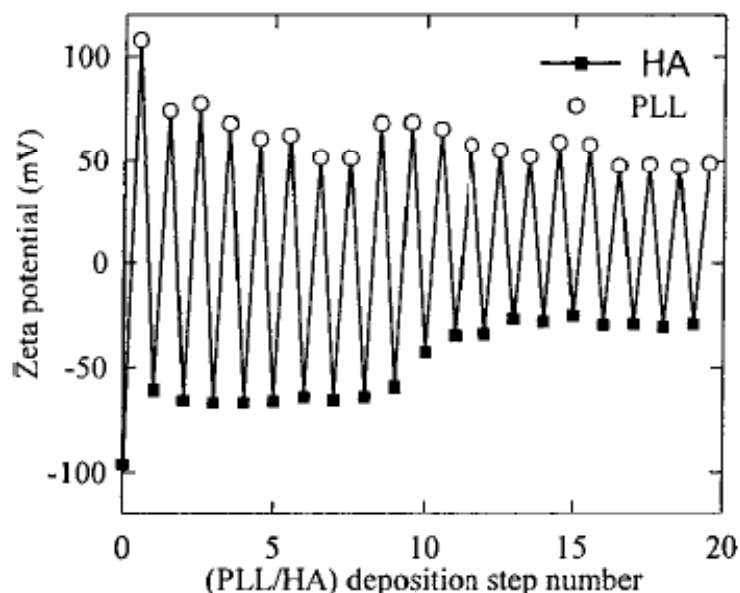


Figure 2.10: Evolution of the ζ -potential for alternated HA and PLL deposition during 20 deposition cycles. Positive (open symbols) values correspond to PLL addition followed by rinsing, and negative values (closed symbols) correspond to HA addition after rinsing [86].

Although the electrical interactions in a system containing oppositely charged polyelectrolytes would be better investigated in the absence of salt, the polyelectrolyte multilayers are usually fabricated in presence of salt. Almost a regular increase in the film thickness has been reported in several studies in which the multilayer films were deposited by PSS and fully ionized PAH in salt free solutions. In addition, Lvov and coworkers [74] have found that the increase in the film thickness was smaller than those obtained in salt-containing solutions. By translating the layer thicknesses into monomoles per unit area, Riegler and Essler [75, 76] found that PAH charges overcompensate the PSS charges in the PSS/PAH deposits. This means that the multilayer film contains some small counterions (Cl^-) for complete charge compensation. Durstock and Rubner [77] reported the presence of 1 small ion per 10,000 repeat units in a PSS/PAH film constructed from salt-free solutions. In all investigations mentioned above, the PSS/PAH films were obtained from

polyelectrolytes of close molecular weights, usually 70 kDa for PSS and 55 or 70 kDa for PAH. In other words, the length of the PAH chain has always been 3–4 times larger than that of the PSS.

The hydrogen-bonded LbL assembly was first demonstrated in 1997 by Stockton and Rubner, and Zhang and coworkers [50, 60, 68].

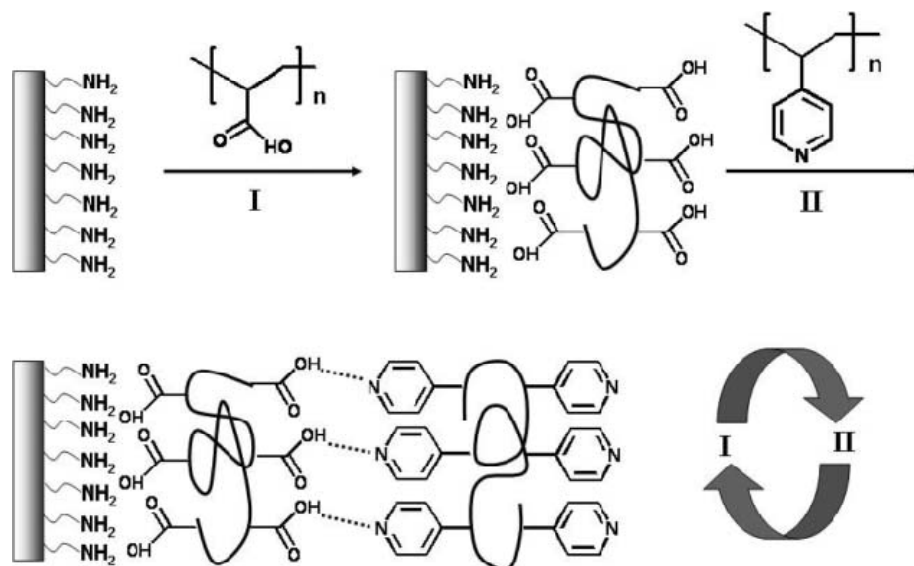


Figure 2.11: Fabrication of LbL multilayer film by hydrogen bonding between carboxylic acid groups and pyridine groups [50].

A multilayer thin films fabricated on the basis of hydrogen bonding is given for an example in Figure 2.11 [50]. In this work, the multilayer thin film is obtained by alternating deposition of poly(acrylic acid) (PAA, hydrogen bond donor) and poly(4-vinylpyridine) (PVP, hydrogen bond acceptor). Hydrogen bonds are sensitive to their environment therefore they can be destroyed by changing the environment. Due to this feature, hydrogen-bonded LbL assembly can be used to fabricate layered, erasable, ultrathin polymer films. Taking the advantage of this feature of hydrogen bonds, Sukhishvili and Granick have demonstrated that LbL multilayers of poly(methacrylic acid) and poly(vinylpyrrolidone) that is stable up to pH 6.9, but dissolve when pH is increased above this point [61]. Caruso et al. reported that the thickness of the hydrogen-bonded layers plays an important role to control the film deconstruction of poly(4-vinylpyridine)/poly(acrylic acid) [63].

Yamamoto and coworkers have introduced a way for building up multilayered films by donor/acceptor interactions using consecutive adsorption of two types of nonionic polymers [64]. They have used 3,5-dinitrobenzoyl group and carbazolyl group at the

ends of the side chains as electron-accepting and electron-donating groups, respectively. The formation of such multilayered films is based on the charge-transfer interactions between donor and acceptor polymers. These films can be prepared in organic solvents. It is possible to introduce hydrophobic functional groups homogeneously into such LbL films. These films can be used as conductive or nonlinear optical materials.

It was found that the degree of ionization of a weak polyelectrolyte within the multilayer film affects the charge of the polyelectrolyte included in the top layer [78-79]. Several investigations have been reported that the last deposited layer has significant importance for the behavior of the whole multilayer film such as the ion permeability. It can influence the swelling of the multilayer due to the changes in the electric potential [80-82].

2.2.4 The zone model For Polyelectrolyte Multilayer Thin Films

Independent of their dynamic properties, polyelectrolyte multilayer (PEM) films can be rationalized by a three-zone model arising from interfacial effects of the substrate and the surrounding medium (e.g., air). A multilayer film composed of an anionic polyelectrolyte and a cationic polyelectrolyte can be considered by subdividing into three distinct zones (Figure 2.12) [1].

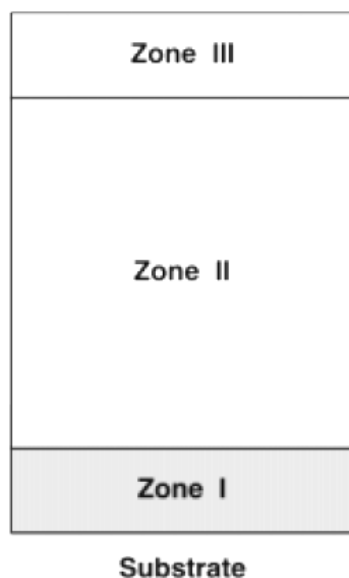


Figure 2.12: The zone model for polyelectrolyte multilayers. Zone I is adjacent to the substrate, Zone II forms the “bulk” of the multilayer and Zone III is adjacent to the film/solution or film/air interface [1].

Zone I is comprised of one or a few polyelectrolyte layers close to the substrate. In this zone the multilayer is influenced by the nature of the substrate. Zone I is comprised of one or a few polyelectrolyte layers close to the surface of the film. In this zone the multilayer is influenced by the interface to the solution or to air. Zone II is “bulk” film, in this region the multilayer is not influenced by either interface. Zones I, II and III would normally differ in both chemical composition and in structure. In the very coarse and simple picture, Zone II is neutral and the Zones I and III are charged. The interface between the zones is diffuse rather than a sharp plane which is indicated here for clarity.

As the adsorption of every layer leads to an overcompensation of the original surface charge, the newly created excess charge is accompanied by the presence of small counterions. Therefore, it is expected that layers further away from the surface will also contribute excess charge on the surface.

Depending on the charge density and roughness of the substrate, varying amounts of small counterions might be present in Zone I. Initially, for the first few layers, the transition between Zones I and III may occur without forming Zone II. Polyelectrolyte pairs, which form a 1:1 complex, will form a Zone II when Zones I and III have reached their final composition and thickness. When more layers are deposited, Zones I and III keep their respective thicknesses and Zone II increase in thickness.

The zone model outlined above is the simplest way to account for effects of the interfaces of the film [1]. However, it is expected to be valid only for simple and relatively flexible polyions. It may become more complicated, especially if polyelectrolytes are employed that are not capable of forming a 1:1 stoichiometric complex. The model of three more or less distinct zones is also only valid once a sufficient number of layers has been deposited.

2.2.5 Growth Process in Polyelectrolyte Multilayer Thin Films

In the literature [83-90, 94], it has been reported that polyelectrolyte multilayer films can grow either linearly or supralinear (exponential growth in most cases) with the number of deposition steps (Figure 2.13). It is reported linear regime occurs preferentially at low temperature and low ionic strength whereas superlinear ones are observed at higher ionic strength or higher temperature.

In the first investigated systems [84,85], it was found that the mass and thickness of the films increase linearly with the number of deposition steps (Figure 2.13). During each layer deposition step, the polyelectrolytes from the solution are electrostatically attracted by only the oppositely charged polyelectrolytes constituting the last deposited layer. In other words, each polyelectrolyte layer interpenetrates only with the neighboring ones. Thus, linear polyelectrolyte deposition leads to charge compensation at the solid/liquid interface [83, 84], which leads to electrostatic repulsion and limits the polyion adsorption to only one additional monolayer. Therefore, the films showing linear growth exhibit a layered structure [85].

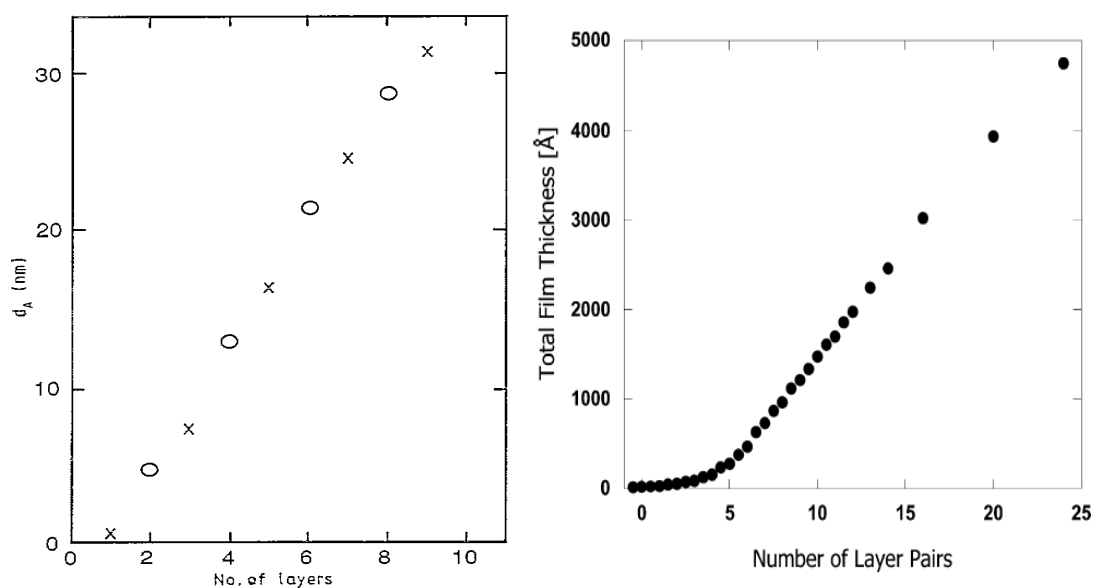


Figure 2.13: Polyelectrolyte multilayer film thickness as a function of layer numbers a) an example for a linear growth regime of ○: PSS, ×: PAH given in literature [44] b) an example of exponential (supralinear) growth obtained by poly(acrylic acid) (PAA) and poly(ethyleneglycol) (PEG) given in literature [43].

The deposition of the exponential regime is often superlinear due to the fact that at least one of the polyelectrolytes can diffuse freely throughout the whole film [86,88]. In fact, when the deposition is performed for a given time, the molecules can only diffuse through a limited critical thickness, which means that the diffusion process cannot affect the whole film thickness any more, and it turns again into a linear regime but for which the thickness increment per layer pair is much higher than for regular linearly growing films. These films are less structured than the linearly growing ones, very hydrated, resemble gel-like and their thickness can reach several

micrometers after only a few tens of deposition steps. Such films were mainly observed with polypeptides, polysaccharides, or synthetic polyelectrolytes [87-90].

It is also known that when a polyanion and a polycation interact, counterions releasing takes place into the solution leading to an increase of the global entropy. Ball and coworkers proposed a correlation between the complexation heat and the nature of the film growth process by using isothermal titration microcalorimetry experiments performed on several polyanion/polycation systems [95, 96]. They have shown that an endothermic complexation process corresponds to an exponential film growth whereas exothermic complexation process corresponds to a linearly film growth. The release of the counterions causes the increase in the entropy which counterbalances the loss of conformational entropy of the polymeric chains leading to exponentially increase in the film thickness. It is suggested that the exponentially growing processes are mainly driven by entropy and also very sensitive to the environmental conditions. Therefore, it is possible to change the buildup regime of every polyelectrolyte multilayer film from linear to exponential or vice versa by a weakening or a strengthening of the polyelectrolyte interactions, by changing the ionic strength and/or the temperature of the dipping solutions. For example, it has been observed that PSS/PAH film may grow exponentially when the polyelectrolyte solutions are prepared in the presence of a high salt concentration. The same observation has been made for the PSS/PDADMA films [102].

Kujawa et al. investigated the influence of the polyelectrolyte molecular weights on the exponential growth regime for the hyaluronic acid/chitosan system. They found that polyelectrolytes of higher molecular weights led to thicker films after a given number of deposition steps [103].

However, not all LBL films fall into simple categories: there are cases in which the growth cannot be described by either a linear or a supralinear growth regime. In a few systems, the growth is best described by a succession of two linear regimes (the first one influenced by the surface and the second one corresponding to “free” growth) [93, 102, 104, 106-109]. Michel et al. [108] reported that exponentially growth film of poly(L-glutamic acid)/poly(allylamine) (PGA/PAH) becomes linear after the deposition of about 20 layers of spraying. In addition, they found that as the number of deposition steps increases transition from exponential growth to a linear increase occurs. Hubsch et al. [104] observed a similar behavior but by depositing

the films from a polyanion solution composed of mixtures of polyanions and a single polycation solution. Salomaki et al. [105] investigated the influence of the effect of temperature and ionic strength on the polyelectrolyte film buildup. They found that the thickness of the films increases linearly with the number of deposition steps at room temperature, but their buildup process becomes exponential if the temperature is raised. The suggestion of these authors for the reason of exponential-to-linear transition (superlinear growth) is the rearrangement of the film and gradual densification of the layers. Restructuring and densification forbids the diffusion of one of the polyelectrolytes over a part of the multilayer matrix so that the film becomes progressively less and less penetrable. The “forbidden” zone moves upward as the total film thickness increases. It grows with the number of deposition steps so that the outer zone of the film that has still diffusion keeps a constant thickness. Porcel et al. [106, 107] investigated hyaluronic acid/poly(L-lysine) (HA/PLL) multilayers by using both dipping and spraying LbL deposition depending on the main parameters such as molecular weight of the polyelectrolytes, spraying rate and time. They have observed that the exponential-to-linear transition is independent of the parameters controlling the deposition process. Although their analysis did not prove the assumption of restructuring of the film, their results are fully compatible with the hypothesis of Hubsch [104] and Salomaki [105]. Porcel et al. [106, 107] suggested that the mechanism of the multilayer film deposition relies on the interaction between the polyelectrolytes with an upper zone of the film. This zone is constituted of polyanion/polycation complexes, which are “loosely bound”, and rich in the polyelectrolyte deposited during the former deposition steps.

Lavalle et al., [109] investigate the buildup of poly(L-glutamic acid)/poly(L-lysine) (PGA/PLL) multilayer films grown under superlinear conditions by means of in situ AFM in order to provide further information on the mechanisms of exponential-to-linear transition. They have proposed a model in which the superlinear growth regime associates with increased surface roughness besides the polyelectrolyte diffusion “in” and “out” of film multilayered film matrix. However, no change in surface roughness was observed for the exponentially growing films made of polypeptides. Unfortunately, since the most investigations have been performed with standard polyelectrolytes, investigation of polyelectrolyte complexation at interfaces is limited to a small subset of systems. Therefore, even if the exponential growth

mechanism begins to be understood, many fundamental questions remain unanswered. The direct proof of film restructuration has been still unknown.

2.3 Polyphosphates

Phosphate, being found in living organisms, plays an important role in carbohydrate, fat and protein metabolism. It is known that condensed linear polyphosphates and its derivatives are produced by a variety of condensation and polymerization reactions in vitro [110].

The earliest differentiation between the various types of phosphates was made Graham, who classified the phosphates into three groups, called linear polyphosphates, ring (cyclo) phosphates (metaphosphates) and ultraphosphates (crosslinked condensed phosphates) [111-119].

Linear polyphosphates (Figure 2.14) are the salts of linear polyphosphoric acid. The basic unit is the (PO_4^{3-}) , and it is the first member of the chain series, with di- and triphosphate being the second and the third members, respectively. Linear polyphosphates with intermediate degree of polymerization ($n = 10 \sim 50$) can usually be obtained in the glassy form [120, 121]. The average degree of polymerization, as measured by the number of phosphorous atoms per chain can range from 3 to 3000.

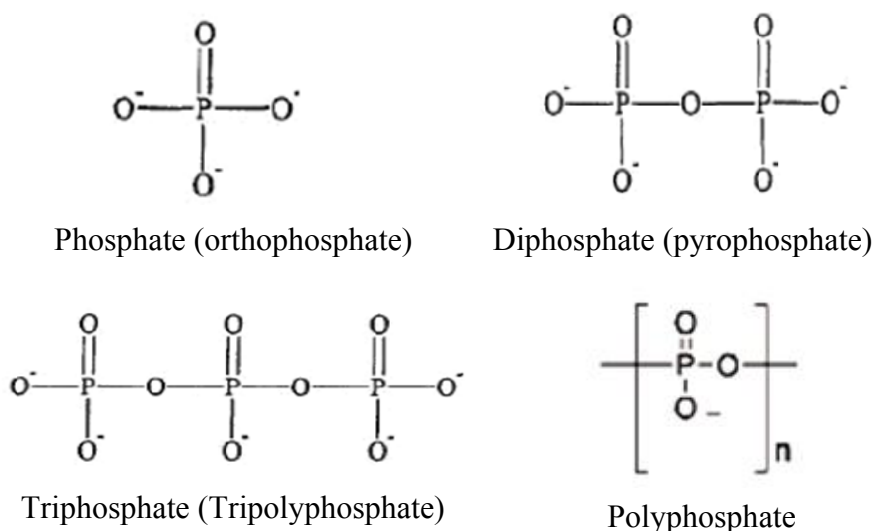


Figure 2.14: Molecular Structures of Linear polyphosphates.

The overall formula of condensed phosphates consisting of either linear or branched chain is given by the formula $M_{n+2}P_nO_{3n+1}$. When the number of units in the

polymeric molecule becomes very large ($n=50$ to 200), in other words if the degree of polymerization is high, the formula is given in the $(\text{PO}_3)_n^{n-}$ form which refers to a ring formation, and called metaphosphate. The ring phosphate composition form well-crystallized salts [121].

Modern studies indicate that linear polyphosphates are reasonably stable in neutral or alkaline solution at room temperature. However, they hydrolyzed to orthophosphates in strongly acid-catalyzed medium by boiling [122]. Alkali and alkaline earth polyphosphate salts have been most studied because of their uses in many fields. For several reasons, the polyphosphates are ideally suited for the study of polyelectrolyte behavior [123, 124].

- They are easily prepared to a much higher degree of purity.
- Their polydispersity can be determined by experimental work.
- The viscosity behavior is uncomplicated since the polyphosphate chains are unbranched.
- Polyphosphates in aqueous solutions of low ionic strength are capable of forming complexes with other polymers, especially proteins, basic polypeptides, and nucleic acids.

Poly(sodiumphosphates) as well as other linear chain phosphates have very similar properties to those of cross-linked, solid ion exchange resin [125]. The behavior of polyphosphates as dissolved ion exchange agents is evidence of their ability to form complexes with counter ions.

Polyphosphates are very good complexing agents for metal ions. This property is widely exploited in the fractionation of polyphosphates, and for other analytical purposes. The chemical and physico-chemical properties of the inorganic polyphosphates will facilitate the development and use of efficient and reliable biochemical procedures for isolation, purification, identification and determination of polyphosphates during their extraction from the alive cell.

Poly(sodiumphosphate) subjected to this study is one of the member of chain polyphosphates having linear polyelectrolyte nature with average degrees of polymerization ranging up to 24, and it is among one of the few inorganic, anionic polyelectrolytes.

3. EXPERIMENTAL PART

3.1 Materials

In this study, poly (sodium phosphate), $((\text{NaPO}_3)_n$, PSP), and poly (allylamine hydrochloride), (PAH), were chosen as polyanion and polycation, respectively. PSP in Analytical Grade (\overline{M}_v : 2900 g/mol, Product No: 04267; CAS: 68915-31-1) and PAH (M_w : 56 000 g/mol, CAS: 71550-12-4; cat. no: 28,322-3) were purchased from Sigma-Aldrich. PEI (Lupasol WF, $M_w=2.5 \times 10^4$) was obtained from BASF (Germany). All the polyelectrolytes were used without further purification. The aqueous solutions prepared with ultrapure water (resistivity=18.2M Ω cm, Milli Q-Gradient system).

Chemical structures of PAH and PSP were given in Figure 3.1.

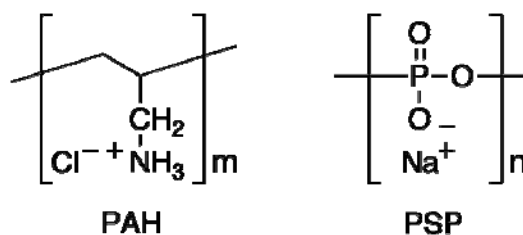


Figure 3.1: Chemical structures of PSP and PAH.

3.2 Methods

3.2.1 Characterization of PSP and PAH

The molar mass and the size of the polyions are one of the important parameters, which provide information for the interested polyions to be suggested in application areas. Therefore, it is necessary to characterize each polyelectrolyte individually prior to used.

3.2.1.1 Determination of molecular weight of PSP by end group titration

The number average degree of polymerization of PSP was obtained by end group analysis [114]. The chain phosphates have one strongly ionized hydrogen for each phosphorus atom and have one weakly ionized hydrogen at each end of the chain. By titrating this weak hydrogen, it is possible to determine the number of end groups

present in the chains. Since there are two types of hydrogen in polyphosphate, two important points on the pH titration curves. Titration of phosphoric acids to an endpoint near pH 4.5 corresponds to the strongly ionized hydrogen associated with each phosphorous atom and gives the total number of phosphorus atoms, whether the phosphorus is in a ring or a chain or in the isolated PO_4^{3-} ion state. Titration between the endpoint pH 4.5 and 9.5 corresponds to the weakly dissociated hydrogen at each end of chain phosphates. The orthophosphate has a third replaceable hydrogen which is so weak that the corresponding inflection point does not show up in a pH titration curve.

The fraction of end group was calculated according to :

$$\%P_2O_5(\text{endgroup}) = \frac{A}{A_h} 100 \quad (3.1)$$

$$\frac{P_2O_5(\text{total})}{P_2O_5(\text{endgroup})} = \frac{n}{2} = \frac{A_h}{A} \quad (2 \text{ indicates two end groups}) \quad (3.2)$$

A = volume of base required to titrate an original aliquot that has been acidified to a pH < 4.5 (if not already sufficiently acidic)

A_h = volume of base required to titrate a hydrolyzed sample from the end point near pH of 4.5 to the end point near pH of 9.5.

Because the solution is titrated before and after hydrolysis, the exact weight of the original sample and the losses are of no importance. This general procedure can be used for chains of any size, assuming that rings and orthophosphate are absent.

A Jenway 3040 pH meter was used for end group titration experiments. 0.5g of PSP was dissolved in 100mL of water and the pH was lowered to about 3 using HCl (1M) in order to convert polyphosphate to polyphosphoric acid, and then, titrated potentiometrically with 0.05M standard NaOH solution until the pH value of 4.5. The volume of added base solution, A (mL), consumed until the first end point was determined. The total phosphorus content of the polyphosphate was determined in another sample containing the same amount of PSP after a complete hydrolysis procedure as described in reference [114]. The complete reversion of the polyphosphate to the orthophosphate form was achieved by gently boiling the sample in a HNO_3 (1M) solution for three hours under reflux. Then, pH was lowered to about 3 and the solution was titrated potentiometrically with 0.05M standard NaOH solution until the pH value of 4.5. The titration was continued beyond the second end

point at about pH 9, and the volume of base, A_h (mL), consumed between two end points was determined. The fraction of end group was calculated according to equations 3.1 and 3.2 and results were given in Table 4.1.

3.2.1.2 Determination of molecular weight of PSP by viscometry

Solution viscosity is a measure of the size of polymer molecules and it is empirically related to molecular weight of polyelectrolytes. Viscosity measurement constitutes an valuable tool for the molecular characterization of polyions. Besides, due to the ease and simplicity of the instrumental technique and the experimental performance it is a widely used method in polyelectrolyte studies.

Dilute solution viscosity is usually measured in capillary viscometer of the Ostwald or Ubbelohde type and concentration, C , is expressed in grams per desiliter (g/dL). Measurements of solution viscosity are usually made by comparing the efflux time, t , required for a specific volume of polymer solution to flow through

a capillary tube with the corresponding efflux time, t_0 , for the solvent. From t_0 , and the solute concentration, C , the following equations are derived (3.3 – 3.6).

$$\text{Relative Viscosity} \quad \eta_r = t/t_0 \quad (3.3)$$

$$\text{Specific Viscosity} \quad \eta_{sp} = \frac{t-t_0}{t_0} = \eta_r - 1 \quad (3.4)$$

$$\text{Reduced Viscosity} \quad \eta_{red} = \eta_{sp} / C \quad (3.5)$$

$$\text{Intrinsic Viscosity} \quad [\eta] = (\eta_{sp}/C)_{C=0} \quad (3.6)$$

t_0 = Efflux time for solvent (distilled water)

t = Efflux time for the polyelectrolyte complex

The molecular weights of linear polyions were calculated from the intrinsic viscosity of the solution by the following Mark Houwink equation:

$$[\eta] = K M^a \quad (3.7)$$

In this equation a and K are constants and dependent to the temperature, type of solvent and polymer and M represents the molecular weight.

In this study, ostwald type viscosimeter was used for the viscosimetry experiments. Viscosity measurements of PSP were carried out in 0.035M NaBr solution at 298.5K

and viscosity averaged molecular weight \overline{M}_v of PSP was calculated as 2900 g/mol by the Equation 3.7 using the constant $K = 69 \times 10^{-5}$ dL/g; $a = 0.61$ for PSP in 0.035 M NaBr .

3.2.1.3 Determination of molecular weight of PAH by viscometry

Ostwald type viscosimeter was used for determination of the molecular weight of PAH. Viscosity measurements of PAH were carried out in 0.5M NaCl at 298K and viscosity averaged molecular weight \overline{M}_v of PAH was found as 52000 g/mol by Equation 3.7 using the constants of $K = 7.19 \times 10^{-5}$ dL/g; $a = 0.794$ for PAH in 0.5M NaCl solutions.

3.2.1.4 Determination of equivalent weight of PSP and PAH

Equivalent weight of PSP was determined by alkalimetry after it has been converted to its acid form, $(\text{HPO}_3)_n$, by ion exchange chromatography using Amberlite IR-120 (strong acid cation exchanger). Similarly, equivalent Weight of PAH was determined by argentimetry after it has been converted to its basic form, PAHOH, by ion exchange chromatography using o Exchanger III (strong base anion exchanger). The ion exchange column were prepared as described in the literature [125].

15g of resin was weighed and put in distilled water and let to stand overnight. After decantation of water, 3M HCl was added, and then it was shaken and filtered. Acid treatment was repeated for three times and washed with large amount of water. Cation and anion exchangers were kept in 1M HCl and in 0.5M NaOH respectively for three hours, and then they are washed several times with water. The 2/3 part of column was filled with the exchangers. In addition, cation exchange column was treated with 150 mL 1 N HCl, and then excess of alkali from anion exchanger column and excess of acids from cation exchanger column were removed by distilled water.

Column length: 50 cm, diameter: 1cm, flow rate: 1.5mL/min, efficiencies of anion and cation exchange column are 98.9% and 98.5% respectively. The eluate $(\text{HPO}_3)_n$ was titrated with standard 0.05M NaOH volumetrically by using methyl orange indicator.

The calculated equivalent weights of PSP and PAH are found 100.46 ± 1.01 g eqw. and 94.50 ± 1.50 g eqw., respectively.

3.2.1.5 Determination of the Dissociation Constants of PSP and PAH

Since the polyelectrolytes exhibit electrolyte properties, dissociation constant of acidic and basic forms of PSP and PAH were determined by conductometric measurements on the basis of Ostwald law.

Electrolyte solutions conduct an electric current by the migration of charged species under the influence of an electric field. Like a metallic conductor, they obey Ohm's law [126].

When a constant potential difference, E , is applied, the electric current, I , flowing between the electrodes immersed in the electrolyte varies inversely with the resistivity of the electrolyte solution, R .

$$R=E/I \tag{3.8}$$

where E is expressed in volts and the I in amperes.

The reciprocal of the electrical resistance, $1/R$, is called the electrical conductance L , and is expressed as S in SI units (the reciprocal ohm, Ω^{-1} , called a siemens, $1 S=1 \Omega^{-1}$). The measured conductance, L , of a solution is inversely proportional to the distance between the electrodes, l , and cross-sectional area, A . Since dimensions of the cell affects conductivity and it is difficult to build a cell with well defined geometrical parameters, any cell should be calibrated with a solution of exactly known specific conductance in order to compensate for variations in electrode dimensions. Therefore, the cell constant, $K=l/A$, in cm^{-1} , is determined by a solution of known specific conductance.

$$L = \frac{1}{R} = \frac{A\chi}{l} = \frac{1\chi}{K} \tag{3.9}$$

Where: χ is specific conductance defined as conductance of a 1 cm^3 of a solution measured between two electrodes 1 cm^2 in area and 1 cm apart and expressed as Sm^{-1} .

Since the charge on ions in solution facilitates the conductance of electrical current, the conductivity of a solution is proportional to concentration of all the ions present in the solution. It depends upon the number of ions per unit volume of the solution and upon the velocities with which these ions move under the influence of the

applied potential. Therefore, a more fundamental unit of electrolytic conductance, which is termed as equivalent conductance, Λ , is used.

Equivalent conductance, Λ , is the value of specific conductance, χ , contributed by one equivalent of ions contained in 1000 cm³ (1 L) of solvent [126].

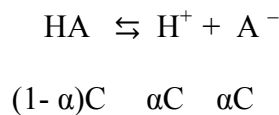
$$\Lambda = \frac{1000 \chi}{C} \quad (3.10)$$

where, C in equiv/L, and the Λ is in cm²equiv⁻¹ohm⁻¹.

Equivalent conductance varies with concentration of the charged species since the degree of ionization, α , strongly depend on concentration. According to the Arrhenius theory, the degree of ionisation increases with increasing dilution for sufficiently weak electrolytes and it is known that the lower the ionic concentration is the weaker the ionic attraction will be. Therefore, ionic attraction is considered independent of concentration and the equivalent conductance approach a constant finite value, Λ_0 , at infinite dilution [127].

$$\alpha \approx \frac{\Lambda}{\Lambda_0} \quad (3.11)$$

All these approaches allows the determination of the dissociation constant of weak electrolyte by measuring its conductivity, knowing that for a weak electrolyte HA is ;



$$K_a = \frac{[\text{H}^+][\text{A}^-]}{[\text{HA}]} = C \frac{\alpha^2}{1-\alpha} \quad (3.12)$$

Substituting and rearrangement of the equations 3.11 and 3.12 leads to Ostwald's law.

$$K_a = \left(\frac{\Lambda^2}{\Lambda_0^2}\right) - K_a \Lambda_0 = \Lambda C \quad (3.13)$$

where; Λ and Λ_0 corresponds to equivalent conductivity at a definite concentration and at infinite dilution respectively.

In order to determine the pK_a values of PSP and PAH, they were converted into their acidic ($(HPO_3)_n$) and basic forms (PAHOH) using Amberlite IR-120 (strong acid cation exchanger) and Ion Exchanger III (strong base anion exchanger) respectively. The ion exchange columns were prepared as given in section 3.2.1.4 above. Then, the series of $(HPO_3)_n$ and basic forms (PAHOH) were prepared in different concentrations. K_a value for $(HPO_3)_n$ and K_b value for (PAHOH) were determined by conductometric measurement using WTW Inolab Level 2 conductometer. pK_a value of PSP and PAH of which were calculated by Equation 3.13.

K_a value for acidic form of PSP ($(HPO_3)_n$) and K_b value for basic form of PAH (PAHOH) were found as 6.63×10^{-3} and 1.64×10^{-3} respectively, corresponding to respective average pK_a values of 2.46 and 9.41.

3.2.2 Preparation of polyion solutions

The PSP and PAH were prepared in 10^{-x} monomol/L (with respect to the monomer repeating unit and with $x=5, 4, 3, 2$) in a solution having an ionic strength of $I=0.01, 0.15, 0.5, 1M$ in NaCl respectively. The pH of each solution was adjusted to 6.70 with addition of appropriate amount of 0.1M NaOH. Hence the solutions contained excessive sodium and chloride ions originating either from the added NaCl or from the polyelectrolyte's counterions. The pH of 6.70 corresponding to the average pK_a values of PSP and PAH was selected on purpose for all experiments in order to keep the degree of dissociation for both polyelectrolytes as identical.

3.2.3 Investigation of PSP/PAH complex formation in bulk

The complex stoichiometry provide further information on the polyelectrolyte complex formation process, degree of conversion and structure of the resulted complex. Besides, the efficiency of the usage of PECs in various processes or in industrial applications is strongly affected by its stoichiometry. In this work, PSP/PAH complex stoichiometry was determined, mainly, by conductometry and viscometry. Besides, analysis of supernatant liquids by FTIR were performed in order to confirm the conductometric and viscometric data.

3.2.3.1 Determination of PSP/PAH stoichiometry by conductometric titration

The conductance measurements provide further information on the polyelectrolyte complex formation, complex stoichiometry as well as the surface charge and stability of the complex aggregates. Due to the fact that the process of complexation is

controlled by the release of the counterions, a simple conductometric titration technique is used to determine the PSP/PAH stoichiometry.

The releasing of Na^+ and Cl^- as counter ions during the PSP/PAH complex formation is taken into consideration in the conductometric titrations. PSP in different concentrations were titrated with PAH as a titrant in both salt free aqueous solutions and at constant ionic strength of 0.15M and 0.5 NaCl depending on pH of 5-8. Reverse titrations were also carried out. The reactions were carried out by slow dropwise addition of titrant to the solution with rapid stirring. The complex was maintained at a constant temperature of $(25\pm 0.02)^\circ\text{C}$ in a thermostated water bath during measurement. The titration plots are shown in Figures 4.1 – 4.5. From the amount of added titrant until the endpoint, the molar ratio of cationic to anionic functional groups was calculated. The stoichiometry of PSP:PAH is given in Table 4.2, 4.3 and 4.4.

Several runs were carried out to check the reproducibility of all titrations.

The direct conductances of polycation and polyanion mixtures prepared in different mol ratios were measured (Figure 4.8).

3.2.3.2 Determination of PSP/PAH stoichiometry by viscometry

Viscometry measurements were performed in order to confirm the PSP/PAH stoichiometry obtained from conductometric studies.

The reliability of these viscosity measurements are sometimes questioned because of the difficulties in measuring the viscosity in the dilute concentration range. Therefore, viscosity measurements were carried out at constant ionic strength, and thus the increase in the viscosity at low polyelectrolyte concentrations is tried to be suppressed.

PSP and PAH were mixed at different mol ratios for salt free and $I=0.01\text{M}$, 0.15M , 0.5M NaCl at original pH and pH of 3 – 8, 10. Viscosities of PSP-PAH complexes were measured at $(25\pm 0.02)^\circ\text{C}$ by comparing the efflux time, t , required for a 2 mL of polyelectrolyte complex solution to flow through a capillary tube with the corresponding efflux time, t_0 , for the water. From t_0 , and the polyelectrolyte concentration, C , specific and reduced viscosities are calculated using the equations 3.4, 3.6 and PSP:PAH mol ratio versus reduced viscosities were plotted. The results are given in Figures 4.6 and 4.7.

3.2.3.3 Kinetic Investigation of PSP/PAH complex formation by Isothermal Titration Calorimetry, ITC

Experiments related with kinetic investigation of PSP/PAH complex formation by ITC was realized in collaboration with Prof. Vincent Ball. Isothermal Titration Microcalorimetry, ITC, experiments of PSP/PAH system was carried out in laboratory of Faculty of Pharmacy in University of Strasbourg.

Thermodynamic data, specifically enthalpy (ΔH) and entropy (ΔS), reveal the forces that drive complex formation and mechanism of action and provide information on conformational changes, hydrogen bonding, hydrophobic interactions, and charge-charge interactions. This information is used to describe the function and mechanism of the complex formation at a molecular level [128].

Heat is evolved or absorbed in liquid samples as a result of mixing of reactants. Isothermal Titration Calorimetry method is a physical technique that directly measures the heat released or absorbed during the reaction [128]. Measurement of this heat allows accurate determination of binding constants (K_B), reaction stoichiometry (n), enthalpy (ΔH) and entropy (ΔS), so that it provides a complete thermodynamic profile of the molecular interaction in a single experiment [129, 130].

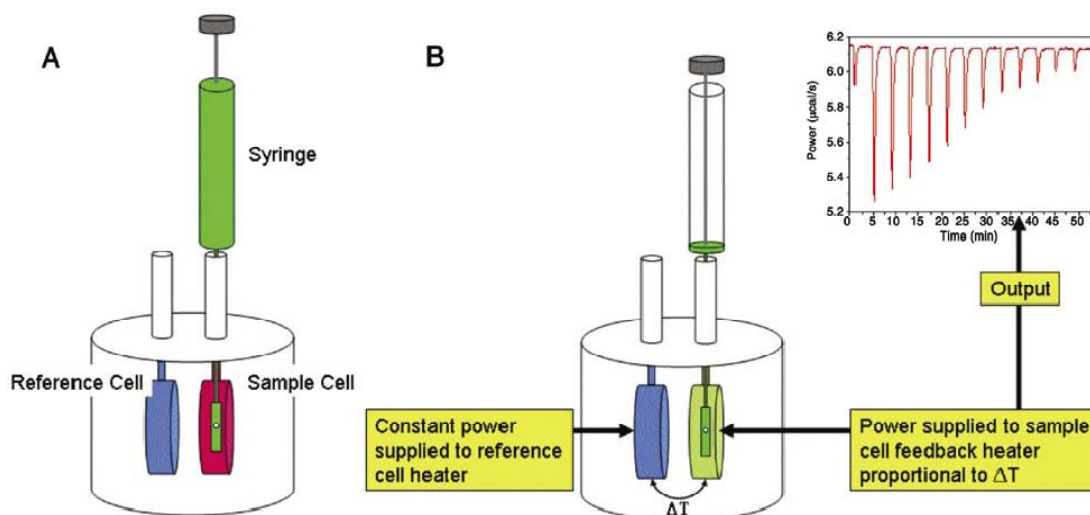


Figure 3.2: Schematic illustration for the set up of isothermal titration calorimeter [128].

An isothermal titration calorimeter is composed of two identical cells made of a highly efficient thermal conducting material such as Hastelloy alloy surrounded by an adiabatic jacket. Temperature differences between the reference cell and the

sample cell are measured using sensitive thermopile/thermocouple circuits and a spinning syringe is utilized for injecting and subsequent mixing of reactants (Figure 3.2).

Measurements consist of the time-dependent input of power is referred to as the differential power between the reference cell and the sample cell, which is denoted by DP. DP signal is the power required to maintain equal temperatures between the sample and reference cells. An injection which results in the evolution of heat (exothermic) within the sample cell causes a negative change in the DP power since the heat evolved chemically provides heat that the DP feedback is no longer required to provide. In an endothermic reaction, the opposite occurs; the feedback circuit increases the power in order to maintain a constant temperature (isothermic/isothermal operation). Since the DP has units of power, the time integral of the peak yields a measurement of thermal energy. This heat is released or absorbed in direct proportion to the amount of binding that occurs. When the macromolecule in the cell becomes saturated with added ligand, the heat signal diminishes until only the background heat of dilution is observed. Observations are plotted as the power in $\mu\text{cal}/\text{sec}$ needed to maintain the reference and the sample cell at an identical temperature. This power is given as a function of time in seconds. These heat flow spikes/pulses are integrated with respect to time, giving the total heat effect per injection. The pattern of these heat effects as a function of the molar ratio of the complex can then be analysed to give the thermodynamic parameters of the interaction under study.

It should be noted that degassing samples is necessary in order to minimize data interference due to the presence of air bubbles within the cells. The presence of such bubbles will lead to abnormal data plots in the recorded results. The entire experiment takes place under computer control.

In a typical ITC experiment, a solution of a one biomolecule (“ligand” such as a drug, protein, DNA molecule, etc...) is titrated into a solution of its binding partner [95-101]. The heat released upon their interaction is monitored over time. Each peak represents a heat change associated with the injection of a small volume of sample into the ITC reaction cell. As successive amounts of the ligand are titrated into the ITC cell, the quantity of heat absorbed or released is in direct proportion to the amount of binding. As the system reaches saturation, the heat signal diminishes until

only heats of dilution are observed. A binding curve is then obtained from a plot of the heats from each injection against the ratio of ligand and binding partner in the cell.

In this study, PSP/PAH complex formation is investigated by ITC in order to have information about the function and mechanism of the PSP/PAH complex formation and to describe the thermodynamic profile of the PSP/PAH interaction. It is known that the enthalpy, ΔH , is a state function of the system and it is equal to the heat exchanged by the system with its surroundings is held at constant pressure. This heat exchanged can be directly measured by means of ITC experiments. Measurement of this heat change associated with the injection of a small volume of PSP into the PAH allows to accurate determination of binding constants (K_B), reaction stoichiometry (n) of PSP/PAH system as well.

The reaction heat between PSP and PAH was measured by means of isothermal titration microcalorimetry (VP-ITC microcalorimeter from Microcal) at 25°C. This microcalorimeter is fitted with two thermostated cells: one reference cell and a sample cuvette containing the buffer or the polyelectrolyte solution to be titrated. Both cells have a volume of 1.44 mL. The polyelectrolyte of opposite sign is injected in successive injections steps by means of an automated microsyringue. Each solution was degassed under vacuum before filling the cells to minimize data interference due to the presence of air bubbles within the cells. 5×10^{-2} M PSP and 2.5×10^{-4} M PAH was prepared at $I=0.15$ M NaCl pH=6.70. The 8 μ L of PSP solution was injected in the PAH solution at each step. The injection needle ended with a propeller which allowed to stir the solution was rotated at 310 rpm 21 consecutive injections were separated by a resting period of 200 s to allow the microcalorimeter trace to come back to a baseline corresponding to the absence of any heat flow between the cell in which PSP/PAH interactions took place and the reference cell which was filled with 0.15 M NaCl at a pH of 6.70 (Figure 4.13).

The polyelectrolyte concentrations, injection volume and injection number were chosen in order provide a final concentration of the PSP in the measurement cell 10 times greater than in the initial concentration of PAH. So that, the stepwised injection of PSP would lead to reach a complex formation process which allows us to make the assumption that all the PSP chains must have reacted with PAH.

Identical microcalorimetry experiments was performed by injecting 8 μL of PSP into 1.44 mL of 0.15M NaCl at a pH of 6.70 for the determination of the reaction heat of dilution (Figure 4.13).

Moreover, PSP and PAH addition to PSP/PAH complex after it is assumed to reach equilibrium were carried out by isothermal titration microcalorimetry in order to investigate the effect of addition excess polyelectrolyte in terms of complexation process once the PSP/PAH complex was formed. These results showed that, the addition of excess of any polyelectrolyte once the PSP/PAH complex formed and reached equilibrium was negligible in terms of thermodynamic properties (Figures 4.14 and 4.15).

For this purpose, the experimental procedure was designed as to have a 1:1 PSP/PAH complex formation in the measurement cell of the microcalorimeter by a single injection. Therefore, $2 \times 10^{-2}\text{M}$ PSP and $1 \times 10^{-4}\text{M}$ PAH was prepared at $I=0.15\text{M}$ NaCl $\text{pH}=6.70$. The reference cell was filled with 0.15M NaCl at a pH of 6.70. Only one main of 7.5 μL PSP solution was injected in the PAH solution, and stirring was carried out at 310 rpm. After this single injection, the PSP/PAH complexation was monitored by a resting period of 5400 s in order to see if it would come back to a baseline corresponding to the absence of any heat flow, and thus to reach the equilibrated complex. After equilibration of about 5400 s, 6 consecutive injections of PSP separated by a resting period of 300 s were carried out in the same cell without changing the solutions (Figure 4.15). Identical microcalorimetry experiments was performed by injecting the PSP into 1.44 mL of 0.15M NaCl at a pH of 6.70 for the determination of the reaction heat of dilution (Figure 4.15).

At the end of each dilution or binding experiment, the injection syringe and cuvette were cleaned with a 5% (v/v) containing detergent solution (Decon) during at least half an hour and intensively rinsed with Milli Q water.

However, some handicaps in these experiments arised due to the instrumental restriction of ITC measurement cell because of the colloidal sticky particles of PSP/PAH complex in the solution and long period of time in the complexation kinetics. This fact is tried to be discussed in detail under the results and discussion section.

3.2.3.4 Kinetic investigation of PSP/PAH complex formation by conductometry and viscometry

PSP/PAH complex formation was investigated depending on the variation in conductivities and viscosities of the PSP/PAH complexes as a function of time in order to provide further information on complex formation in terms of complexation kinetics.

PSP-PAH complex was prepared in 1:1 mol ratio for $1 \times 10^{-2} \text{M}$ and $1 \times 10^{-4} \text{M}$ polyion concentration at $I=0.15 \text{M}$ NaCl, pH: 6.70. Then, the specific conductivity of the PSP-PAH complexes were measured as a function of time. The complex was maintained at a constant temperature of $(25 \pm 0.02)^\circ \text{C}$ in a thermostated water bath during all measurements (Figure 4.9).

PSP-PAH complex was prepared in 1:1 mol ratio for $1 \times 10^{-2} \text{M}$ and $1 \times 10^{-4} \text{M}$ polyion concentration at $I=0.15 \text{M}$ NaCl, pH:6.70, and kept at room temperature in a closed container. The viscosity measurements from this solution were carried out for different time intervals by taking 2 mL of aliquot from the prepared PSP-PAH complex using Ostwald capillary type viscometer at a constant temperature of $(25 \pm 0.02)^\circ \text{C}$. Specific and reduced viscosities are calculated using the equations 3.4 and 3.5. Time versus reduced viscosities were plotted. the results are given in Figure 4.9.

3.2.3.5 Analysis of Supernatant Liquids by Vicsometry

Analysis of supernatant liquids of PSP/PAH complex were carried out by viscometry and FTIR spectroscopy in order to confirm the stoichoimetric data. Besides, the FTIR spectra of the solid PSP/PAH complex samples which are obtained from the supernatant liquids by drying were carried out in order to reveal if there is a complex formation and to identify the molecular structure of PSP/PAH complex.

A- PSP and PAH prepared in $1 \times 10^{-4} \text{M}$ concentration at $I=0.15 \text{M}$ NaCl, pH: 6.70. The PSP-PAH complex was prepared in 1:1 mol ratio and allowed to reach equilibrium more than 3000 minute. Then, 5ml of $1 \times 10^{-2} \text{M}$ PSP (at $I=0.15 \text{M}$ NaCl, pH: 6.70) added to that supernetant and viscosity was measured at 25°C . A control solution of $3.3 \times 10^{-3} \text{M}$ PSP was prepared at the same conditions. Then the viscosity of the PSP control solution was measured at 25°C . The viscosity of supernatant+PSP and PSP control solution were compared. The same experiment was carried out by adding a control solution of $3.3 \times 10^{-3} \text{M}$ PAH at the same conditions.

B- PSP and PAH prepared in 1×10^{-4} M concentration at $I=0.15$ M NaCl, pH:6.70. PSP-PAH complex was prepared in 1:1.5 PSP: PAH mol ratio and allowed to reach equilibrium more than 3000 minute. Then the viscosity of supernatant was measured at 25°C . A control solution of 2×10^{-5} M PAH was prepared at the same conditions by taking into consideration of the excess amount PAH present in the supernatant. Then the viscosity of the PAH control solution was measured at 25°C and the viscosity of supernatant and PAH control solution were compared. The same experiment was carried out for PSP-PAH complex prepared in 1.5:1 PSP: PAH mol ratio at the same conditions.

The same experiments given in the A and B was carried out for 1×10^{-2} M PSP and PAH concentration at $I=0.15$ M NaCl, pH: 6.70. The results are given in Table 4.5.

3.2.3.6 Analysis of Supernatant Liquids by FTIR Spectroscopy

Infrared (IR) spectroscopy is a widely used analytical method for characterizing the chemical composition of compounds. It is the subset of spectroscopy that deals with the infrared region of the electromagnetic spectrum. The main purpose of this technique is to identify the compounds and information about the chemical bonding or molecular structure of materials [127].

The basis of the IR spectroscopy depends on absorption of specific frequencies which are characteristic to that molecule. The frequency of the absorbed radiation matches the frequency of the bond/group that vibrates. The resonant frequencies are related to the strength of the bond, and the mass of the atoms at either end of it. Thus, the frequency of the vibrations can be associated with a particular bond type.

The Fourier Transform –Infrared Spectroscopy, FTIR, measures the absorption or transmittance of versus wavelength or wavenumber (reciprocal of the wavelength) as the x-axis and absorption intensity or percent transmittance as the y-axis. The IR absorption bands identify the molecular components and structures.

Transmittance, T , is the ratio of radiant power transmitted by sample (I) to the radiant power incident on the sample (I_0). Absorbance (A) is the logarithm of the base 10 of the reciprocal of the transmittance (T).

$$A = \log_{10} (1/T) = - \log_{10} T = - \log_{10} (I/I_0) \quad (3.14)$$

The transmittance spectra provide better contrast between intensities of strong and weak bands because transmittance ranges from 0 to 100% whereas absorbance ranges from from infinity to zero. Therefore, in this work, transmittance spectra of the complex were given.

In principle, a beam of infrared light is passed through the sample, and the IR spectrum of the compound is recorded. The examination of the transmitted light can be carried out in either by a monochromatic beam, which changes in wavelength over time, or by a Fourier transform instrument in order to find out how much energy was absorbed at each wavelength. Then, the data is evaluated so that a transmittance or absorbance spectrum is produced, showing at which IR wavelengths the sample absorbs. The molecular structure of the sample is revealed by the analysis of these absorption characteristics [127].

The FTIR spectrometer uses the an interferometer to modulate the wavelngth from a broad infrared source. A dedector measures the intensity of transmitted or reflected light as a function of its wavelength. The signal is obtained from the dedector is an interferogram, which must be analyzed with computer using Fourier transforms to obtain a single beam infrared spectrum. The FTIR spectra are usually presented as plots of intensity (Transmittance or Absorbance) versus wavenumber in cm^{-1} .

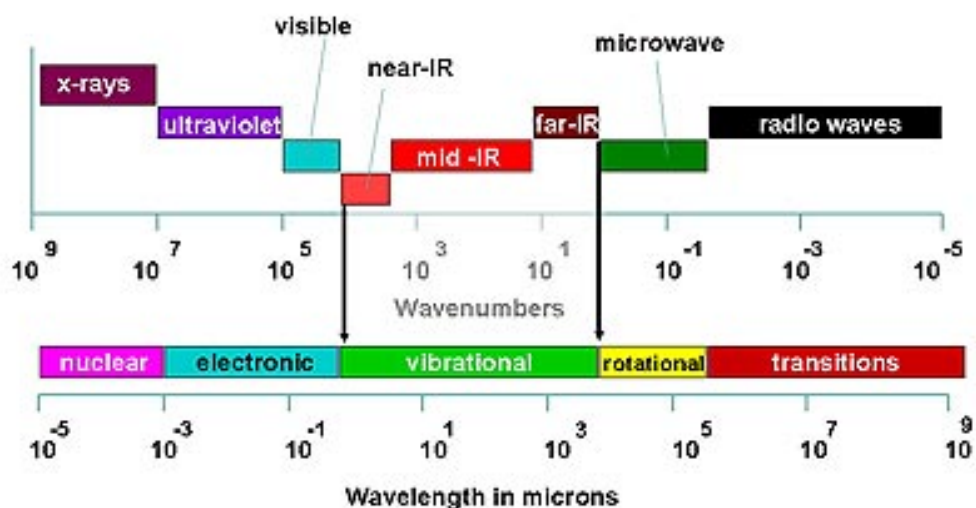


Figure 3.3: Infrared region of the electromagnetic spectrum.

Typical application areas of FTIR are;

- Identification of foreign materials : Fibers, residues etc...
- Identification of bulk material compounds

- Identification of constituents in multilayered materials
- Quantification of silicone, esters, etc.. as contamination on various materials.

The aim of FTIR experiments in this study is to identify the molecular structure of PSP/PAH complex as well as to reveal the existence of complex formation. It is, also aimed to find out whether the commercial $(\text{NaPO}_3)_n$ is pure or contains even a little amount of cyclic phosphate. It was thought that the structures and properties of PSP/PAH complex could be affected by the impurities.

PSP/PAH complexes prepared in 1:1 mol ratio at 1×10^{-2} M, 1×10^{-3} M, and 1×10^{-4} M, I:0.15M NaCl and pH:6.70, then allowed to reach equilibrium more than 24 hours. Then 10mL of an aliquot from the supernatant liquid was taken and dried at 55°C in the oven. The solid residue is examined by FTIR spectroscopy using Thermo Nicolet 380 FT-IR Spectrometer and transmission spectra were recorded (Figures 4.11 and 4.12).

Besides, it has been known that type and structure of the polyelectrolytes play a role on the properties of PECs. Therefore, different types of PSP were synthesised and the FTIR spectrums were compared with that of commercial PSP, $(\text{NaPO}_3)_n$, used in this study.

Preparation and Characterization of Amorphous PSP (Graham Salt), linear $(\text{NaPO}_3)_n$, (n=10-50) [119, 120]:

3 different sample were prepared by heating 4.9148 g $\text{NaH}_2\text{PO}_4 \cdot 2\text{H}_2\text{O}$ at 700°C for 2, 4 and 24 hours (Sample 1, 2, and 3) respectively, and FTIR spectra were taken by using Thermo Nicolet 380 FT-IR Spectrometer and transmission spectra were recorded (Fig 4.10).

Preparation and Characterization of Crystalline PSP (Kurrol Salt), $(\text{PO}_3)_n^{-n}$, cyclic (n=50-200) [119, 120]:

4.9148 g $\text{NaH}_2\text{PO}_4 \cdot 2\text{H}_2\text{O}$ was weighed, heated at 400°C for 24 hours (Sample 4) and FTIR spectrum was taken by using Thermo Nicolet 380 FT-IR Spectrometer and transmission spectra were recorded (Figure 4.10).

3.2.3.7 Dynamic Light Scattering

The most significant characteristics of many colloidal dispersions are the size and shape of the particles and most properties of the colloidal dispersions; such as, stability and chemical reactivity, are influenced to some extent by these factors.

The important aspect of product quality is the ease with which the material can be handled. A product's stability and handling qualities are determined by its bulk properties, and many of these can also be understood through particle sizing. They include dispersion/flocculation, viscosity and rheology. Decreasing particle size enlarges the overall surface area for a pigment volume concentration, increasing the particle-particle interactions and the driving force for agglomeration. Thus, while achieving a fine particle size may be beneficial with regard to the optical properties of the film. The rheological properties of the pigment suspension are important in defining how it behaves during storage and application.

One of the most common techniques for determining the particle size and particle size distribution of colloidal systems is dynamic light scattering, DLS.

Scattering methods can provide information on the mass and size of the scattering particles, their polydispersity, particle-solvent interactions and structure properties of the resulting aggregates. Therefore, light-scattering experiments are of special importance to characterize nanoparticles as well as macromolecules in solution.

Dynamic light scattering is based on the Brownian motion theory of the scattering particles in solution, and gives information about only the particle surface but not the polyelectrolytes in solution. Brownian motion is the movement of particles due to the random collision with the solvent molecules that surround them. The larger the particle, the slower the Brownian motion will be. Smaller particles can collide with the solvent molecules and move more rapidly. The velocity of the Brownian motion is defined by the translational diffusion coefficient, D . The size of a particle is calculated from the translational diffusion by using various algorithms depending on the Stokes-Einstein relation [126].

$$d(H) = \frac{kT}{3\pi\eta D} \quad (3.15)$$

where; $d(H)$, D , k , T and η are the hydrodynamic diameter, diffusion coefficient, Boltzmann's constant, absolute temperature and viscosity, respectively. The diameter measured in DLS refers to how a particle diffuses within a fluid, therefore it is considered as a hydrodynamic diameter. The apparent size of the particle is strongly affected by any change on the surface of a particle. The ionic concentration

of the medium, which correspondingly change the diffusion, speed also affect size of the particle as well as the PEC conformation.

PSP/PAH complex formation was investigated depending on the variation in particle size as a function of time in order to characterize the PSP/PAH particles in bulk solution leading to a better comparison of complex aggregates formed in bulk and at interfaces.

In this study, measurements of particle size were carried out using Zetasizer Nano ZS (Malvern Instruments, Ltd., UK) at a scattering angle of 173° having a wavelength of 632.8 nm He/Ne laser. All measurements were performed at a constant temperature of 25°C using standard disposable sizing cuvettes (Malvern Ins. Ltd., UK, and DTS0012). The PSP and PAH prepared in $1 \times 10^{-4}\text{M}$ at $I=0.15$ and 1M NaCl. pH of each solution was adjusted to 6.70. The PSP-PAH complex was prepared in unit mol ratio by mixing of PSP and PAH. The measurements were carried out for both type of complex prepared by adding of PSP to PAH and vice versa (Fig. 4.11). Prior to preparation of complex, the polyanion and polycation were filtered through $0.2\mu\text{m}$ pore size filters (Carl Roth GmbH, CHROMAFIL, RC 20/25). The z-average diameter of PSP-PAH particles was calculated using Stokes-Einstein equation 3.27. The results are given in Figure 4.17.

3.2.3.8 Measurement of Zeta Potential

In general, the zeta potential is a measure of the magnitude of repulsion or attraction between particles since it reflects the effective charge on the particles. Its measurements provides a detailed information about the dispersion mechanism, therefore, it is a key to control the electrostatic dispersion, colloidal stability and flocculation processes.

Development of the net charge at the particle surface affects the distribution of ions in the surroundings leading to an increase in the concentration of counter ions close to the surface. Thus electrical double layer exist around each particle [126].

Each particle dispersed in a solution is surrounded by oppositely charged ions called Stern layer or fixed layer (Figure 3.4.). Outside the fixed layer, there are varying compositions of ions of opposite polarities, forming a cloud-like area. This area is called the diffuse “double layer”, and the whole area is electrically neutral.

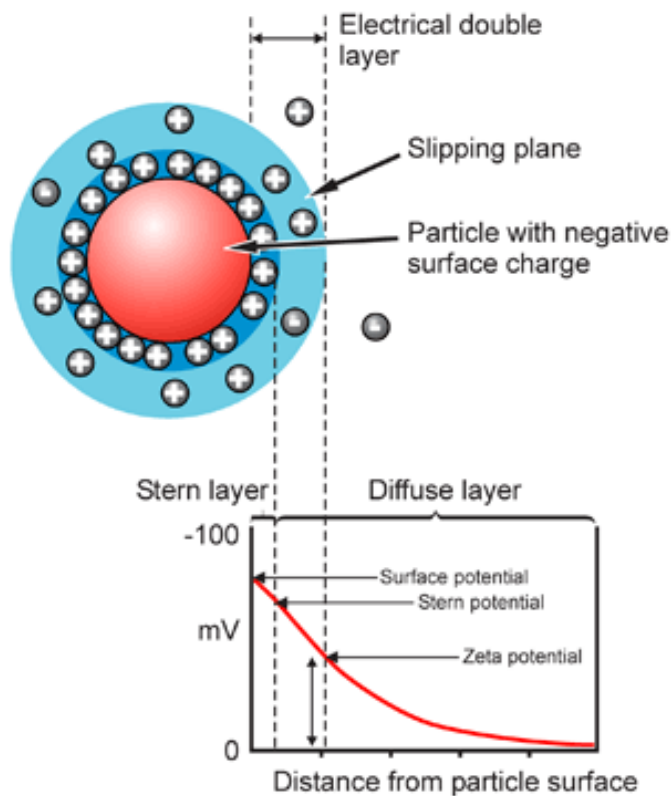


Figure 3.4: Schematic of Zeta potential Measurement [154].

If the particle moves under Brownian motion, diffuse layer moves as a part of the particle together with the some part of surrounded liquid, but sometimes some part of the surrounded liquid is not carried by particle. When a voltage is applied to the solution in which particles are dispersed, particles are attracted to the electrode of the opposite polarity, accompanied by the fixed layer and part of the diffuse double layer. Within this diffuse layer, there is a notional boundary which known as “slipping plane” where the particle acts as a single entity.

Zeta potential is considered to be the electric potential of this inner area including "slipping plane" which is dragged in the bulk solution. In other words, the potential difference between the solid surface and sliding surface of the diffuse layer is defined as the zeta potential. Therefore, the zeta potential is a function of surface charge of the particle.

The purpose of these experiments is to investigate the PSP/PAH complex formation depending on the variation ζ - potential of PSP-PAH particles as a function of time in order to characterize the surface charge of the PSP/PAH particles in bulk solution. It is also aimed to provide further comparison of complex aggregates formed in bulk and at interfaces.

In this work, ζ - potential of PSP-PAH particles in bulk were performed using Zetasizer Nano ZS (Malvern Instruments, Ltd., UK). All measurements were performed at a constant temperature of 25°C using disposable folded capillary cuvettes (Malvern Ins., DTS1060). The PSP and PAH prepared in 1×10^{-4} M at $I=0.15$ M NaCl. pH of each solution was adjusted to 6.70. The PSP-PAH complex was prepared in 1:1 mol ratio. The measurements were carried out for both type of complex prepared by adding of PSP to PAH and vice versa. Prior to preparation of complex, the polyanion and polycation were filtered through 0.2 μ m pore size filters (Carl Roth GmbH, CHROMAFIL, RC 20/25). Average potential of PSP-PAH particles were calculated according to Smoluchowski approximation using Monomodal model (Figure 4.16).

3.2.4 PSP/PAH complex formation and characterization at interfaces

3.2.4.1 Cleaning Procedure

The silicon wafers were purchased from WaferNet, Inc. (San Jose, CA). They were cut in the form of rectangles ($4 \times 1 \text{ cm}^2$), cleaned with acetone and allowed to stand in MeOH:HCl (1:1) solution for 20-30min. This treatment was followed by extensive rinsing with Milli-Q water and blowing-dry with nitrogen. Finally, the wafers were immersed into concentrated H_2SO_4 for at least 4 hours, rinsed extensively with Milli-Q water and blown-dry again with nitrogen.

3.2.4.2 Deposition of PEI-(PSP-PAH)_n multilayers

Alternated deposition of PSP and PAH on substrates was performed by alternatively spraying the polyelectrolyte solutions (at 10^{-x} M in the presence of 0.01, 0.15, 0.5, and 1M NaCl and at pH 6.7) using “AIR –BOY” (Roth Sochiel E.U.R.L) spray bottles. The solutions were sprayed onto vertically hold silicon substrates from a distance about 15 cm (Figure 3.5). All (PSP/PAH)_n multilayers were deposited on a single PEI anchoring layer. PEI was dissolved at 2.5 mg/mL in MilliQ water and sprayed on the cleaned silicon wafer for 10s. This step was followed by spray-rinsing 10 sec. with Milli-Q water, and blow-drying with nitrogen. The same spraying time of 10 s was always used for each subsequent spraying step, either PSP, PAH or Milli-Q water. The spraying sequence was PEI-(PSP/PAH)_n.

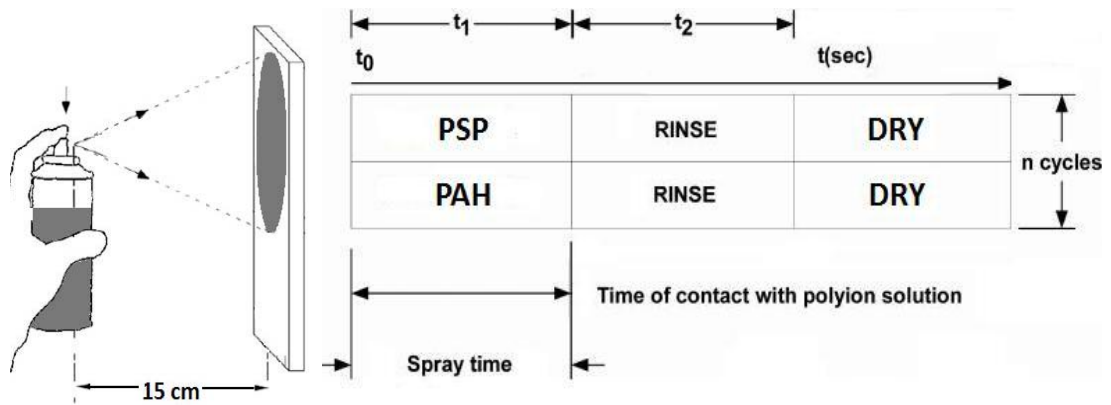


Figure 3.5: Standard procedure for LbL-Spray PSP/PAH deposition.

3.2.4.3 Ellipsometry Measurements

Ellipsometry is a completely nondestructive optical technique for determining the properties of surfaces and thin films. An ellipsometer measures the changes in the polarization state of light when it is reflected from a sample. In fact, the change in the reflection depends on the optical properties of the samples, such as; thickness, refractive index. Therefore, ellipsometry is a widely used technique in order to determine film thickness and optical constants [131]. It is also applied to characterize composition, crystallinity, roughness, doping concentration, and other material properties associated with a change in optical response

In principle, the beam emitted by a light source and linearly polarized by a polarizer, and pass through an optional compensator, then falls onto the sample. After reflection the incident passes a compensator (optional) and an analyzer, and falls into the detector. In ellipsometry, the angle of incidence equals the angle of reflection (Figure 3.6).

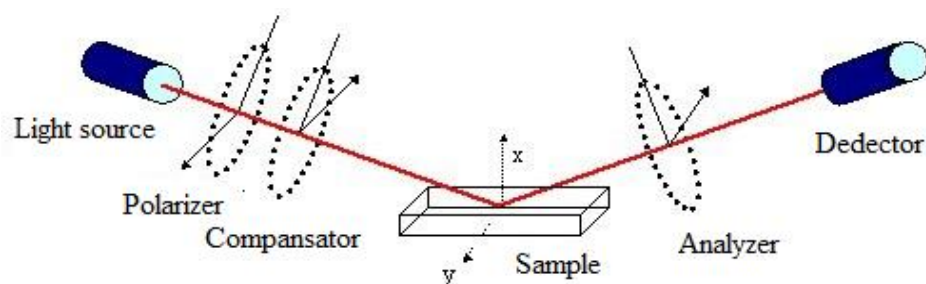


Figure 3.6: Schematic representation of an ellipsometry set up [157].

Ellipsometry measures the complex reflectance ratio, ρ , of a system, of which parameters are Ψ and Δ . where Ψ is the amplitude and the Δ is the phase difference. The polarization state of the incident beam is decomposed into an s and a p

component (the s component is oscillating perpendicular to the plane of incidence and parallel to the sample surface, and the p component is oscillating parallel to the plane of incidence). After reflection, the amplitudes of the s and p components are normalized to their initial value and denoted by r_s and r_p , respectively. Thus, the measured complex reflectance ratio, ρ , is the ratio of r_p to r_s :

$$\rho = \frac{r_p}{r_s} = \tan(\psi)e^{i\Delta} \quad (3.16)$$

Ellipsometry is, in fact, an indirect method, since the measured Ψ and Δ cannot be converted directly into the optical constants of the sample. A model analysis must be established in order to direct inversion of Ψ and Δ is only possible in very simple cases of isotropic, homogeneous and infinitely thick films. Therefore, an iterative procedure, like least-squares minimization, is performed and unknown optical constants and/or thickness parameters are varied, and then, Ψ and Δ values are calculated. The calculated Ψ and Δ values matching with the experimental data best provide the optical constants and thickness parameters of the sample.

In this study, the measurement of total thickness of the PEI-(PSP/PAH)_n multilayers were performed by using a PLASMOD SD2300 ellipsometer with He-Ne laser (632.8 nm) illumination at an incidence angle of 45°. The refractive index for the polyelectrolyte multilayers was assumed to be 1.465. Although this procedure could lead to slightly incorrect values with respect to the absolute film thicknesses, it allows for the quick monitoring of the deposition process. For each studied polyelectrolyte deposit, 10 different measurements acquired at regularly spaced locations along the main axis of the wafer were performed to obtain an average thickness as well as to determine the homogeneity of the deposit. The average thickness of the PEI-(PSP/PAH)_n deposits was measured at ambient temperature and moisture by means of ellipsometry as a function of the spraying step. The measurement was carried out on the sample after blow-drying with nitrogen. The results are given in Figures 4.18 - 4.24, 4.30, and 4.33.

3.2.4.4 Characterization of PEI-(PSP-PAH)_n multilayer by Atomic force microscopy

The atomic force microscope (AFM) is a very high-resolution type of scanning probe microscopy. AFM consists of a cantilever with a sharp tip (probe) at its end that is used to scan the specimen surface (Fig. 3.7). AFM measures the forces acting

between a the tip and a the sample. The tip is attached to the free end of a cantilever and is brought very close to a surface. Attractive or repulsive forces resulting from interactions between the tip and the surface cause a positive or negative bending of the cantilever. The bending is detected by means of a laser beam reflected from the back side of the cantilever and collected in a photodiode [131, 132].

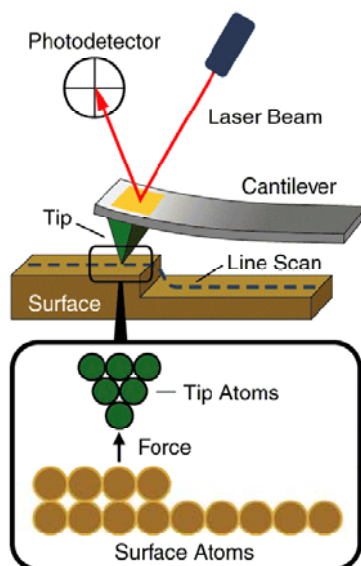


Figure 3.7: Principle of AFM [132].

The primary modes of operation for an AFM are classified in two categories; static mode(also called contact mode) and dynamic mode.

In dynamic mode operation, the force between the tip and the surface is kept constant during scanning by maintaining a constant deflection. Therefore, the use of dynamic mode allows scanning the shape of the sample without being influenced by the tip-sample forces, and it is also called as non contact mode [132].

In this work, AFM images were obtained in tapping mode. In this mode, the cantilever is oscillating close to its resonance frequency and oscillation amplitude remains constant so that a constant tip-sample interaction is maintained during scanning. The amplitude is used for the feedback and the vertical adjustments of the piezoscanner are recorded as a height image. Simultaneously, the phase changes are presented in the phase image.

In this study, AFM images were obtained on the same deposits as those used for ellipsometry measurements in tapping mode and at room temperature, in air, using a Nanoscope IIIa Multimode AFM (Digital Instrument Inc., Santa Barbara, CA). Tips with a terminal radius of curvature less than 10 nm and silicon cantilevers with a

nominal spring constants of 40 N/m (resonance frequency of 300 kHz) were used. Several scans were performed over a given area in order to produce reproducible images to ascertain that there was no sample damage induced by the tip. Height and phase images were scanned simultaneously at a fixed scan rate between 0.5–1 Hz with a resolution of 512x512 pixels². The scan sizes varied from 1x1 μm² to 5x5 μm². The root-mean-squared roughness (RMS) values of roughness were calculated from images corresponding to a fixed area of 5x5 μm². Images were acquired, stored, and visualized using the NanoScope Software Version 5.3. The results are given in Figures 4.25, 4.26, 4.29, 4.32, 4.34, 4.35, and 4.37.

3.2.4.5 Grain Size Analysis of the AFM topographies

Grain size analyses of the AFM topographies were carried out using the “ImageJ” software [<http://rsbweb.nih.gov/ij/download.html>]. More than 100 grains were measured for each sample (Figure 4.28).

3.2.4.6 Optical Microscopy Experiment

Optical microscopy experiments are used to obtain an enlarged image of a small object, using visible light. In general, it consists of a light source, a condenser, an objective lens, and an eyepiece, which can be replaced by a recording camera. The quality and design of the lens system determines the magnifying power, details of image formation, and color correcting capabilities of a light microscope [133].

The magnifying power of a microscope is the product of the magnification of the objective and the magnifying power of the eyepiece.

Since the obtained deposit exhibited a too large roughness to allow for imaging by AFM owing to the limited displacement of the piezoelectric scanner. The optical microscopy experiments were carried out .

The PSP and PAH prepared in 1x10⁻⁴M at I=0.15M NaCl. pH of each solution was adjusted to 6.70 with addition of 0.1M NaOH. The PSP/PAH complex was prepared in 1:1 mol ratio. A silicon substrate coated by a single PEI precursor layer prepared as described above and dipped into the PSP/PAH complex solution for 18 hours. Then, it was rinsed with milliQ water by dipping in steps of 60s, 60s and 100s and blow-dried with nitrogen. The optical microcopy images of the sample were taken using a Axiotech Vario (from Carl Zeiss) microscope trough objectives with different magnifications of 10x0.20, 20x0.50, and 50x0.70. Pictures were taken by

Nikon COOLPIX 4500 camera with a MDC lens. HAL 100 lamp, Osram was used for illumination (Figure 4.35).

3.2.4.7 Zeta potential measurement of PEI-(PSP-PAH)_n multilayers on glass substrate

This work is carried out in collaboration with Prof. Vincent Ball in International Center for Frontier Research in Chemistry, INSERM UMR 977.

The streaming potentials of the PSP/PAH coated surfaces are measured with a ZetaCAD device (CAD Instrumentation, Les Essarts le Roi, and France). The ζ -potential of each particular deposit on glass slides were calculated from the streaming potential using the Smoluchowski relationship [126]:

$$\zeta = \frac{\Delta E \eta \lambda}{\Delta P \epsilon \epsilon_0} \quad (3.17)$$

where ζ , η , λ and $\epsilon \epsilon_0$ are the ζ -potential, the solution viscosity, the solution conductivity and the dielectric permittivity of water. $\Delta E/\Delta P$ is the streaming potential, which is the slope of the potential difference versus pressure difference curve. The potential difference ΔE is measured between two Ag/AgCl reference electrodes located on both sides of the measurement cell. The pressure difference ΔP between the two electrolyte compartments is varied with compressed air by increments of 5 kPa between -30 kPa and +30 kPa. The solution conductivity is measured in situ. Since the viscosity and the dielectric permittivity are temperature dependent, the temperature of the solution is also regularly measured in situ and its value is used to calculate temperature corrected values of the dielectric permittivity and viscosity.

PEI-(PSP-PAH)_n or PEI-(PSP-PAH)_n-PSP deposits were prepared at the same time by LbL-spraying on 2 vertically hold glass surfaces in the same manner as for the silicon wafers. The schematic illustration for the LbL-Spraying set up of the glass slides is given in Figure 3.8.

The two covered glass slides are mounted parallel to each other in the plexiglass sample holder and are separated by a 500 μm thick poly(tetrafluorethylene) (PTFE) spacer. For all measurements, NaCl with a concentration of 5 mM is circulated between the samples. The ionic strength during zeta potential measurement with respect to ionic strength used during the spray deposition (0.15 M) is decreased in

order to reduce the influence of ionic screening. It is assumed that this reduction in ionic strength does not influence the structure of the deposit, which is reasonable due to the fact that a reduction in salt concentration tends to freeze in the mobility of polyelectrolyte chains [85]. The streaming potential is measured 5 times on the same substrate, before and after functionalization with sprayed deposits and the obtained values are averaged. The result is given in Figure 4.36.

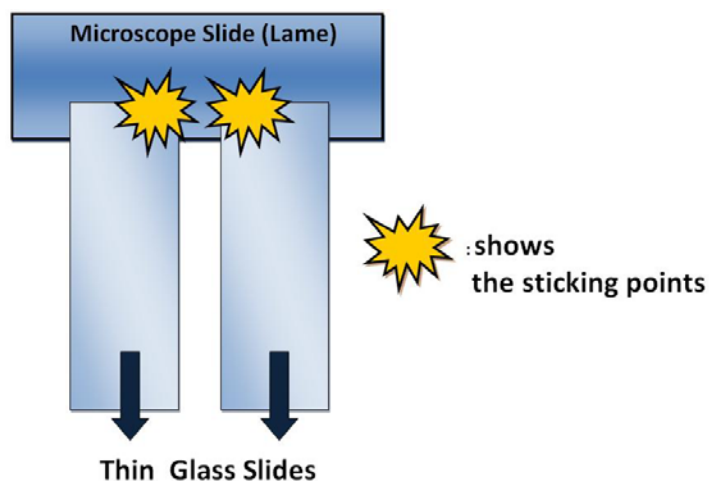


Figure 3.8: Schematic illustration of the LbL-spraying set up for 2 vertically hold glass surfaces.

4. RESULTS AND DISCUSSION

4.1 Characterization of PSP and PAH

4.1.1 Determination of molecular weight of PSP and PAH

P₂O₅ % (end group) and P₂O₅ % (total) was found 8.33 and 99.96, respectively. The number average degree of polymerization of PSP was determined as 24 and hence the molecular weight was found 2500 g/mol as indicated in Table 4.1.

Table 4.1: The results of end group titration.

| Titration Procedure | Added NaOH (V mL) | P ₂ O ₅ % |
|--|-------------------|---------------------------------|
| Before Hydrolysis (end group) | 5.5 | 8.33 |
| After Hydrolysis (total) | 66.0 | 99.96 |
| n ≈ 24, $\bar{M}_w \approx 2500$ g/mol | | |

Viscosity averaged molecular weight \bar{M}_V of PSP and PAH was calculated as 2900 and 52000 g/mol by using Mark Houwink equation 3.7.

4.1.2 Determination of equivalent weight of PSP and PAH

The experimental determination of the equivalent weight of polyelectrolytes, which corresponds to the equivalent weighed of repeated units are found to be 100.46±1.01 and 94.50±1.50 g.eqw for PSP and PAH, respectively.

4.2 Investigation of PSP/PAH complex formation in bulk

4.2.1 Determination of PSP/PAH stoichiometry by conductometric titration

Due to the fact that the process of complexation is controlled by the release of the counterions, a simple conductometric titration technique is used to determine the PSP/PAH stoichiometry.

The releasing of Na⁺ and Cl⁻ as counter ions during the PSP/PAH complex formation is taken into consideration in the conductometric titrations. The results are given in Figures 4.1 – 4.5, and 4.8, 4.9.

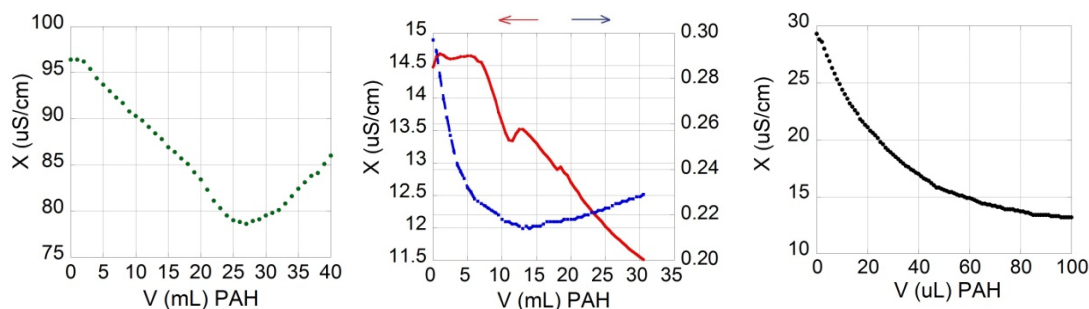


Figure 4.1: Conductometric titration curves of PSP with PAH at pH:6.70 in salt free solution. PSP and PAH are in equimolar concentration (Red: 1×10^{-2} M, Green: 1×10^{-3} M, Blue: 1×10^{-4} M, Black: 1×10^{-5} M, PSP and PAH). The error in these data is of the order of $0.2 \mu\text{S}$.

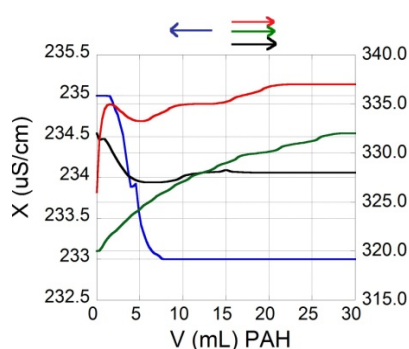


Figure 4.2: Conductometric titration curves of PSP with PAH at pH:6.70 in 0.15M NaCl. PSP and PAH are in equimolar concentration (Red: 1×10^{-2} M, Green: 1×10^{-3} M, Blue: 1×10^{-4} M, Black: 1×10^{-5} M, PSP and PAH). The error in these data is of the order of $0.2 \mu\text{S}$.

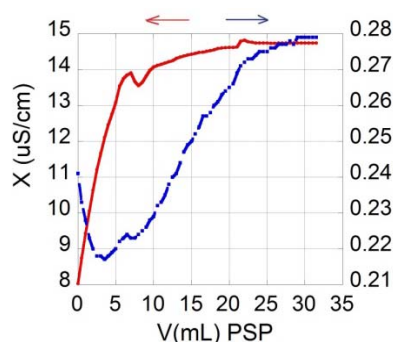


Figure 4.3: Conductometric titration curves of PAH with PSP at pH:6.70 in salt free solution. PSP and PAH are in equimolar concentration (Red: 1×10^{-2} M, Blue: 1×10^{-4} M, PSP and PAH). The error in these data is of the order of $0.2 \mu\text{S}$.

In general, the release of counterions during the titration of the PSP and PAH leaves negligible charge on, and around the close neighborhood of the polyions, but as the amount of titrant increased the more counter ions are liberated. Therefore, the conductivity increases with the counterion releasing [4-25].

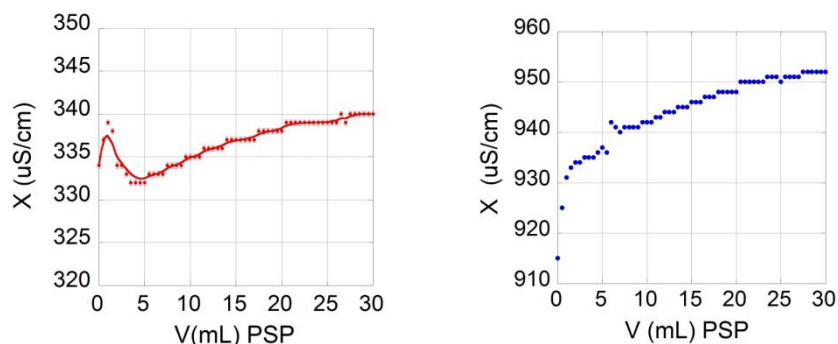


Figure 4.4: Conductometric titration curves of PAH with PSP at pH:6.70 in 0.15M NaCl. PSP and PAH are in equimolar concentration (Left: 1×10^{-2} M, Right: 1×10^{-4} M). The error in these data is of the order of $0.2 \mu\text{S}$.

The decreased part of the figure shows the complexation of PSP and PAH with the equivalent release of counterions, then due to the increase in the effective charge density, the reaction slows down, and the coiling of polyion takes time to bring the active functions to mutual position. At the high ionic strength, the added salts screen the effective charges on the free polyions. Thus, the conductivity either remains constant or increases slowly beyond the end point of the titration (Figures 4.1-4.5).

The constant conductivity can be explained by Manning's theory [134-139] that the counter and the added low molecular weight ions can be distributed either on the chain of free polyion (Territorial-binding) or around the polyions (Site-binding) as an excess but with opposite sign of the effective charge of polyions, and thus the conductivity remains constant.

Table 4.2: Stoichiometry of PSP/PAH complex determined at pH:6.70.

| Results by Conductometry | | | |
|--------------------------|--------------------------|--------------------|-------------------|
| Titrant | Solution | PSP:PAH mol ratio | |
| | | Salt Free Solution | I=0.15 mol/L NaCl |
| 1×10^{-2} M PAH | 1×10^{-2} M PSP | 0.91:1 | 0.77:1 |
| 1×10^{-3} M PAH | 1×10^{-3} M PSP | 1:1.40 | 1:1 |
| 1×10^{-4} M PAH | 1×10^{-4} M PSP | 0.77:1 | 1.25:1 |
| 1×10^{-5} M PAH | 1×10^{-5} M PSP | 1.61:1 | 1.25:1 |
| 1×10^{-2} M PSP | 1×10^{-2} M PAH | 1:1.67 | 1:1 |
| 1×10^{-4} M PSP | 1×10^{-4} M PAH | 1.61:1 | 0.91:1 |

Table 4.3: The stoichiometry of PSP/PAH complexes by viscosimetry and direct conductometry.

| Methods | PSP | PAH | PSP:PAH mol ratio |
|----------------------|-------------------------------|-------------------------------|-------------------|
| Viscosimetry | $9.8 \times 10^{-4} \text{M}$ | $9.8 \times 10^{-4} \text{M}$ | 1:1 |
| Direct Conductometry | $1 \times 10^{-3} \text{M}$ | $1 \times 10^{-3} \text{M}$ | 1:1.47 |

It is observed that the stoichiometry of PSP/PAH complex in bulk is close to unit mol ratio (Tables 4.2 and 4.3)

The conductometric titrations also carried out at pH 3, 4, and 10. However, the results at pH 3, 4, and 10 are not satisfactory. It might due to the fact that these pH values are closer to the pKa values of PSP and PAH (Figure 4.5).

Conductometric studies show that the complexation is stoichiometric but excess of PSP or PAH is present (Tables 4.2 and 4.3). Since the stoichiometry depends on polyion concentration, ionic strength and pH, the deviation from 1:1 mol ratio is associated with the losses in ion transference. Deviation from the unity arises due to screening effect of small ion, charge condensation (in this case Bjerrum Length is larger than the Coulomb Distance), the unreacted fraction of one polyion, reaction between unreacted polyions with the free fraction of polyions of opposite sign, conformational changes in the chain of polyion in order to bring the active sites of one polyion to react with the polyion of opposite charge.

Table 4.4 : Stoichiometry of PSP/PAH complex determined at pH:5 and 8.

| Titrant | Solution | PSP:PAH mol ratio | | |
|---------|----------|------------------------------|--------|-------|
| | | Ionic Strength (NaCl), mol/L | | |
| | | pH | 0.5 | 0.15 |
| PSP | PAH | 5 | 1:1 | 1:1 |
| | | 8 | 1.11:1 | 1.2:1 |
| PAH | PSP | 5 | 1.15:1 | - |
| | | 8 | 0.9:1 | 1:1 |

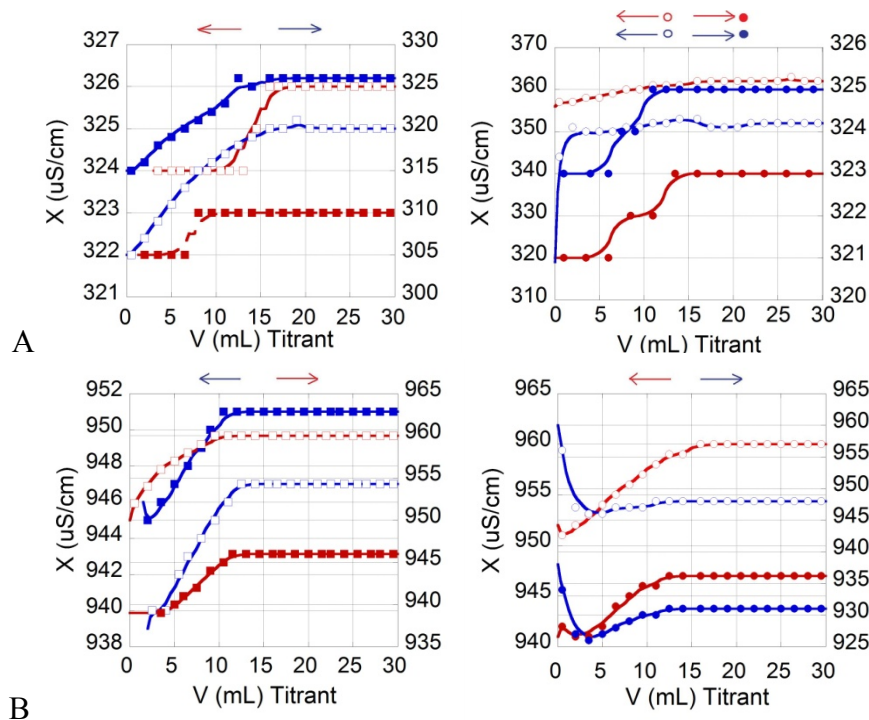


Figure 4.5: Conductometric titration curves of 1×10^{-4} M PSP and PAH in A: $I=0.15$ M NaCl, B: $I=0.5$ M NaCl, Red:PSP titrant, Blue:PAH titrant at pH; \circ : 5, \blacksquare : 6, \square : 7, and \bullet : 8. The error in these data is of the order of $0.2 \mu\text{S}$.

4.2.2 Determination of PSP/PAH stoichiometry by viscometry

Viscometry measurements were performed in order to confirm the PSP/PAH stoichiometry obtained from conductometric studies.

Figure 4.6 shows the changes in the reduced viscosity of the PSP/PAH system as a function of molar ratios of equimolar polyanion to polycation in aqueous solution at pH:6.70.

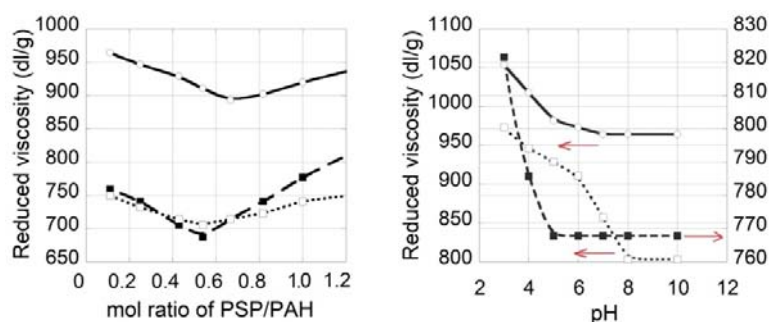


Figure 4.6: Reduced viscosity of PSP/PAH complex as a function of (left): mol ratio and ionic strength, (right): pH and ionic strength. ($C_{\text{PSP}}=1 \times 10^{-3}$ g/dl, PSP and PAH are prepared in equimolar concentration, \circ — : 0.01 M NaCl, \blacksquare - - : 0.15 M NaCl, \square ... : $I=0.5$ M NaCl). The error in these data is of the order of 10.3 dl/g.

It was observed that reduced viscosity decreases until pH of 5 and 7 and then remains constant at I=0.15 and 0.5M NaCl respectively at maximum complexation ratio (Figure 4.6) . Ireduced viscosity of PSP-PAH complex decreases as a function of pH until pH of 7 for I=0.01M NaCl and then remains constant at maximum complexation ratio (Figure 4.7).

Reduced viscosity has a minimum point for all ionic strenghts and pH values at maximum complexation ratio. The unit mole ratio of PSP/PAH was shifted from to 0.54:1 to 0.67:1 with the increasing of ionic strenght at original (natural) pH (Figures 4.6 and 4.7).

The decrease in the viscosity is due to the complex formation in the medium. The minimum viscosity is reached when more or less all free polyions have complexed. The viscosity increases since the free PSP polyions are in excess over the PAH molecules.

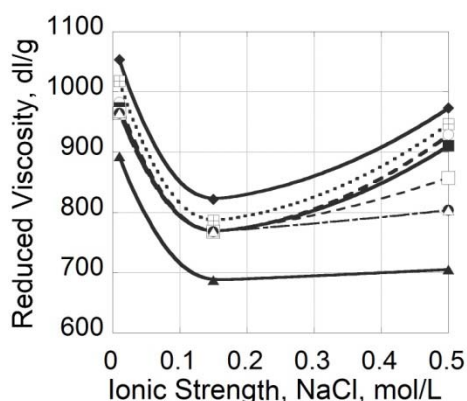


Figure 4.7: Dependence of reduced viscosity of PSP/PAH complex as a function of ionic strength and pH. ($C_{PSP}=1 \times 10^{-3}$ g/dl, PSP and PAH are prepared in equimolar concentration, pH; ◆: 3, ◻: 4, ○: 5, ■: 6, ◻: 7, ●: 8, △: 10, ▲: original pH). The error in these data is of the order of 6.3 dl/g.

The decrease in reduced viscosity with the increasing of ionic strength support the work of Hsiao and Luijten [80, 140]. In their work, an initial decrease of reduced viscosity due to the collapse of the polyelectrolyte chains as a result of coulombic screening by the counterions and subsequent increase of solution viscosity. It is also assumed that the change in viscosity is due to the transition from a more extended conformation of the polyelectrolyte chains to a more coiled up conformation depending on the low charge densities and high charge densities of polyions

respectively. This transition might be caused by intramolecular hydrophobic interactions of polyions. According to the Monte Carlo simulations [137, 141], this can happen due to the intramolecular competition between Coulombic and hydrophobic interactions. In the coiled conformation, the polyelectrolyte chains reach their most compact state and the lowest reduced viscosity is achieved.

The increase of reduced viscosity at higher salt concentration might also be attributed to intrachain interaction due to the counterion condensation on the chains leading to charge overcompensation.

Since the added salt concentration is much larger than the number of released low molecular ions the influence of the degree of counterion binding on viscosity can be neglected.

Besides, the direct conductometry and viscometry measurements as a function of different mol ratios were also carried out in salt free solution at pH:6.70. All the results confirmed that the complexation stoichiometry is in unit mol ratio. The results are given in Figure 4.8.

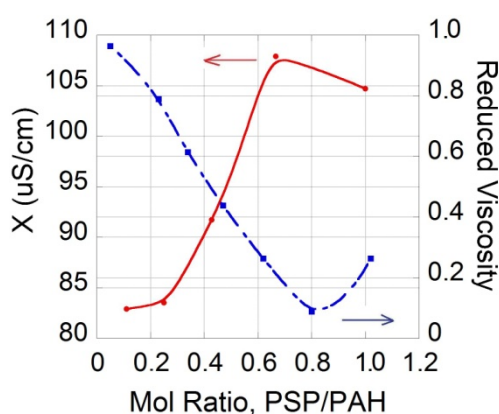


Figure 4.8: Reduced viscosity and specific conductivity change as a function of mol ratio ($C_{\text{PSP}}=0.01\text{g/dl}$, PSP and PAH are prepared in equimolar concentration in salt free solution, Blue: viscosity data, Red: conductivity data). The error in these data is of the order of 6.3 dl/g and $0.2\mu\text{S}$ respectively.

4.2.3 Kinetic investigation of PSP/PAH complex formation by conductometry and viscometry

PSP/PAH complex formation was investigated depending on the variation in conductivities and viscosities of the PSP/PAH complexes as a function of time in order to provide further information on complex formation in terms of complexation kinetics.

Time dependent studies by direct conductometry and viscometry showed that specific conductivity increases with time for $1 \times 10^{-2} \text{M}$ and $1 \times 10^{-4} \text{M}$ PSP-PAH complex respectively (Figure 4.9).

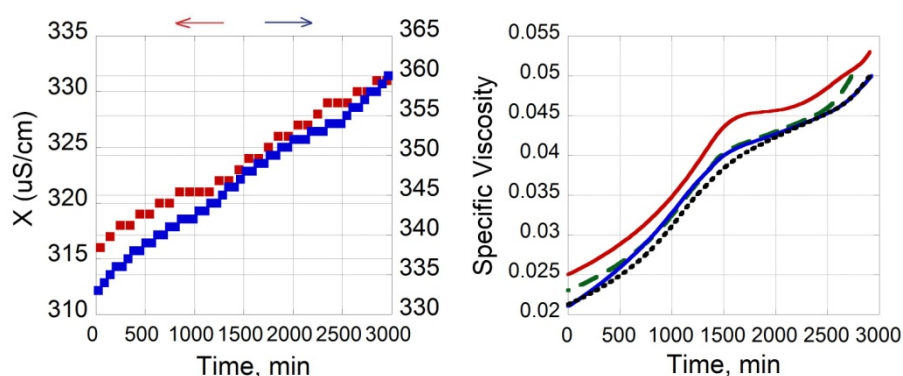


Figure 4.9: Time dependency of specific conductivity and specific viscosity of PSP/PAH complex prepared at $I=0.15 \text{M}$ NaCl, $\text{pH}:6.70$ (Red: $1 \times 10^{-2} \text{M}$, Green: $1 \times 10^{-3} \text{M}$, Blue: $1 \times 10^{-4} \text{M}$, Black: $1 \times 10^{-5} \text{M}$ PSP and PAH).

It is observed that there is a counter ions releasing after the complex has been formed and the PSP/PAH complexation is very dynamic. The continuous counter ion releasing be due to the rearrangement of the complex particles during complexation. It can be assumed that PSP and/or the PAH chains are so mobile that PSP/PAH complex particles might go under rearrangement during complexation leading to the charge increase in the specific conductance. The same assumption is suggested by Kotz et al. [27] in which they studied with acryl-based polyelectrolytes of different chain length, however, their model for the structural rearrangement is not demonstrated. They suggested that dominating influence on structural changes is considered to be mainly caused by differences in overall structural density of the particles and also some differences in the chain loops and chain end surface structure.

These results are in good agreement with time dependent dynamic light scattering and zeta potential experiments and with the studies carried out at interfaces given in sections 4.3.1, 4.3.2, and 4.3.3.

4.2.4 Analysis of Supernatant Liquids by Viscosity

Analysis of supernatant liquids of PSP/PAH complex were carried out by viscometry in order to confirm the stoichiometric data.

Table 4.8 compares the measured supernatant liquid and control sample specific viscosities for the PSP/PAH mixtures. The specific viscosity of supernatant solutions is almost equal to those of control samples which are made up to contain the ionic excess of more concentrated polyion plus NaCl equivalent to maximum counter ion release from the PEC.

It is observed that for all mixtures, $\eta_{sp(\text{supernatant})}/\eta_{sp(\text{control})}$ slightly deviates from unity. The amount of unreacted moieties and counterions are found to be less than from the expected in supernatant mixtures. If perfect pairing does not occur, those unpaired free polyions will be accompanied by their corresponding counterions, and cause departures from unity.

The same experiments given in page 47 (A and B) was carried out for 1×10^{-2} M PSP and PAH concentration at $I=0.15$ M NaCl, pH: 6.70 (Table 4.5).

Table 4.5: Supernatant liquid and control sample specific viscosities for solution PSP/PAH mixtures.

| Complex Composition | Preparation | Control sample | η_{SP} (supernetant) | η_{SP} (control) | $\eta_{SP(\text{control})} / \eta_{SP(\text{supernatant})}$ |
|------------------------------|---|----------------------------|------------------------------|--------------------------|---|
| 1×10^{-4} M PSP-PAH | (1:1 mol ratio, allowed to settled down and then PSP added) | 3.3×10^{-3} M PSP | 0.063 | 0.069 | 1.10 |
| | (1:1 mol ratio, allowed to settled down and then PAH added) | 3.3×10^{-3} M PAH | 0.068 | 0.079 | 1.16 |
| | (1.5:1 mol ratio, allowed to settled down) | 2×10^{-5} M PSP | 0.102 | 0.110 | 1.08 |
| | (1:1.5 mol ratio, allowed to s settled down) | 2×10^{-5} M PAH | 0.113 | 0.127 | 1.12 |
| 1×10^{-3} M PSP-PAH | (1:1 mol ratio, allowed to settled down and then PSP added) | 3.3×10^{-2} M PSP | 0.044 | 0.049 | 1.11 |
| | (1:1 mol ratio, allowed to settled down and then PAH added) | 3.3×10^{-2} M PAH | 0.059 | 0.060 | 1.02 |
| | (1.5:1 mol ratio, allowed to s settled down) | 2×10^{-4} M PSP | 0.081 | 0.091 | 1.12 |
| | (1:1.5 mol ratio, allowed to settled down) | 2×10^{-4} M PAH | 0.093 | 0.104 | 1.12 |

4.2.5 Analysis of Supernatant Liquids by FTIR Spectroscopy

It has been known that type and structure of the polyelectrolytes play a role on the properties of PECs. Therefore, different types of PSP were synthesised and the FTIR spectra were compared with that of commercial PSP, $(\text{NaPO}_3)_n$, used in this study. It is, basically, aimed to find out whether the commercial $(\text{NaPO}_3)_n$ is pure or contains even a little amount of cyclic phosphate. It was thought that the structures and properties of PSP/PAH complex could be affected by the impurities.

Comparison of the IR spectra between PSP obtained in different procedures and commercial PSP (Sigma Aldrich-04267) revealed that the commercial PSP does not contain crystalline, cyclic Kurrol's salts (Figure 4.10).

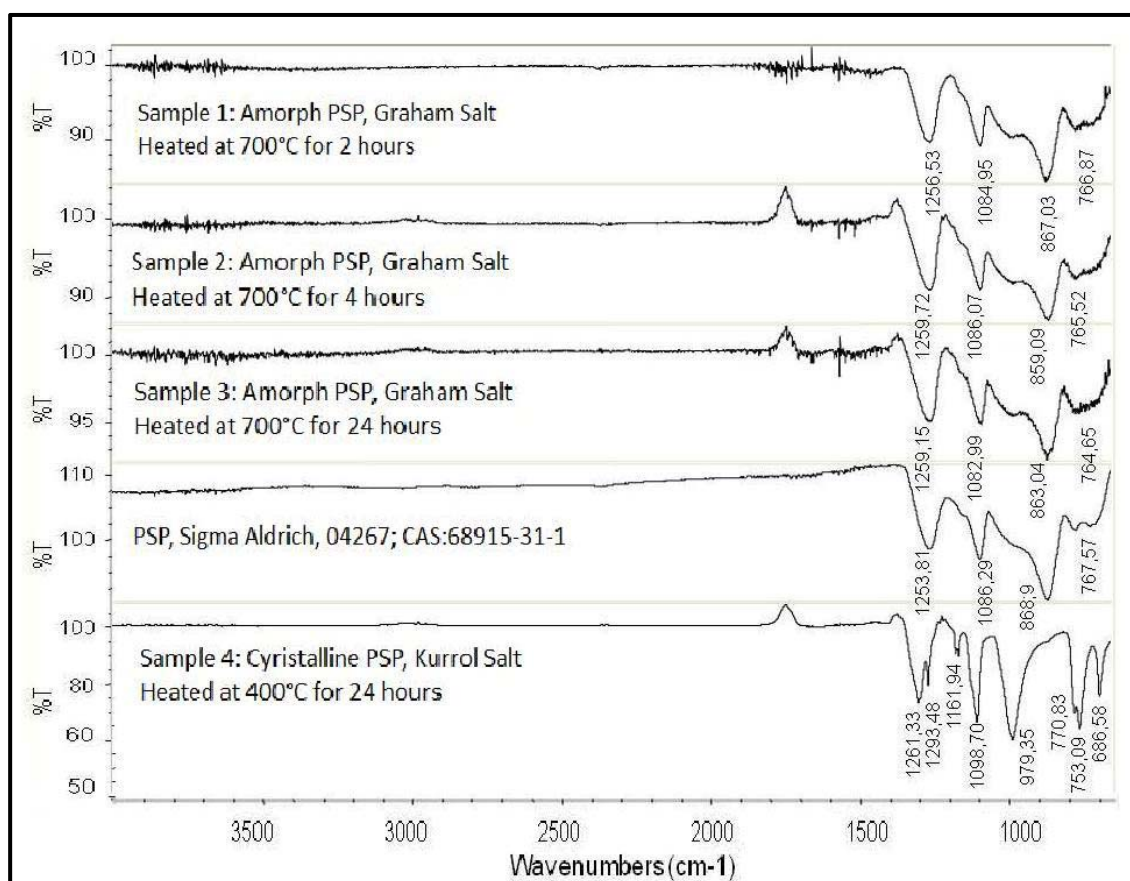


Figure 4.10: FTIR spectra of PSP prepared by different procedures.

It is evident from the IR spectrum that the crystalline form of poly(sodiumphosphate) (Kurrol's salt) has a strong and sharp doublet peaks at 745 and 770 cm^{-1} which is due to asymmetric and symmetric stretching of P-O-P bond [120]. This is characteristic for cyclic phosphates. This peak was not observed in IR spectra of commercial and also synthetic poly(sodiumphosphate) (Figure 4.10).

FTIR spectra of PSP-PAH complexes obtained by different procedures showed that the PSP-PAH complexes in bulk solution and in the solid form obtained by LbL deposition were the same (Figure 4.11). Besides, the existence of PSP-PAH complex formation is confirmed by FTIR spectra (Figure 4.11).

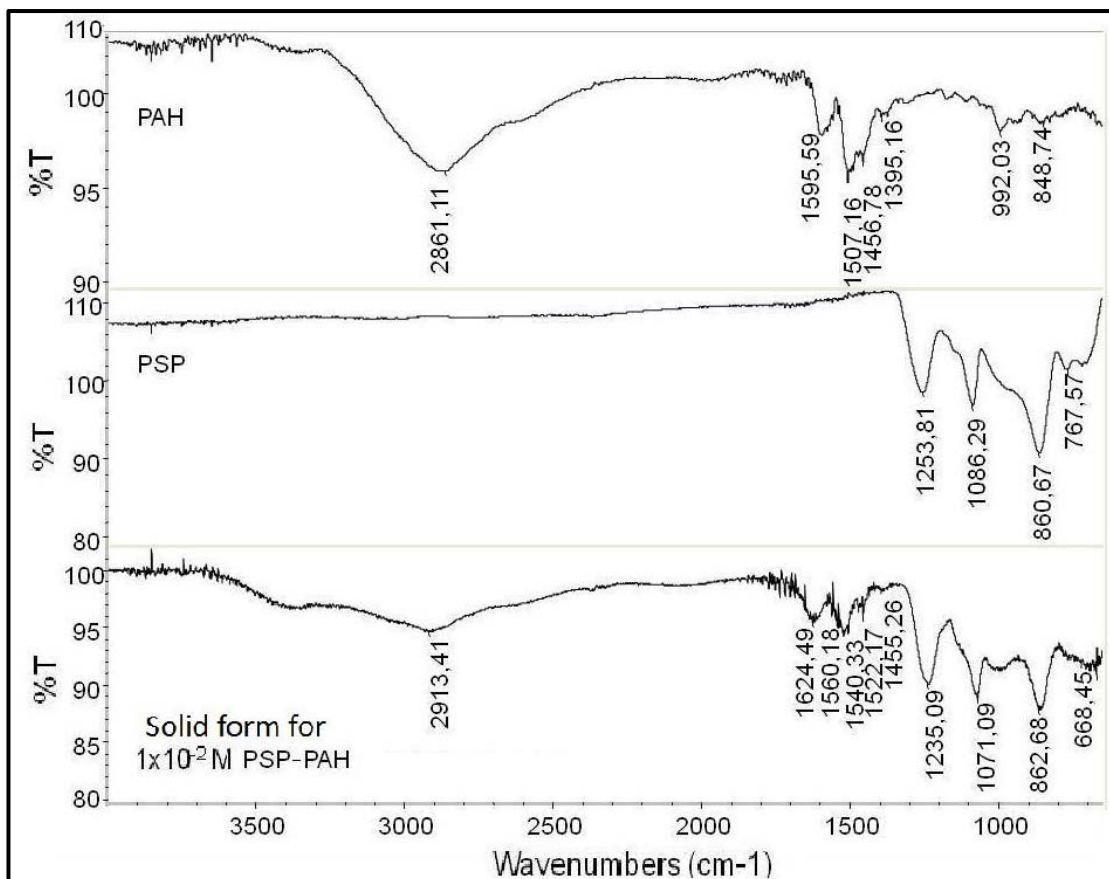


Figure 4.11: FTIR spectrum of solid PSP and PAH, and PSP/PAH complex prepared by 1:1 mol ratio at $1 \times 10^{-2} \text{M}$ polyelectrolyte concentration, $I=0.15 \text{M}$ NaCl at pH 6.70.

Besides, the FTIR spectrum of the solid PSP/PAH complex samples which are obtained from the supernatant liquids by drying were carried out. The aim of FTIR experiments is to identify the molecular structure of PSP/PAH complex as well as to reveal the existence of complex formation.

PSP/PAH complexes prepared in 1:1 mol ratio at $1 \times 10^{-2} \text{M}$, $1 \times 10^{-3} \text{M}$, and $1 \times 10^{-4} \text{M}$, $I:0.15 \text{M}$ NaCl and pH:6.70, then allowed to reach equilibrium more than 24 hours. Then 10mL of an aliquot from the supernatant liquid was taken and dried at 55°C in the etuve. The solid residue is investigated by FTIR spectroscopy (Figure 4.12).

It was observed from these results that, after reaching equilibrium, the supernatant liquid does not contain any PSP/PAH complex prepared at $1 \times 10^{-3} \text{M}$ and $1 \times 10^{-4} \text{M}$

polyelectrolyte concentrations. However, when the complex is prepared at higher concentration of $1 \times 10^{-2} \text{M}$, there can be free PAH exist together with the complex.

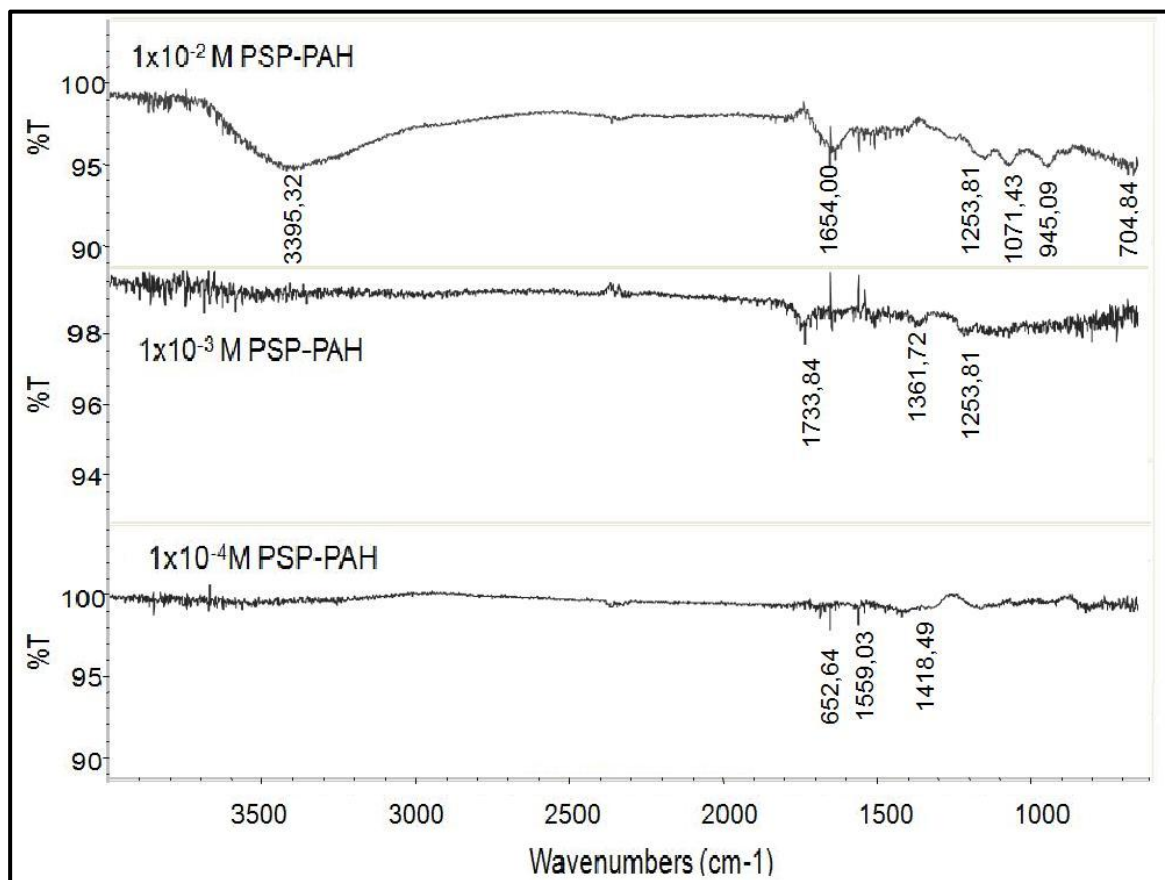


Figure 4.12: FTIR spectrum of the solid PSP/PAH complex samples obtained from the supernatant liquids by drying.

4.2.6 Isothermal Titration Microcalorimetry, ITC, Measurements

Experiments related with kinetic investigation of PSP/PAH complex formation by ITC was realized in collaboration with Prof. Vincent Ball. Isothermal Titration Microcalorimetry, ITC, experiments of PSP/PAH system was carried out in laboratory of Faculty of Pharmacy in University of Strasbourg.

It is known that the enthalpy, ΔH , is a state function of the system and it is equal to the heat exchanged by the system with its surroundings is held at constant pressure. This heat exchanged can be directly measured by means of ITC experiments.

In this study, PSP/PAH complex formation is investigated by ITC in order to have information about the function and mechanism of the PSP/PAH complex formation and to describe the thermodynamic profile of the PSP/PAH interaction. Measurement of this heat change associated with the injection of a small volume of PSP into the

PAH allows to accurate determination of binding constants (K_B), reaction stoichiometry (n) of PSP/PAH system as well.

It is known that the measured heat effects are the sums of two contributions: the heat of binding of PSP to PAH and the heat of dilution of the PSP. However, it has been observed that the heat of dilution is negligible (Figure 4.13).

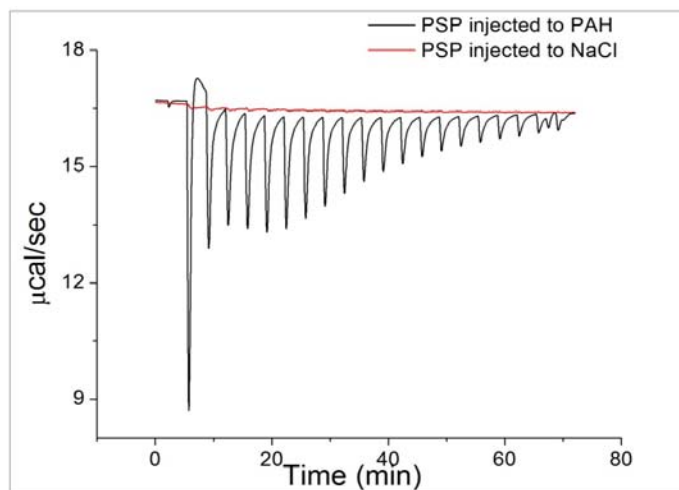


Figure 4.13: Experimental heat flow obtained at 25 °C in the presence of a 0.15M NaCl at pH 6.70 for 21 stepwise injection of 8 μ L, 5 $\times 10^{-2}$ M PSP into 2 $\times 10^{-4}$ M PAH with a stirring rotation at 310 rpm. Consecutive injections were separated by a resting period of 200s.

Negative change in differential power indicates the PSP/PAH complex formation is exothermic which supposed to have a linear growth regime in PSP/PAH multilayers deposits. The correlation between the complexation heat and the nature of the film growth process is suggested by Ball and coworkers in literature [95, 96]. In their work, it is indicated that linearly growing processes are associated with strongly exothermic reactions, whereas exponentially growing ones are associated with endothermic complexation reactions. It is expected that when the polyanion/polycation complexation process is exothermic, both the enthalpy and entropy changes favor the complexation and the complexes are expected to be “strong”. This is expected to be the case for linearly growing films. On the other hand, when the polyanion/polycation complexation process is endothermic, enthalpy and entropy can play opposite roles in the complexation process so that the complexes should be much weaker. This is expected to be the case for exponentially growing films.

Besides, since there is still a change in differential power even after more than one hour, it was not possible to calculate the binding constants for PSP/PAH system. Therefore, ITC results gave only qualitative information about the PSP and PAH interaction.

Moreover, PSP and PAH addition to PSP/PAH complex after it is assumed to reach equilibrium were carried out by isothermal titration microcalorimetry in order to investigate the effect of addition excess polyelectrolyte in terms of complexation process once the PSP/PAH complex was formed. Therefore, PSP/PAH complex formation was obtained in the measurement of the cell by a single only one main injection of 7.5 μL PSP solution followed by consecutive injections of PSP to this complex as described in section 3.2.3.3.

After only one main injection of PSP, it is observed that the time required to allow the microcalorimeter to come back to a baseline corresponding to the absence of any heat flow, thus to reach the equilibrated complex is not sufficient and the PSP/PAH complex formation is, indeed, an extremely slow process and equilibrium was not reached even after a few hours (Figure 4.14). However, the addition of excess of any polyelectrolyte once the PSP/PAH complex formed was negligible in terms of thermodynamic properties (Figure 4.15).

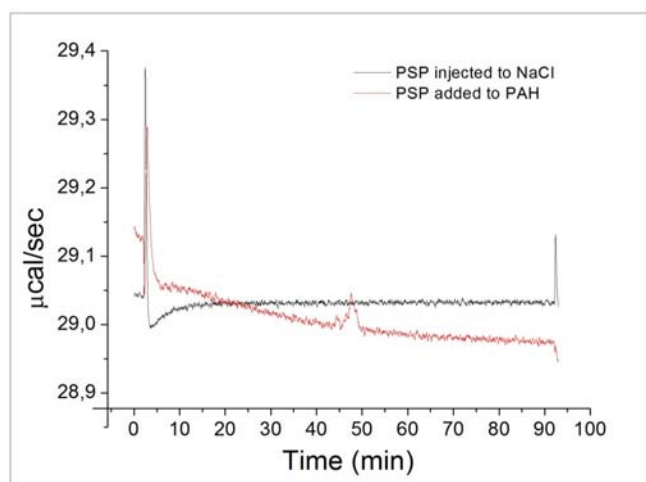


Figure 4.14: Experimental heat flow obtained at 25 °C in the presence of a 0.15M NaCl at pH 6.70 for a single injection of stepwise injection of 7.5 μL , 2×10^{-2} M PSP into 1×10^{-4} M PAH with a stirring rotation at 310 rpm. The reference cell was filled with 0.15M NaCl at a pH of 6.70.

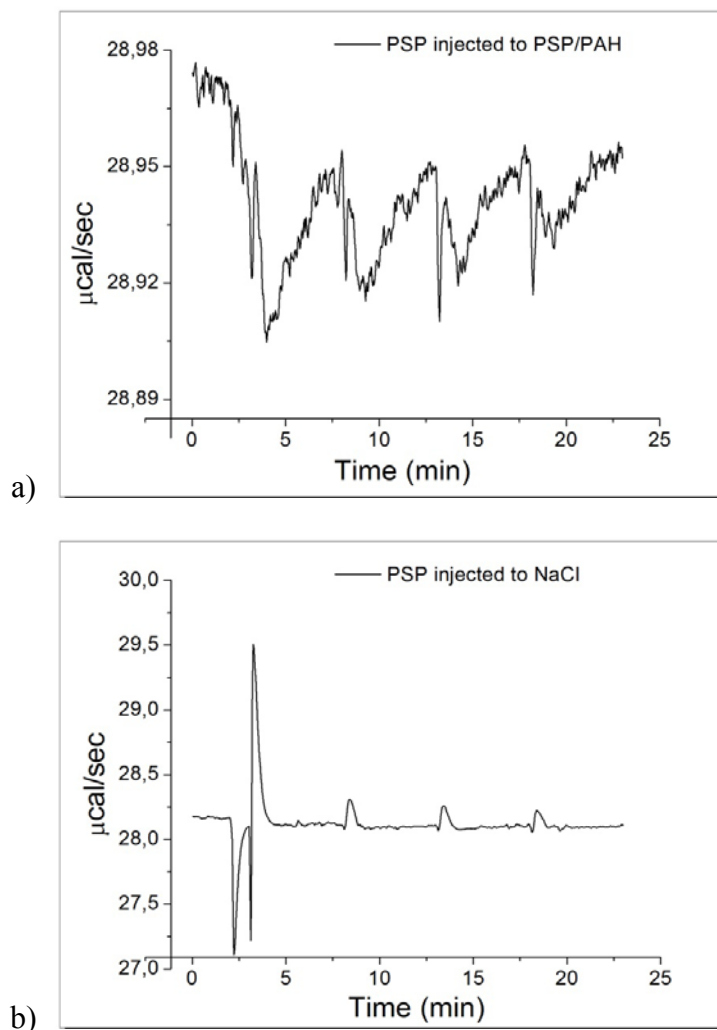


Figure 4.15: a) Experimental heat flow obtained at 25°C in the presence of a 0.15M NaCl at pH 6.70 for 4 stepwise injection of 5 μL , $2 \times 10^{-2}\text{M}$ PSP into $1 \times 10^{-4}\text{M}$ PAH with a stirring rotation at 310 rpm. The reference cell was filled with 0.15M NaCl at a pH of 6.70. b) Experimental heat flow obtained at the same conditions and parameters for the dilution step.

The particular slow process property of PSP/PAH complex formation is one of the big handicaps in these experiments. The formation of colloidal sticky particles of PSP/PAH complex in the solution and, hence, the instrumental restriction in the microcalorimetry cell is another handicap arises in the investigation of PSP/PAH complex formation mechanism by isothermal titration microcalorimetry. This problem originated because of the long duration time in the complexation kinetics and particle size increasing leading to an unstable aggregate formation which prevents to study ITC experiments. Particle size increasing and aggregate formation depending on time will be discussed in the following sections.

4.2.7 Dynamic Light Scattering (DLS) and Zeta Potential Measurements.

Experiments related with the Dynamic Light Scattering (DLS) and zeta potential measurements, and molecular fluorescence studies were realized in collaboration with Prof. Vincent Ball.

The most significant characteristics of many colloidal dispersions are the size and shape of the particles and most properties of the colloidal dispersions; such as, stability and chemical reactivity, are influenced to some extent by these factors [142-144]. Therefore, PSP/PAH complex formation was investigated depending on the variation in particle size as a function of time in order to characterize the PSP/PAH particles in bulk solution leading to a better comparison of complex aggregates formed in bulk and at interfaces.

Besides, PSP/PAH complex formation was investigated depending on the variation ζ - potential of PSP-PAH particles as a function of time in order to characterize the surface charge of the PSP/PAH particles in bulk solution. It is also aimed to provide further comparison of complex aggregates formed in bulk and at interfaces.

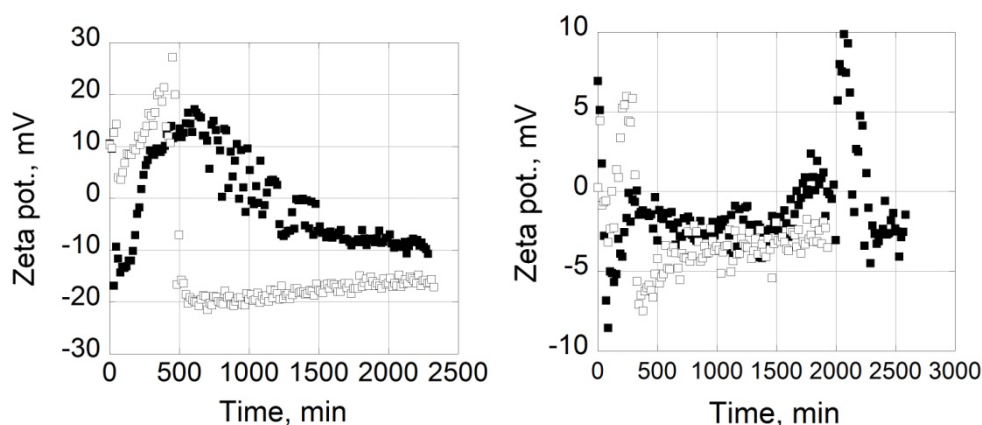


Figure 4.16: Time dependency of zeta potential of PSP/PAH complex particles prepared in unit mol ratio at pH:6.7, Left: $I=0.15$ M NaCl, Right: $I=1$ M NaCl; ■: PSP added, □:PAH added, PSP and PAH: 1×10^{-4} M.

It has been observed that the dynamics of the PSP/PAH complexation is very slow (characteristic time of a few hours), and the complexes carrying a negative zeta potential of about -15 to -20 mV after around 24 hours of equilibration of PSP and PAH (Figure 4.16) and a slow increase in the particle size up to $2.5 \mu\text{m}$, at the same time scale so that a reversal in the zeta potential occurred from a positive to a negative value (Figure 4.17).

As a result, PSP/PAH complex formation is very dynamic and close to equilibrium, and within a certain time of period ζ -potential alternates and particle sizes slightly increases. The order of addition either polyion to form the complex does not effect complex equilibrium.

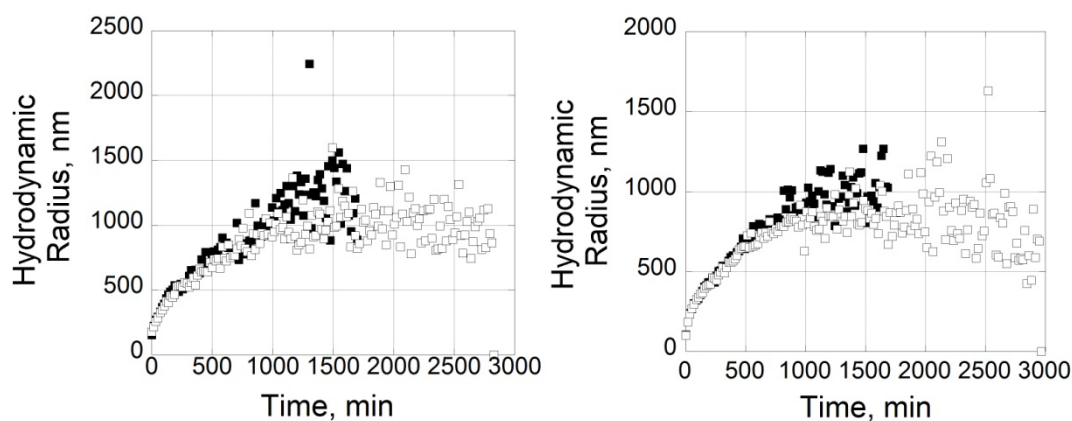


Figure 4.17: Time dependency of hydrodynamic radius of PSP/PAH complex particles prepared in unit mol ratio at pH:6.7, Left: $I=0.15M$ NaCl, Right: $I=1M$ NaCl; ■: PSP added, □:PAH added, PSP and PAH: $1 \times 10^{-4} M$.

When the charge provided by one of the adsorbed polyelectrolyte is sufficient to neutralize other one on the surface, the particles have strong tendency to form aggregates and the particle size increases. The reason behind this assumption might be the non-homogeneous overcompensation of surface charge. When the surface charge is close to zero, electrostatic repulsion between complexes is absent on average and the presence of an attractive potential leads to strong particle aggregation. In addition, the presence of small polydispersity indicates that the aggregation process might not involve only the particle size increment, but also an accumulation of aggregates. Formation of such aggregates can be also explained by the presence of long-range electrostatic repulsions and short-range attractive forces [30, 66, 67, 72, 134-142]. If the repulsion forces between particles are not sufficient to counterbalance the short-range attraction, particles sticks together. During this clustering of the aggregates, a sufficient charge should be accumulated and the aggregate stops to grow up which means a critical aggregate size is reached. At these conditions, the charge is close to zero. This clustering might proceeds over a long time scale, typically hours, even days. The results obtained are well correlated with this assumption.

Besides, PSP and PAH addition to PSP/PAH complex after it is allowed to reach equilibrium were carried out by conductometry, viscometry, isothermal titration microcalorimetry and dynamic light scattering. For this purpose, always the same amount of PSP or PAH were added to the equilibrated complex. These experiments were carried out in order to investigate the effect of addition of excess polyions on PSP/PAH complex, and on particle size increment (once the PSP/PAH complex formed) as well. The results showed that, the addition of excess of any polyelectrolyte after the PSP/PAH complex formed and reached equilibrium was negligible in terms of thermodynamic properties.

4.3 PSP/PAH complex formation and characterization at interfaces

4.3.1 Ellipsometry measurements

The purpose of these experiments is to characterize the PSP/PAH complex formation at interfaces, and then to compare the properties of the same complex obtained in bulk at close-to-identical conditions at an interface (multilayer film) in order to work out the fundamental differences and similarities between these two systems.

In fact, regularly growing LbL deposits were not obtained at the early stages of the interface studies. The PSP/PAH film deposition was achieved nearly after three months of work. During this period, the parameters effecting the PEC complex formation at interfaces; such as pH, ionic strength of the solution as well as the different type of multilayer build up procedures; such as spraying and dipping were tried to obtain a homogenous PSP/PAH coated surface. For this purpose, contact time of polyions to the surface in spraying and dipping procedure as well as the effect of drying step and duration of rinsing step during the buildup of PSP/PAH multilayers were examined and the parameters yielding a homogeneous, nanoscaled surfaces were tried to be optimized. From these pre-trial and optimization experiments, it was observed that the PSP/PAH complex formation at interfaces can only takes place in the presence of low molecular salt. Besides, it was found that LbL-dipping method was nearly unsuccessful in PSP/PAH deposition which leads to a nonhomogeneous surfaces whose change in the total thickness with the deposition number gives a distorted curves with very low R^2 values. The result of obtaining nonhomogeneous films by LbL- dipping method might be due to characteristics of the build up process, in which the longer contact time of each polyions comparing to

the LbL-spraying method. In the dipping method, due to the longer contact time removal of the complex from the surface occurs because of loosening the interactions between PEC and substrate. In addition, Quartz Crystal Micro Balance- Dissipation, QCM-D, experiments was also performed in PSP/PAH system in order to observe whether the surface of the multilayer film is viscoelastic or not. However, experiments were not successful because of the absence of drying step in this method.

PAH and PSP deposits are produced according to the LbL spray deposition method as a function of concentration of polyelectrolytes and ionic strength (Figures 4.18 - 4.21, 4.30, and 4.32).

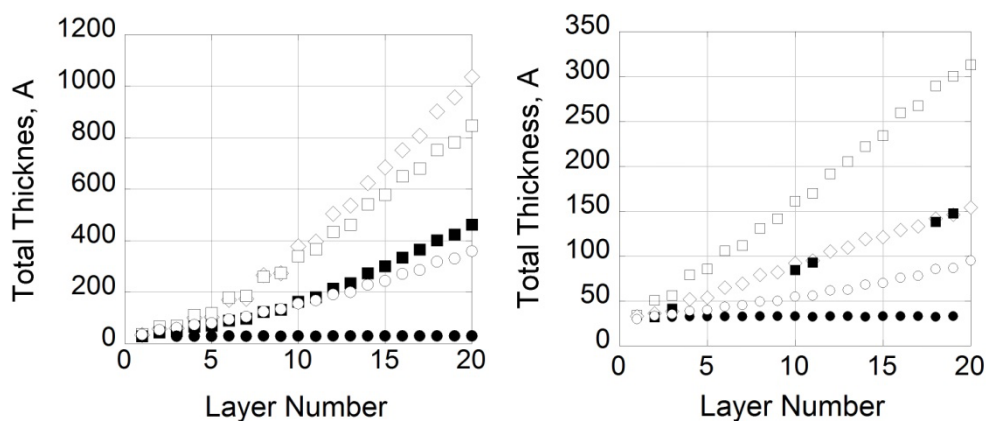


Figure 4.18: Evolution of the thickness of a PEI-(PSP/PAH) $_n$ deposits with layer numbers showing the effect of ionic strength at pH:6.70 for $1 \times 10^{-3} \text{M}$, (left) and for $1 \times 10^{-4} \text{M}$ polyelectrolyte concentration (right), ●: salt free, ○: $I=0.05 \text{M NaCl}$, ■: $I=0.15 \text{M NaCl}$, □: $I=0.5 \text{M NaCl}$, ◇: $I=1 \text{M NaCl}$.

No film deposition was observed in salt free solution. It was demonstrated that an increase in PSP and PAH concentration allowed for a progressive transition from linear growth to a supralinear (Figure 4.18). Besides, as shown in Figure 4.19, intersection of two linear growth is observed for the polyion concentration of $1 \times 10^{-2} \text{M}$ and $1 \times 10^{-3} \text{M}$. In other words, the combination of an exponential growth followed by a linear one has been observed at $1 \times 10^{-2} \text{M}$ and $1 \times 10^{-3} \text{M}$. Observation of a two linear growth regimes with a transition between them might be due to the mobility of higher polyelectrolyte chains because of entropic reasons.

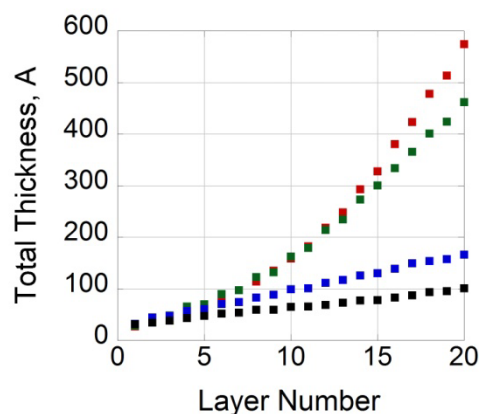


Figure 4.19: Evolution of the thickness of a PEI - (PSP/PAH)*n* deposits with the layer numbers showing effect of polyelectrolyte concentration at pH 6.70, I=0.15M NaCl, Red: 1×10^{-2} M, Green: 1×10^{-3} M, Blue: 1×10^{-4} M Black: 1×10^{-5} M PSP and PAH.

In literature, there are some studies in which a transition between two linear growth regimes is observed [73, 86, 87, 93, 104, 106-109]. The suggestion of these authors for the reason of transition is the rearrangement of the film and gradual densification of the layers. Restructuring and densification forbids the diffusion of one of the polyelectrolytes over a part of the multilayer matrix so that the film becomes progressively less and less penetrable. However, the direct proof of film restructuring has been still unknown.

It appears that by increasing the concentration of both polyelectrolytes from 1×10^{-5} to 1×10^{-2} M, the growth regime changes from linear with a slow thickness increment of 0.35 nm per layer pair at 1×10^{-5} M to markedly exponential growth at 1×10^{-3} and 1×10^{-2} M. The quality of the exponential fit to the thickness data is particularly good for the deposition experiment performed at 1×10^{-2} M and a bit less good at 1×10^{-3} M but nevertheless satisfactory (Figures 4.18—4.19).

It is also found that increasing the ionic strength from 0.05 to 0.5 M results in thicker films, however, if the concentration of the ionic strength is increased up to 1 M, the average total thickness of the PSP/PAH deposits decreases (Figure 4.20). It is due to the screening effect of the small Na^+ and Cl^- ions due to Coulomb interaction. As it is mentioned in the literature [39, 48, 80, 85, 94, 134-139] increasing the salt concentration screens the charges on the polyelectrolyte chains so that electrostatic interaction between oppositely charged polyions are weakened.

It was found that the complex formation decreases with increasing polyelectrolyte concentration in LbL deposition (Figure 4.21). Indeed, Schlenoff and co-workers [145] have shown a complete loss of the polyanion which inhibits the multilayer film growth by using “short” polyelectrolytes (of molecular weight ca. 10 kDa).

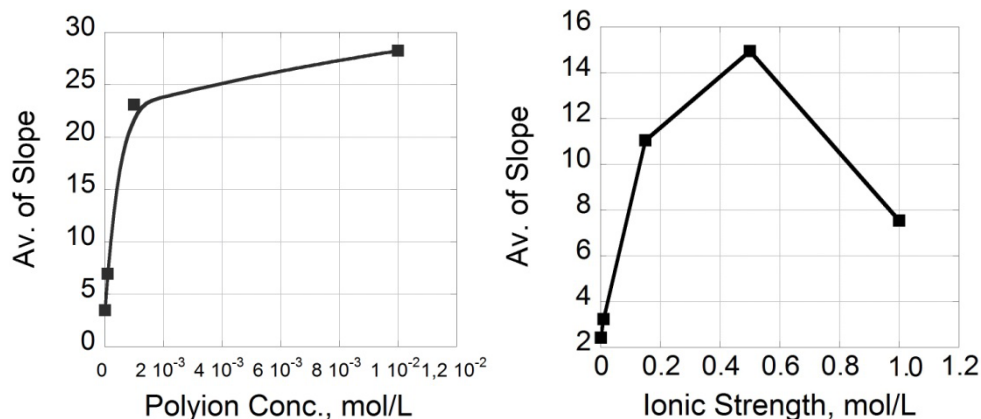


Figure 4.20: Left: represent the variation of linear fit slope values as a function of polyelectrolyte concentration, Right: represent the variation of linear fit slope values as a function of ionic strength for 1×10^{-4} M PSP/PAH deposits at pH 6.70.

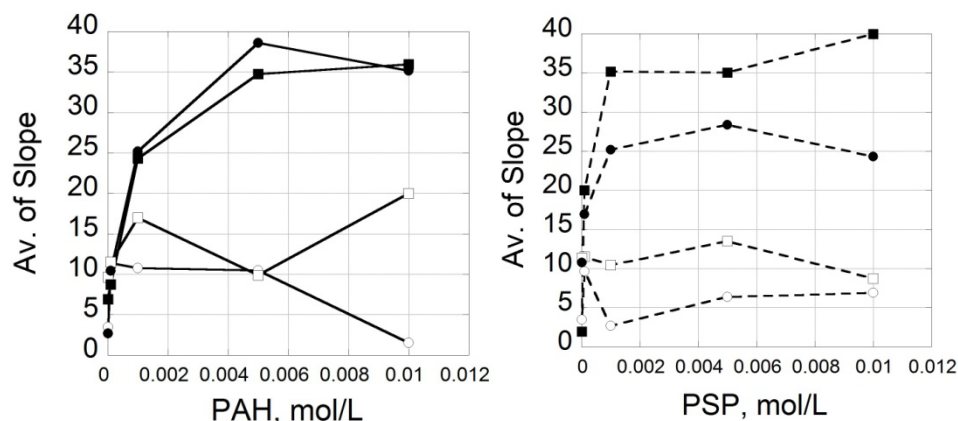


Figure 4.21: Change in the average slope of linear growths for PSP/PAH deposits at equimolar of ■: 1×10^{-2} M, □: 1×10^{-3} M, ●: 1×10^{-4} M, ○: 1×10^{-5} M PSP and PAH as a function of polyanion and polycation concentration at $I=0.15$ M NaCl and pH:6.70.

It has been observed that a combination of “short” and “long” polyelectrolytes causes a net increase in the film thickness as a function of layer number, but the thickness increment is partially lost when the shorter polyelectrolyte was deposited onto the longer one. It is due to removal of the shorter polyelectrolyte by the oppositely charged longer polyelectrolyte [145].

On the other hand, Caruso and co-workers [146] showed that partial removal of the deposited low charged polyelectrolyte upon adsorption of the next layer of highly charged polyelectrolyte is responsible for no significant film growth. Observation of no film deposition in salt free solution might be explained considering above approaches since there is a big difference in chain length of PSP with a lower degree of polymerization of 24 and PAH having a higher molecular mass (56000 g/mol) than PSP.

Several experiments were also carried out for more than 100 layers at the conditions of 1×10^{-4} M and 1×10^{-3} M (Figure 4.22). Deviation from the linearity was observed almost after 120 layers at the conditions of 1×10^{-4} M.

In order to understand if this deviations arise due to a misperfection during deposition or if it is a characteristic growth regime for particular PSP/PAH complex; the same experiment was repeated several times in the same spraying conditions. In some experiments, the position of substrate was changed in order to ensure if the deviation was due to the deposition protocol. As a matter of fact, as seen in Figure 4.22, the different experiments were independent from each other gave the result that the deviation was not due to the parameters which controls the deposition process.

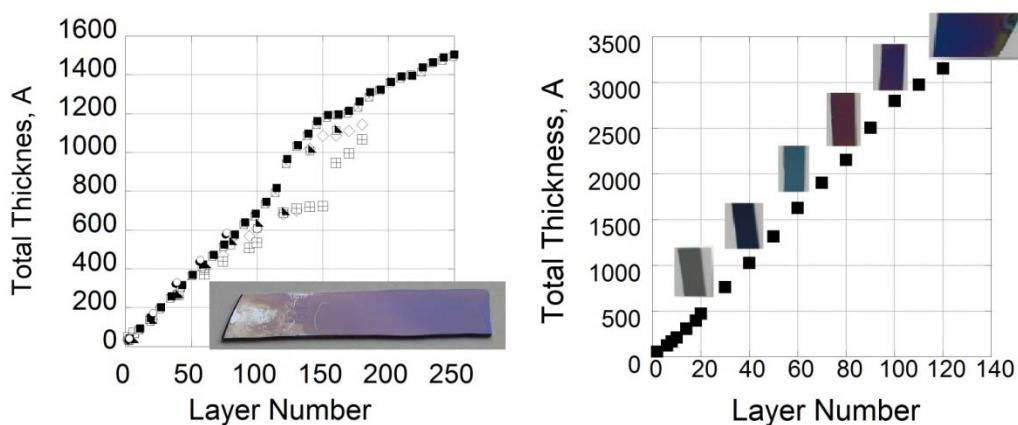


Figure 4.22: Evolution of the thickness of PEI-(PSP/PAH) n deposits with the layer numbers at pH:6.70, I=0.15M NaCl, for 1×10^{-4} M PSP/PAH. The insets show the photographic image of a deposit obtained after 150 deposition steps (left), and after 30, 40, 60, 80, 100 and 120 deposition steps (right). Different symbols correspond to different experiments carried out independent from each other.

The average thicknesses obtained at 1×10^{-3} M was found to be higher than that of 1×10^{-4} M. The increase in the average thickness with increasing the concentration of

the polyelectrolytes could originate from either kinetic or thermodynamic reasons. Indeed at the lowest concentration the amount of provided polyelectrolyte may not be sufficient to ensure full surface coverage, or the interaction between the already deposited polyelectrolyte with the one being deposited is concentration dependent.

Besides, in order to investigate the reasons of different growing regimes at 1×10^{-4} and 1×10^{-3} M in polyelectrolytes concentration, a control experiment was carried out, in which the polyelectrolyte concentration was hold constant but the spraying time was decreased from 10 to 5 s. The lines correspond to the fit of a linear function ($y=ax+b$) where $x=0.59$ nm/deposition step, $b=2.1$ nm and $x=0.70$ nm/deposition step, $b=2.8$ nm were obtained for 5s and 10s spraying time respectively (Figure 4.23). It was found that the growth regime remained linear with only a 15 % increase in slope (0.59 nm per PSP/PAH deposition cycle versus 0.70 nm when the spraying time per polymer is of 5 and 10 s respectively) ie upon doubling the spraying time (Figure 4.23).

This shows that a spraying time of 5 s is almost sufficient to reach steady state film growth for all polyelectrolyte concentrations higher than 1×10^{-4} M. The spraying time of 10s is hence sufficient to reach the maximal amount of deposited polyelectrolytes at 1×10^{-4} M and at higher concentrations.

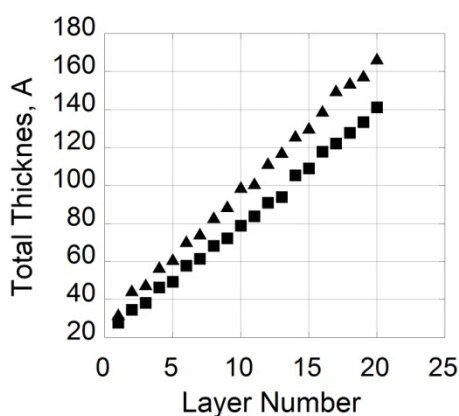


Figure 4.23: Evolution of the average thickness of a PEI-(PSP/PAH)_n deposits with the layer numbers at 1×10^{-4} M in the presence of 0.15 M NaCl at pH 6.7 for spraying time per deposition step: ■ : 5s, ▲ : 10s.

In addition, several experiments were carried out in different spraying modes in order to see the effect of drying on PSP/PAH multilayer deposition (Figure 4.24). The description of the spraying modes are illustrated in Figure 4.24.

It is revealed that drying step is an important parameter in PSP/PAH deposition LbL films and the increasing the contact time with polyion solution results in thicker films.

| | |
|---|--|
| <p>S mode 1</p> <p>t_1:5 s t_2:25 s t_3:15 s (water) t_4:15 s n: 25 Dry after each layer</p> | <p>S mode 2</p> <p>t_1:5 s t_2:25 s t_3:15 s (NaCl) t_4:15 s</p> <p>After n:5 rinsed with water 15s, and waited 15s Dry after each 5 layer pairs. n_{total}:25</p> |
| <p>S mode 3</p> <p>t_1:5 s } Repeated 2 times t_2:25 s } Dry after each 5 layer pairs n_{total}:25</p> <p>t_3:15 s (NaCl) t_4:15 s</p> <p>After n:5 rinsed with water 15s and waited 15s</p> | |

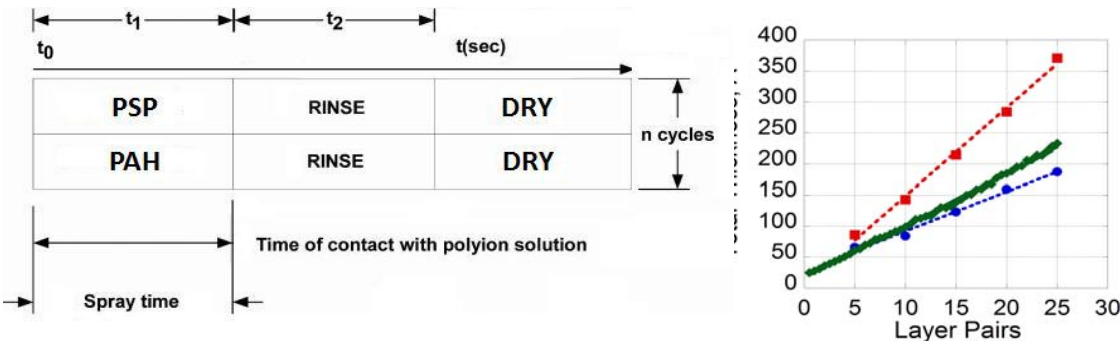


Figure 4.24: Evolution of the thickness of a PEI-(PSP/PAH)_n deposits with the layer numbers at 1×10^{-4} M in the presence of 0.15 M NaCl at pH 6.7 obtained by different spraying conditions given above. (Green: S mode 1, Blue: S mode 2, Red: S Mode 3).

4.3.2 Characterization of PEI-(PSP-PAH)_n multilayer by Atomic force microscopy, AFM, and Grain Size Analysis

The AFM images were taken by Mr. Christophe Contal who is in charge of the AFM laboratory.

Despite of the appearance of interference colors (Figure 4.22), atomic force microscopy (AFM) topographies of PSP/PAH coated surface show that the deposits obtained at 1×10^{-4} M are islandlike which increase in size up without reaching coalescence even after a layer number of at least 150 (Figures 4.22 and 4.25). The

situation is a similar that of observed for polyelectrolyte multilayer films made from chitosan as a polycation and from hyaluronic acid as a polyanion in which the film is initially island-like [93]. However, in this previous investigation the islands coalesce into a smooth film after a few layers and the variable parameter was the concentration of the salt not that of the polyelectrolytes.

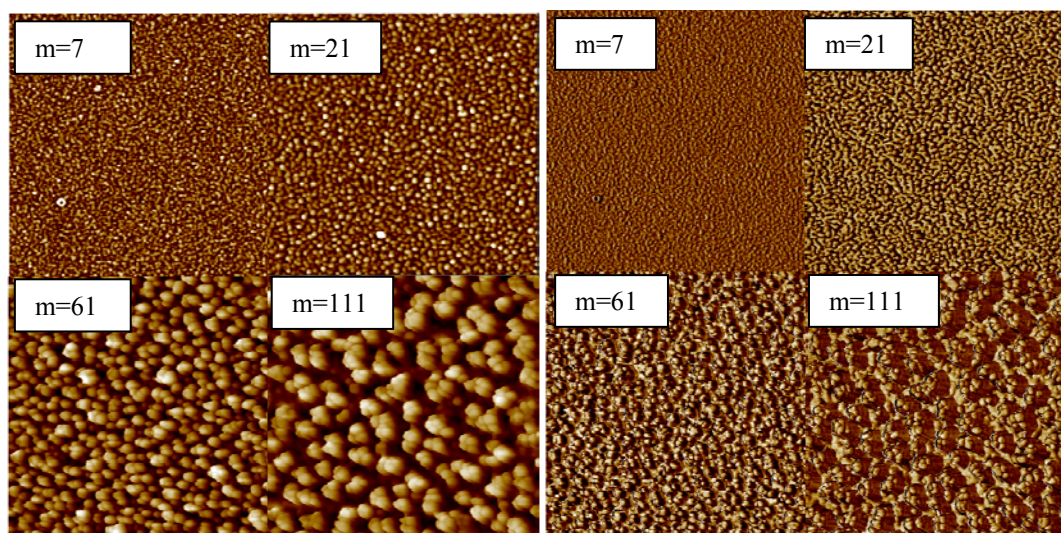


Figure 4.25: (Left) AFM height images, (right) AFM phase images of the surface of PSP/PAH deposits prepared at 1×10^{-4} M polyelectrolyte concentrations, $I = 0.15$ M NaCl, pH:6.7. m represents deposited the number of layers.. The image size is $2 \times 2 \mu\text{m}^2$. The z scales ranges from 0 to 250 nm.

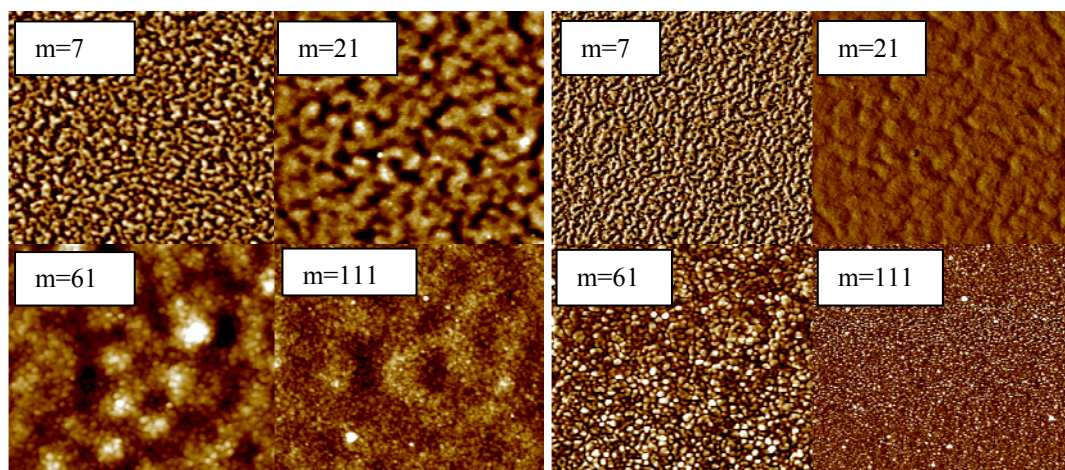


Figure 4.26: (Left) AFM height images, (right) AFM phase images of the surface of PSP/PAH deposits prepared at 1×10^{-3} M polyelectrolyte concentrations, $I = 0.15$ M NaCl, pH:6.70. m represents deposited number of layers. The image sizes are $2 \times 2 \mu\text{m}^2$. The z scales ranges from 0 to 20 nm.

It was obtained that the roughness of the PSP/PAH deposits increases almost linearly as a function of the number of deposition steps and average film thickness.

On the other hand, analysis of the root-mean-square (RMS) roughness of the deposits as a function of the number of deposition steps showed a markedly different behavior depending on the polyelectrolyte concentration. For the deposition experiment performed at $1 \times 10^{-2} \text{M}$ and $1 \times 10^{-3} \text{M}$ in polyelectrolyte, the morphology of the deposits are flat and homogeneous (Figure 4.27). It was observed that the PPS/PAH deposits have the morphology of smooth films at $1 \times 10^{-3} \text{M}$ polyelectrolyte concentration at the same ionic strength and pH (Figure 4.27). The roughness was found to be decreased from ~ 5 to ~ 1 nm at $1 \times 10^{-3} \text{M}$ PPS and PAH, while it increased from ~ 5 to ~ 75 nm at $1 \times 10^{-4} \text{M}$ polyelectrolyte concentration (Figure 4.27).

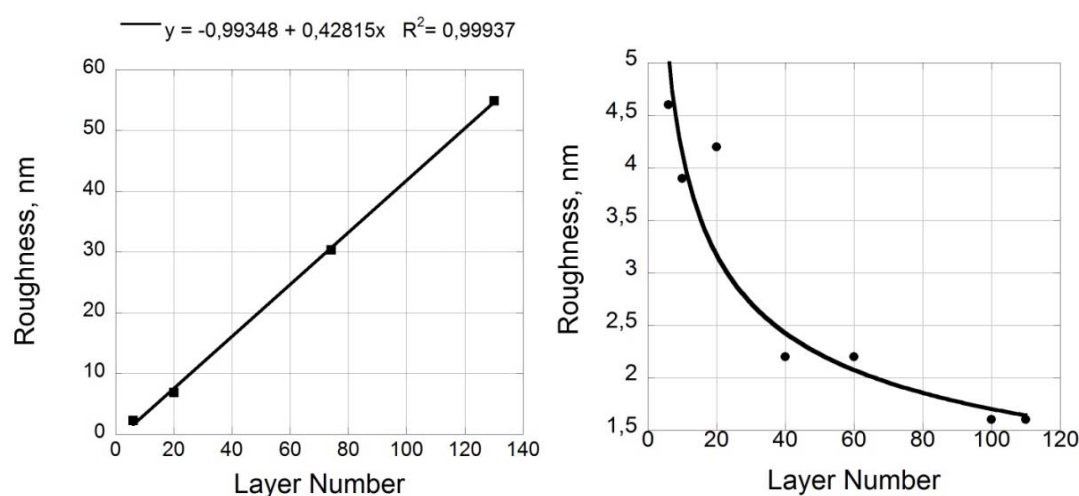


Figure 4.27: Evolution of the RMS roughness determined from AFM topographies as a function of layer number: (left): $1 \times 10^{-4} \text{M}$; (right): $1 \times 10^{-3} \text{M}$ polyelectrolyte concentrations at $I=0.15 \text{M}$ NaCl and $\text{pH}:6.70$.

It has been observed that $1 \times 10^{-4} \text{M}$ in polyelectrolyte, the deposit grows as islands, probably through lateral motion of deposited polyelectrolytes and that the PEI covered substrate is progressively decorated with PSP/PAH complexes. Indeed the adsorption of equilibrated PSP/PAH complexes (prepared 1/1 ratio in bulk at the same concentration as used in the spray deposition) leads to a similar structure, however larger deposited structures. The difference in the obtained grain size could be understood on the basis that the time scale for both experiments are very different: 24 h of aging in solution before deposition whereas the alternated spraying of 150 layer pairs takes around 1 h when the process is not interrupted by intermediate thickness measurements. In addition, the complexes in solutions have a higher number of accessible conformations than those deposited on the substrate by means of alternated spraying. Indeed, in this latter case the polyelectrolyte chains are forced

to diffuse in a quasi bi-dimensional environment and their mobility may be restricted by their interactions with the substrate.

As it is mentioned above, there are examples of supralinear growth LbL processes in which the deposition starts with the formation of islands that progressively coalesce to form an homogeneous film when more polyelectrolytes chains are provided, hence by increasing the number of deposition steps [86, 87, 102]. It can be suggested that a change in PSP and PAH concentration allows to cover the whole repertoire of known LbL film growth mechanisms and that the island growth regime could constitute a new intermediate regime between extremely low mobility (associated with linear growth) and extremely high chain mobility (associated with supralinear-exponential growth).

Besides, the grain size analysis showed that there is a strong linear correlation with the grain sizes and film roughness, the average film thickness, and so deposition number (Figure 4.28). These findings show that the material accumulated at the interface clusters in islands of increasing size hence leading to an increased roughness. These interesting findings, observed for the first time, indicates that the PSP/PAH deposits have an exceptional self-patterning behavior in which the layer number controls the grain size.

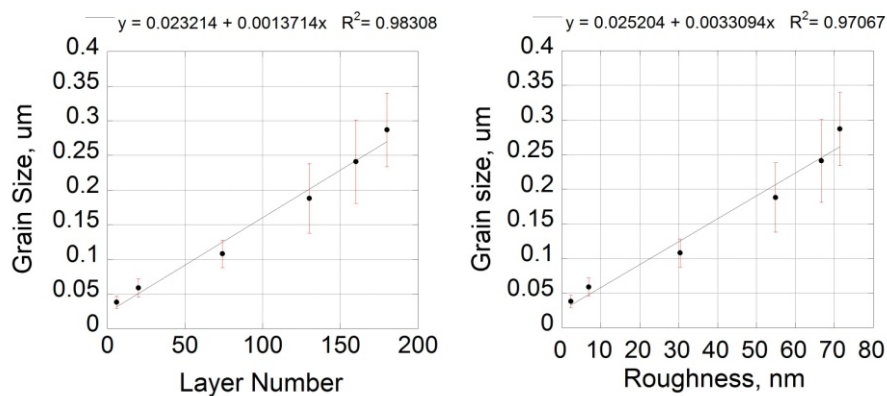


Figure 4.28: Evolution of the average grain size (determined from AFM topographies in Figure 4.26) with the thickness and number of layers given in Figure 4.22. The error bars corresponds to the standard deviation for the size of more than 100 grains measured in each individual image.

The AFM topographies were also obtained for 1×10^{-4} M polyelectrolytes at higher ionic strength ($I=1$ M NaCl). The results showed that increasing the ionic strength

leads to smoother films at the same polyelectrolyte concentrations (Figures 4.29 and 4.30).

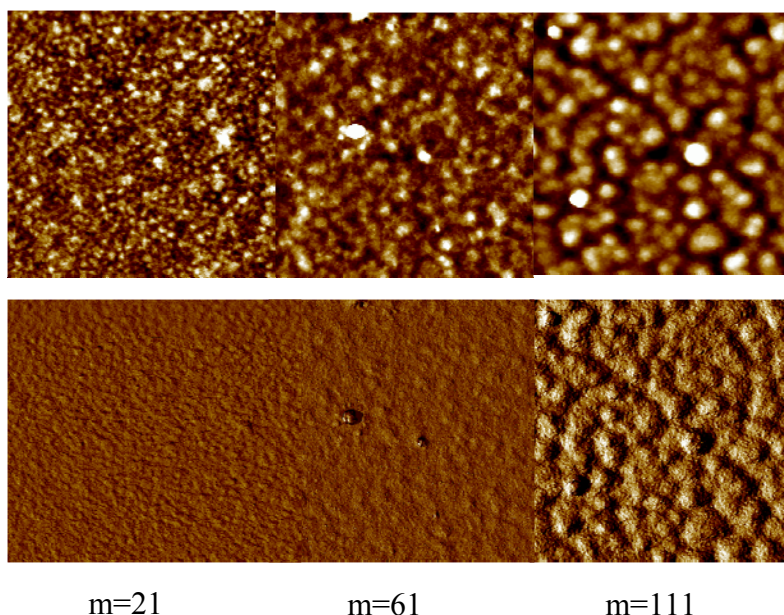


Figure 4.29: (above) AFM height images (below) AFM phase images of the surface of PSP/PAH deposits prepared at $1 \times 10^{-4} \text{ M}$ polyelectrolyte concentrations, $I = 1 \text{ M NaCl}$, $\text{pH}: 6.70$. m represents deposited number of layers. The image size is $2 \times 2 \mu\text{m}^2$. The z scales ranges from 0 to 100 nm.

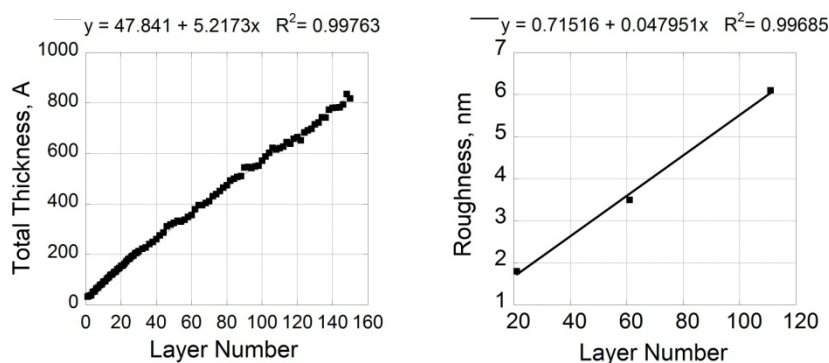


Figure 4.30: (Left) Evolution of the thickness of a PEI-(PSP/PAH) n deposits with the layer numbers (right) evolution of the RMS roughness (determined from the AFM topographies) as a function of deposition step. PSP and PAH are prepared at $1 \times 10^{-4} \text{ M}$, $I = 1 \text{ M NaCl}$ and $\text{pH}: 6.70$.

The surface topography of PSP-Lupamin multilayers were also obtained by AFM in order to compare if the molecular weight of the polycation plays a role in surface morphology. Lupamin was chosen since the structure of the lupamin (Figure 4.31) ($M_w = 10000 \text{ g/mol}$, purchased from BASF), is very similar to PAH but has a lower

polymer molecular weight and one $-\text{CH}_2-$ group less than PAH used the experiments.

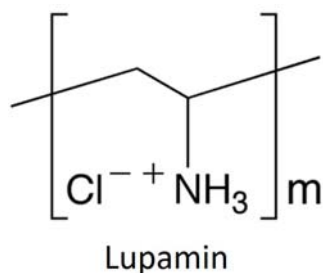


Figure 4.31: Chemical Structure of Lupamin.

PSP-Lupamin complex has deposited by LbL spraying at the same conditions of PSP-PAH complexes as explained in section 3.2.4.2 and 4.3.

It has been observed that the general aspects of the AFM images for PSP/PAH and PSP/Lupamin are the same (Figure 4.32). However, the roughness value for PSP-Lupamin deposits are found as 2.0 nm that is almost 5 nm lower than PSP-PAH deposits at 20th layer number. The lines correspond to the fit of a linear function ($y=ax+b$) where $x=0.59$ nm/deposition step, $b=2.1$ nm and $x=0.16$ nm/deposition step, $b=0.85$ nm were obtained at the same experimental conditions for PSP/PAH and PSP/Lupamin deposits respectively (Figure 4.33) .

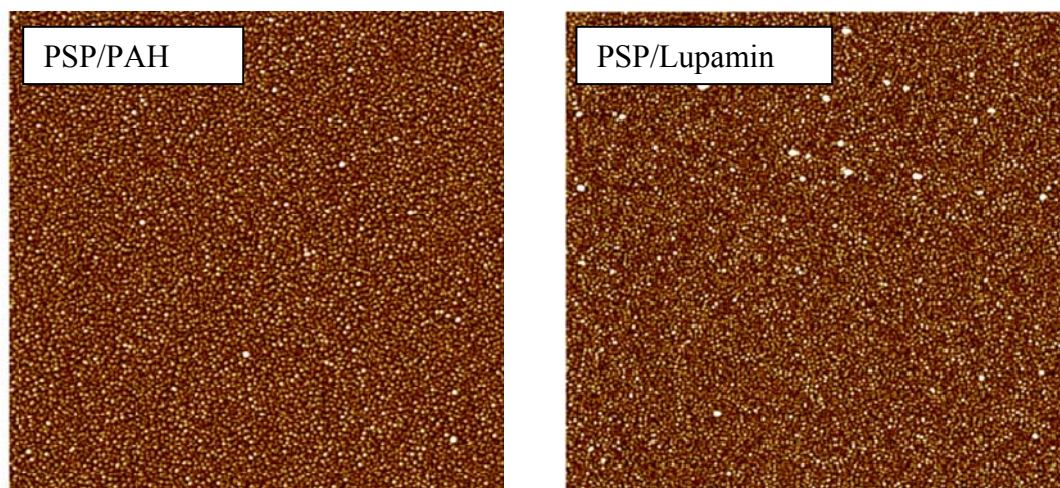


Figure 4.32: AFM height images for the 20th layer of PSP/PAH and PSP/Lupamin deposits prepared at 1×10^{-4} M polyelectrolyte concentrations, $I= 0.15$ M NaCl, pH:6.70. The image size is $5 \times 5 \mu\text{m}^2$. The z scales ranges from 0 to 30 nm.

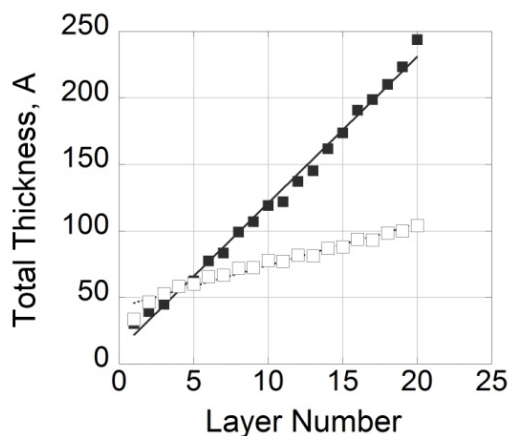


Figure 4.33: Evolution of the average thickness of ■:PEI-(PSP/PAH)_n and □:PEI-(PSP/Lupamin)_n at 1×10^{-4} M polyelectrolyte concentrations, $I = 0.15$ M NaCl, pH:6.70.

4.3.2.1 Decomposition of PSP/PAH deposits

Decomposition of the PSP/PAH complex formed on the solid substrate was investigated by AFM imaging after dipping the PSP/PAH coated slide into NaCl solution.

AFM images were obtained for the PSP/PAH deposited up to layer number of 120 and after dipping of the 120 layered deposited sample into a solution of 0.15M NaCl at pH:6.70 for 1 and 2 hours (Figure 4.34A-C).

The PSP/PAH deposition was carried by LbL spray method at the conditions of 1×10^{-4} M polyelectrolyte concentration $I = 0.15$ M NaCl, pH=6.70 as before. After, it is dipped into 0.15M NaCl solution for 1 hour and then blow-dried with nitrogen. The AFM sample is prepared by carefully cutting the substrate and the total thickness of is measured with ellipsometry. Then, the rest same sample was dipped into a freshly prepared second 0.15M NaCl solution for another 1 hour and the same procedure was carried out.

The small islands like aggregates are still observed on the surface but with a more denser particles. The grain sizes are determined as (0.19 ± 0.05) nm before dipping, (0.32 ± 0.12) nm after 1hour dipping, and (0.40 ± 0.19) nm after 2 hours of dipping, respectively. This results showed that the PSP/PAH deposits swells in salt solution and the roughness of the film is reduced although the decrease in the thickness of the film is negligible amount.

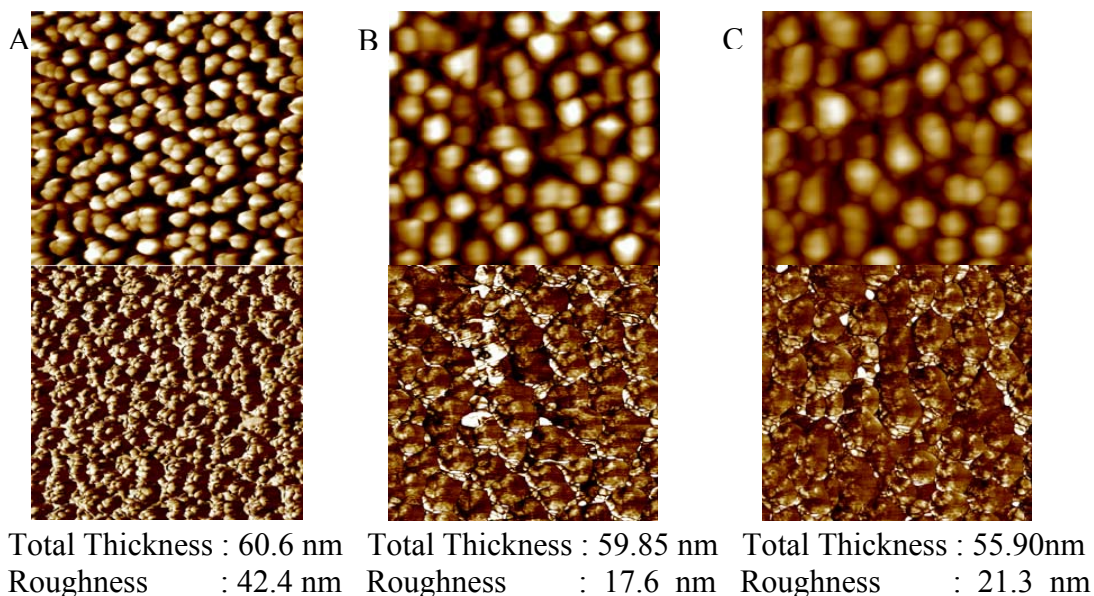


Figure 4.34: AFM height (above) AFM phase images (below) for the surface of PSP/PAH deposits prepared at 1×10^{-4} M polyelectrolyte concentrations, $I = 0.15$ M NaCl, pH:6.70. (A) PSP/PAH deposited up to layer number of 120 and (B) after dipping of the 120 layered deposited sample into 0.15M NaCl for 1 and (C) 2 hours. The image size is $2 \times 2 \mu\text{m}^2$. The z scales ranges from 0 to 200 nm.

4.3.2.2 Optical Microscopy Experiments

The aim of these experiments was to compare the morphology of the deposits obtained from a solution containing 1/1 mixture of PSP and PAH on a PEI coated silicon substrate and with that obtained by alternated spray of the two components in order to demonstrate the complex formation occurs in bulk and at interfaces by the same phenomena.

To try to correlate the build-up process at the solid-liquid interface to the PSP/PAH complexation process in solution, we performed a control experiment in which the PSP/PAH complexes (aged during 24 h in solution) were put in contact with a PEI coated silicon substrates. The obtained deposit exhibited a too large roughness to allow for imaging by AFM owing to the limited displacement of the piezoelectric scanner. Therefore, optical microscopy experiments were carried out on the same sample (Figure 4.35).

It appears clearly that the surface is covered by micrometer sized islands which are bigger than about a factor of 5 than the islands obtained after 150 alternated spraying steps of PSP-PAH (given section 4.3.1 and 4.3.2, Figures 4.25 and 4.28). The

analogy between the structures obtained in solution (micrometer sized aggregates) and those obtained after alternated spraying (around 300 nm) is only compared qualitatively (Figure 4.35).

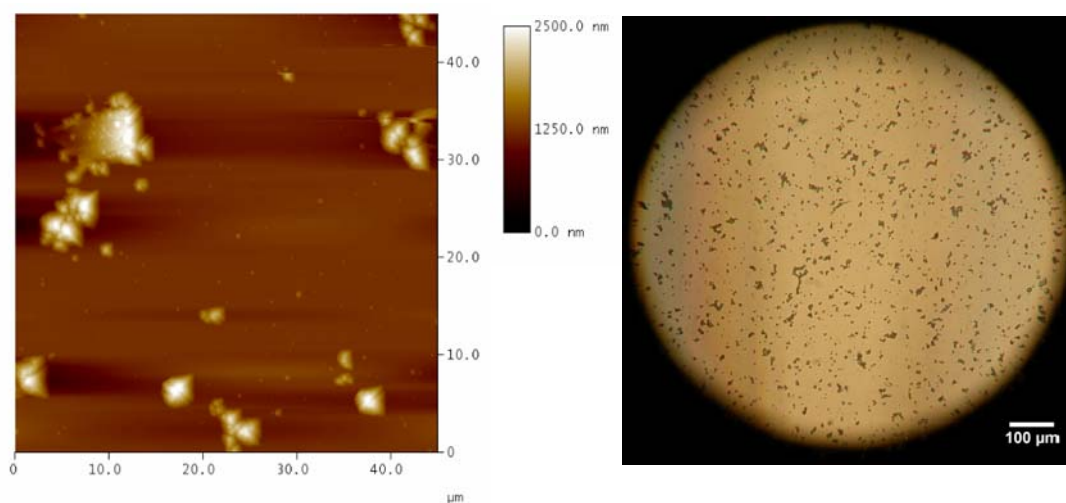


Figure 4.35: (left) AFM images (right) Optical microscop images for the PSP/PAH complex adsorbed on a silicon wafer after. 1:1 mol ratio of PSP/PAH complex prepared and PEI coated wafer was dipped for 24 hours into 0.15M NaCl solution. Total Thickness: (51.70 ± 0.17) Å.

4.3.3 Zeta potential measurement of PEI-(PSP-PAH)_n multilayers on glass substrate

This work is carried out in the International Center for Frontier Research in Chemistry Laboratory, INSERM UMR 977 with the assistance of technician Mr. Christian.

As it is mentioned in section 4.3.1 deviation from the linearity almost after 120 layers at the conditions of 1×10^{-4} M was observed and as a matter of fact, the different deposition experiments at the same conditions carried out independent from each other showed that the deviation was not due to the parameters which controls the deposition process. In order to understand the reason behind the particle size increase at interface as a function of layer number despite a deviation that is seen, always, at the same number of deposition cycle, streaming potential measurements at the interface of PSP/PAH multilayers were carried out.

The glass slides, never used before LbL spray coating, were cleaned in a 2 % (v/v) Hellmanex (Hellma GmbH, Germany) solution at 70°C during half an hour,

extensively rinsed with Milli Q water, immersed in a hot (70°C) 0.1 M hydrochloric acid solution, rinsed again with Milli-Q water and blown dry with nitrogen.

These experiments are aimed to define if the LBL deposition follows the regular charge inversion which is usually observed during the alternated deposition of polycations and polyanions.

As long as the ζ potential was positive (i.e., for $m=75$), the ζ potential continuously decreased with increasing layer number at the condition of 1×10^{-4} M polyelectrolytes. When the ζ potential approached zero, an instability occurred with respect to the previously regular film growth (Figure 4.36, left). The experiment related with the right hand side of the Figure 4.36 was carried out by one of my friend, Mrs. Francine Valenga, who is also in the research group of Prof. Gero Decher, during my absence in France.

It is revealed that drying step is an important parameter in PSP/PAH deposition LbL films and the increasing the contact time with polyion solution results in thicker films.

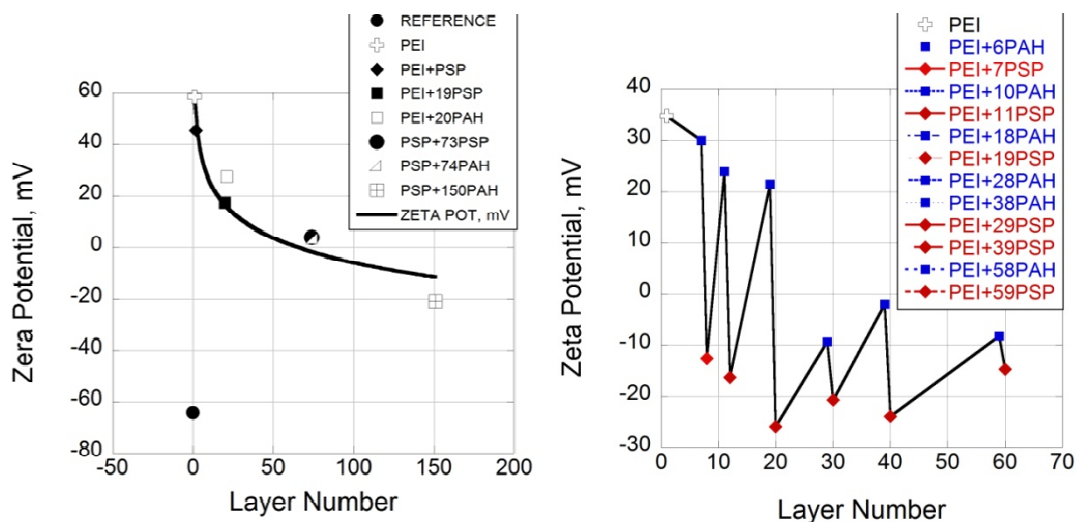


Figure 4.36: Evolution of the ζ potential (mV) during the alternated deposition of PSP and PAH layers at $I= 0.15$ M NaCl, pH:6.70 as a function of the layer number (left): for 1×10^{-4} M, (right): 1×10^{-3} M PSP/PAH concentration. Red: correspondes to PSP last layer, Blue corresponds to PAH ended last layer.

After ζ reached a plateau value of about -20 mV after 150-200 deposition steps, the film growth continued with approximately the same slope as observed at small layer numbers (Figure 4.36). It should be noted that the spray deposition of poly(styrene sulfonate) and PAH under identical conditions led as expected to an alternation of the

ζ potential between positive and negative values [73, 83, 93, 139, 142, 143, 147]. In fact, a surface charge reversal as well as the deposition of islands observed during the deposition of the first "layers" in a previous study where chitosan and HA were used as polyelectrolytes [93].

This is an interesting example of a growth process in which the zeta potential does not alternate whose sign is normally expected to correspond to the sign of the charge of the polyelectrolyte adsorbed as the last layer. Hence, It is an interesting example of film growth process in which the chains of the polycation PAH can adsorb onto a surface with a macroscopically positive ζ -potential.

The zeta potential is found to be changing from positive to negative value for the small layer number ($m < 20$) at the conditions of $1 \times 10^{-3} M$. This indicates that each newly deposited layer leads to an overcompensation of the previous charge as has been observed for other polyanion/polycation couples before. After layer number of 20 the sign of the zeta potential does not alternate but it can be said that the overcompensation occurs regarding as the relatively decrease in the potential value. It is an interesting result that the zeta potential reaches almost a zero value at the layer number of 40 in which the AFM topographies and ellipsometry data at this stage showed that there is PSP/PAH deposits on the surface with an average thickness of 100 nm (Figures 4.22, 4.25, and 4.27) having 2.2 nm roughness. The AFM images for the layer number of 40 is given in Figure 4.37.

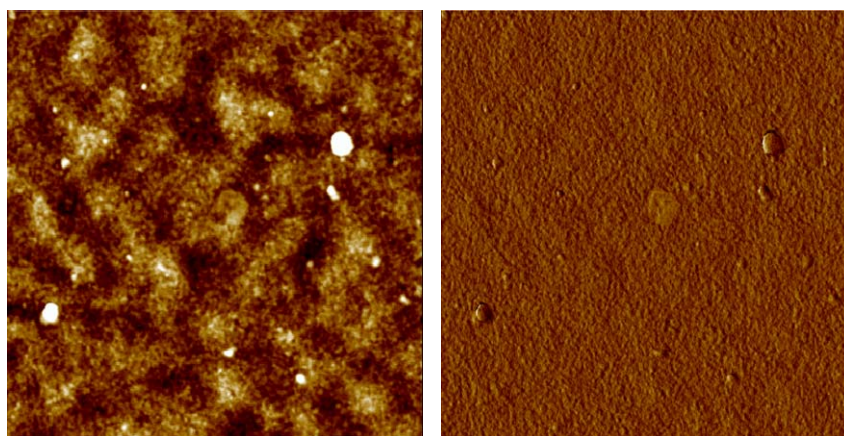


Figure 4.37: AFM image obtained after layer PEI-(PSP/PAH)₄₀. For both images, the dimensions are $5 \times 5 \mu m^2$. (left:height, right:phase mode images).

The adsorption of a polyelectrolyte onto a surface of the same sign is exotic but has been observed previously [147, 148] This indicates that interactions other than

electrostatic ones contribute to the buildup of the multilayer deposit and/or that dynamic structural changes occur in the polyelectrolyte complexes on the surface. These assumptions are in good agreement with the bulk studies given in section 4.2. Possible explanations for this phenomenon include unusually strong hydrogen bonding and/or nanoscale heterogeneities in the ζ potential. Such heterogeneities could for example arise from the growth of negatively charged islands on the initial layer of cationic poly(ethylene imine). This would suggest that the unusual growth process at $1 \times 10^{-4} \text{M}$ may be substrate-dominated and thus restricted to zone I in the three-zone model for multilayer growth, whereas at higher concentrations a more regular film growth is observed. Even, the development of islands growing to sizes of more than 300 nm without coalescing into a continuous film is probably due to a permanent structural reorganization of the deposit allowing for the accumulation of both PAH and PSP.

Note that, the zeta potential of the complexes (24 h after mixing) and the zeta potential of the film after the deposition of 150 layers is found almost in the same range (Figures 4.16 and 4.35). Therefore, it can be assumed that PSP and/or the PAH chains are so mobile on the solid substrate. The mobility of the polyelectrolyte chains on the solid substrate may originate from the huge difference in size between PSP (average degree of polymerization of 24) and PAH. Unfortunately, there is no water soluble PSP of high degree of polymerization that is available to validate or invalidate this assumption.

At higher concentration in polyelectrolytes, the mobility of the chains may become higher because of entropic reasons. This mechanism would allow the transition from the observed "linear" increase in thickness to the supralinear regime (and the formation of an homogeneous film).

It can be concluded that evolution of the PEI-(PSP-PAH)_n deposits and PSP/PAH complex formation occurs in the same range both in bulk and in LbL deposition in which the complexation process can even be interrupted by drying and the kinetically trapped states can be investigated.

5. CONCLUSIONS

Most of the polyanions as charged moieties used in polyelectrolyte multilayer films up to now were carboxylates, sulfates or sulfonates, but to our knowledge, no investigations have been done on with polyphosphates, which display interesting behavior due to being an interesting water soluble, integral type of inorganic, anionic polyelectrolyte with some unique properties concerning its interactions with positively charged species [16, 20-24]. There is a large gap in the literature, which involves the interaction between the polyions having low and high degree of polymerization. Therefore, in this study poly (sodium phosphate), PSP, with a degree of polymerization, $n=24$ and poly (allylamine hydrochloride), PAH, having a higher molecular weight (56000 g/mol) were chosen as polyanion and polycation, respectively.

Both used polyelectrolytes, PSP and PAH, were carefully characterized and the complex formation between PSP and PAH in bulk and with those of a PEC formed at close-to-identical conditions at an interface (multilayer film) were compared in order to work out the fundamental differences and similarities between such systems.

The complexation was investigated by conductometry, viscosimetry, spectroscopy, isothermal titration microcalorimetry, dynamic light scattering, zeta potential determination methods depending on different parameters, such as: concentration of polyions, ionic strength and pH in the bulk solution. PSP/PAH complex formation at interface was carried out mostly by LbL spray-deposition with the identical parameters as in bulk studies, and the behavior of the complex at interface is examined by ellipsometry, AFM, zeta potential and optical microscopy techniques.

It is observed that the stoichiometry of PSP/PAH complex in bulk is close unit mol ratio but excess of PSP or PAH is present in several conditions. The deviation from 1:1 mol ratio depends on polyion concentration, ionic strength and pH. Errors associated with the losses in transference might cause the deviation from unit mol ratio. Besides, the unreacted fraction of one polyion might also react with the free fraction of polyions of opposite sign, leading to departures from stoichiometry.

The decreased and increased curves obtained during the conductometric titration in the presence of low molecular salt is due to the formation of small aggregates, coulombic screening by the counterions and subsequent increase of solution viscosity. It is also assumed that the change in viscosity is due to the transition from a more extended conformation of the polyelectrolyte chains to a more coiled up conformation. This transition might be caused by intramolecular hydrophobic interactions in bulk. This approach will be examined in details in the forthcoming studies. The increase of reduced viscosity at higher salt concentration might also be attributed to intrachain interaction due to the counterion condensation on the chains leading to charge overcompensation.

It is observed that there is a counter ions releasing after the complex has been formed and the PSP/PAH complexation is very dynamic. The continuous counter ion releasing is due to the rearrangement of the complex particles during complexation. It can be assumed that PSP and/or the PAH chains are so mobile that PSP/PAH complex particles might go under rearrangement during complexation leading to the charge increase in the specific conductance. The same assumption is suggested by Kotz et al [27] in which they studied with acryl-based polyelectrolytes of different chain length, however, their model for the structural rearrangement is not demonstrated. They suggested that dominating influence on structural changes is considered to be mainly caused by differences in overall structural charge density of the particles and also some differences in the chain loops and chain end surface structure. These results are in good agreement with time dependent dynamic light scattering and zeta potential experiments in bulk and at interfaces. The results showed that PSP/PAH complex formation is very dynamic, close to equilibrium, and order of the addition either polyion to form the complex does not effect complexation [20-24].

Besides, isothermal titration microcalorimetry results showed that the time required to reach the equilibrated complex is not is, indeed, an very long. Therefore, PSP/PAH complexation is extremely slow process and equilibrium was not reached even after a few hours. However, the addition of excess of any polyelectrolyte once the PSP/PAH complex formed was negligible in terms of thermodynamic properties, and PSP/PAH complexation is very dynamic. The time dependent PSP/PAH complexation experiments carried out by conductometry, viscometry and dynamic

light scattering at the identical conditions and parameters parallel to microcalorimetry experiments confirmed this findings.

The PSP/PAH complex prepared in 1:1 mol ratio by mixing of PSP and PAH reaches a negative zeta potential of about -15 to -20 mV after around 24 hours of equilibration. In addition, it was found that the complexes formed in solution upon mixing PSP and PAH in a 1/1 molar ratio display a slow increase in their size (up to 2.5 μm at the same time scale after the PSP mixing with PAH) and a reversal in their zeta potential from a positive to a negative value. It is assumed that when the charge provided by one of the polyelectrolyte is sufficient to neutralize the surface of the other particle, the particles have strong tendency to form aggregates of particles. The particle size increases due to non-homogeneous overcompensation of surface charge.

These results also indicate that interactions other than electrostatic ones (in forthcoming studies) might contribute the complex formation in bulk and in the building up of the multilayer deposits so that dynamic structural changes occur in both cases.

It was demonstrated that an PSP/PAH multilayer growth regime can be controlled by the polyelectrolyte concentration. The increase in PSP and PAH concentration allowed for a progressive transition from linear growth to a supralinear. Besides, a two linear growth regimes with a transition between has been observed at $1 \times 10^{-2}\text{M}$ and $1 \times 10^{-3}\text{M}$. This transition might be due to the mobility of higher PE chains because of entropic reasons. In literature, there are some studies in which a transition between two linear growth regimes is observed [73, 86, 87, 93, 104, 106-109.] The suggestion of these authors for the reason of transition is the rearrangement of the film and gradual densification of the layers. Restructuring and densification forbids the diffusion of one of the polyelectrolytes over a part of the multilayer matrix so that the film becomes progressively less and less penetrable. However, the direct proof of film restructuring has been still unknown.

A very interesting point to be noted in this study is that the ellipsometric thickness increases linearly with the number of deposited layers (at $1 \times 10^{-5}\text{M}$ and $1 \times 10^{-4}\text{M}$ in each polyelectrolyte) which would indicate to make the assumption that a regular LbL film is deposited. It was observed that the film growth seems to be linear at the lowest concentrations ($1 \times 10^{-5}\text{M}$ and $1 \times 10^{-4}\text{M}$) and can be fitted by an exponential

growth at $1 \times 10^{-3} \text{M}$; the combination of an exponential growth followed by a linear one has been observed at $1 \times 10^{-2} \text{M}$. Furthermore, it is revealed that drying step is an important parameter in PSP/PAH deposition LbL films and the increasing the contact time with polyion solution results in thicker films.

The linear growth at small polyelectrolyte concentration was not due to kinetic limitations related to insufficient spraying time but an intrinsic property of the used PSP and PAH. The most interesting finding is that the linear increase in the deposit thickness is not accompanied by the deposition of a film but the deposition of islands whose average diameter grows in proportion to the average film thickness without coalescing into a continuous film. Despite of the appearance of optical interference colors, AFM topographies show that the islands increase in size up to a layer number of at least 150 deposits at $1 \times 10^{-4} \text{M}$.

The alternated deposition for 10^{-4}M polyion concentration does not lead to alteration in the zeta potential as it is, usually, observed for the regular LbL films. It decreases monotonously from the zeta potential value of PEI which is the first layer on the glass slide, to around -21 mV . Note that, the zeta potential of the complexes (24 hours after mixing) and the zeta potential of the film after the deposition of 150 layers is found almost in the same range. Therefore, it can be assumed that PSP and/or the PAH chains are so mobile on the surface and that the PEI-(PSP-PAH)_n deposits evolve on the surface in a similar manner to the complexes in solution. The mobility of the polyelectrolyte chains on the solid substrate may originate from the huge difference in the chain length of PSP and PAH.

On the other hand, although the roughness increases almost linearly with the average thickness at $1 \times 10^{-4} \text{M}$ concentration of polyelectrolytes, the deposits have the morphology of smooth films at the $1 \times 10^{-3} \text{M}$ polyion concentrations.

These findings allowed us to propose a model in which the deposit builds by progressive accumulation of PSP and PAH accompanied by their lateral diffusion to build up complexes that would correspond to a minimal free energy of the PSP/PAH system in these conditions (Figure 5.1)

Our assumption that the deposit growth is related to a diffusion process leading to formation of PSP and PAH complexes at the interface may also explain the transition from a linear increase in the average film thickness. In this study, a new growth

regime of deposits is discovered in which deposition of islands growth without coalescing up to a very high number of deposition steps has been observed. This findings are in opposition to the coalescence of the islands after only a few deposition steps observed in some exponential growth processes in literature [93]. The existence of this growth regime forces researchers in the field of LbL deposition of so called polyelectrolyte "multilayers" to be extremely cautious in the denomination of their coatings.

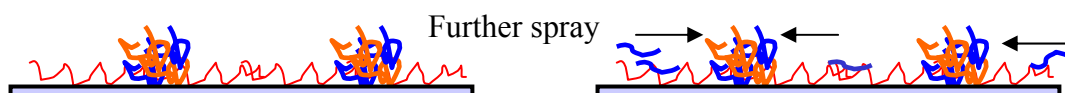


Figure 5.1: Proposed build-up mechanism of PEI-(PSP-PAH)_n deposits prepared by alternated spray deposition. The arrows are aimed to represent quasi 2D diffusion of the polyelectrolyte chains.

Note that Adusumilli and Bruening [149] found that the zeta potential of [poly(diallyldimethyl ammonium)-poly(4-styrene sulfonate)]_n deposits becomes permanently positive after the deposition of 14-15 "layer pairs" whatever the nature of the last deposited layer even if the film continues to grow (in an exponential manner. However, it was postulated, and many findings confirmed [73, 83, 93, 139, 142, 143, 147] that a reversal of surface charge is mandatory to get deposition. Therefore, the findings in this study points out that this assumption is not valid and should be seriously questioned.

As a consequence, the dimensions of the nanoscale pattern are obtained as a function of the number of deposition cycles. The evolution of the PEI-(PSP-PAH)_n deposits and PSP/PAH complex formation occurs in the same range both in bulk and in LbL deposition in which the complexation process can be interrupted by drying and the kinetically trapped states are investigated.

The most important results of this work is to obtain self-patterning polyelectrolyte multilayers which are described for the first time using polyphosphates.

5.1 Future Perspectives

The kind of observed island growth found in this study could have very interesting applications. Indeed, the progressive increase in grain size and the apparent existence of different scales of roughness could allow to design super-hydrophobic

coatings [150-152], bio-active surfaces (transfection, bio-sensors, separation of proteins), bio-remediation surfaces [36, 41, 46, 49, 108, 153], and polyphosphate functions in living organisms [110, 121, 123].

Besides, the results of PSP/PAH system in the bulk solution might be a model system for the reactions between the natural polyions in the eukaryot and prokaryot organisms.

Moreover, it will be more interesting to give a scientific explanation to demonstrate the core/shell structure of colloidal particles in the bulk solution using PSP/PAH system [27].

A part of the result related with the complexation at interface has already been published in Journal of American Chemical Society as short communication and a print copy of it is given at the end part of thesis. The results related with the complex formation in bulk solution is in preparation for publication as well.

REFERENCES

- [1] **Decher, G.; Schlenoff, J. B.**, (eds) 2003. *Multilayer Thin Films-Sequential Assembly of Nanocomposite Materials*, Wiley-VCH.
- [2] **Dubin, P; Bock, J.; Davies, R. M.; Schulz, D. N.; Thies, C;** (eds) 1994. *Macromolecular Complexes in Chemistry and Biology*, Springer – Verlag.
- [3] **Koetz, J.; and Kosmella, S.**,(eds) 2007. *Polyelectrolytes and Nanoparticles*, Springer – Verlag.
- [4] **Micheals, A. S., Miekka R. G.**, 1961. Polycation-Polyanion Complexes of Poly-(Vinylbenzyltrimethylammonium) Poly-(Styrenesulfonate), *J. Phys. Chem.*, **65 (10)**, 1765-1773.
- [5] **Fuoss, R. M. and Sadek, H.**, 1949. Mutual interaction of polyelectrolytes, *Science.*, **110**, 552-554.
- [6] **Kossel, A.**, 1896. Ueber die basischen Stoffe des Zelikerns, *J. Phys. Chem.* **22**, 176–187.
- [7] **Tsuchida, E., Abe, K.**, 1982. Interactions between macromolecules in solution and intermacromolecular complexes., *Adv. Polym. Sci.*, **45**, 1–119.
- [8] **Tsuchida, E.**, 1980. Formation of interpolymer complexes. *J. Macromol. Sci. Part .*, **17**, 683–714.
- [9] **Tsuchida, E., Osada, Y., Abe, K.**, 1974. Formation of polyion complexes between polycarboxylic acids and polycations carrying charges in the chain backbone, *Makromol. Chem.*, **175**, 583–592
- [10] **Bekturov, E. A., Bimendina, L.A.**, 1981. Interpolymer complexes., *Adv. Polym. Sci.*, **41**, 99–147.
- [11] **Nakajima, J.**, 1980. Formation of polyelectrolyte complexes. *J. Macromol. Sci. Part B* **17**, 715–721.
- [12] **Dautzenberg, H., Hartman, J., Grunewald, S., Brand, F.**, 1996. Stoichiometry and structure of polyelectrolyte complex particles in dilute solutions, *Phys. Chem.*, **100**, 1024-1032.
- [13] **Dautzenberg, H., Karibyants, N.**, 1999. Polyelectrolyte complex formation in highly aggregating systems. Effect of salt: response to subsequent addition of NaCl, *Macromol. Chem. Phys.*, **200**, 118–125.
- [14] **Overbeek, J.T.G.; Voorn, M.J.J.**, 1957. Phase separation in polyelectrolyte solutions. Theory of complex coacervation, *J. Cell. Comp. Physiol.* **49**, 7–26.
- [15] **Bungenberg de Jong, H.G.**, in: **H.R. Kruyt (Ed.)**, 1949. Colloid Science, vol. II, Elsevier Publishing Company, Amsterdam, , pp. 335–384.

- [16] **Kabanov, V. A. and Zezin, A. B.**, 1985. Soluble interpolymeric complexes as a new class of synthetic polyelectrolytes., *Pure Appl. Chem.*, **56**, 343-354.
- [17] **Kabanov, V.A., Zezin, A.B., Izumrudov, V.A., Bronich, T.K., Bakeev, K.N.**, 1985. Cooperative interpolyelectrolyte reactions. *Makromol. Chem. Suppl.*, **13**, 137–155.
- [18] **Izumrudov V. A., Bronich T. K., Saburova O. S. Zezin A. B., Kabanov V. A.**, 1988. The influence of chain length of a competitive polyanion and nature of monovalent counterions on the direction of substitution reaction of polyelectrolyte complexes., *Makromol. Chem., Rapid Commun.*, **9**, 7-12.
- [19] **Kabanov, V. A. et al.**, 1981. A new family of crystallizable polyelectrolyte complexes., *Macromol. Chem. Rapid Commun.*, **2**, 343-346.
- [20] **Acar, N. and Tulun, T.** 1996. Studies on the Interaction of Poly(4-vinylpyridiniumchloride) with Poly(sodiumphosphate) in an Aqueous Solution by Conductometry, *J. Polym. Sci. Part:A, Polymer Chemistry*, **34(11)**, 1251-1260.
- [21] **Acar, N.; Huglin, M. B.; Tulun, T.**, 1999. Complex formation between poly(sodium phosphate) and poly(4-vinylpyridinium chloride) in aqueous solution, *Polymer*, **40**, 6429 -6435.
- [22] **Acar, N. and Tulun, T.**, 2001. Interactions of polymer-small molecule complex with cupric (II) ions in aqueous ethanol solution, *European Polym. J.*, **37**, 1599-1605.
- [23] **Acar, N. and Tulun, T.**, 2001. Investigation of interaction between poly(sodium phosphate) and p-aminobenzoic acid, hydrochloride, *European Polym. J.*, **37**, 651-657.
- [24] **Gun, H.**; 1990. Ms. Sci Thesis, Studies on polyelectrolyte properties of polyphosphates.
- [25] **Philipp, B.; Dautzenberg, H.; Linow, K.J.; Koetz, J.; Dawydoff, W.**, 1989. Polyelectrolyte complexes—recent developments and open problems., *Progr. Polym. Sci.* **14**, 91–172.
- [26] **Izumrudov, V. A.**, 2007. Polyelectrolyte Complexes of Carboxyl-Containing Polyanions: Stabilization of Complexes in Neutral and Weakly Acidic Media and Factors Affecting This Phenomenon? *Polymer Science, Ser. A*, **49**, 456–462.
- [27] **J. Koetz, J.; B. Philipp, B.; Sigitov, V.; Kudaibergenov, S.; Bekturov, E.A.**, 1988. Amphoteric character of polyelectrolyte complex particles as revealed by isotachopheresis and viscometry, *Colloid Polym Sci*, **266**, 906-912.
- [28] **Krotovaa, M. K. et al.**, 2009. The Effect of a Low Molecular Mass Salt on Stoichiometric Polyelectrolyte Complexes Composed of Oppositely Charged Macromolecules with Different Solvent Affinities, *Polymer Science, Ser. A*, **51(10)**, 1075–1082.

- [29] **Kovacevic, D.; Borkovic, S.; Pozar, J.**, 2007. The influence of ionic strength, electrolyte type and preparation procedure on formation of weak polyelectrolyte complexes, *Colloids and Surfaces A: Physicochem. Eng. Aspects*, **302**, 107–112.
- [30] **Viktoria, M. and Radeva, T.**, 2007. Effect of chain length and charge density on the construction of polyelectrolyte multilayers on colloidal particles, *Journal of Colloid and Interface Science*, **308**, 300–308.
- [31] **Izumrudov, V. and Sukhishvili, S. A.**, 2003. Ionization-Controlled Stability of Polyelectrolyte Multilayers in Salt Solutions, *Langmuir*, **19 (13)**, 5188–5191.
- [32] **Kovacevic, D.; van der Burgh, S.; de Keizer, A.; Cohen, S. M. A.**, 2002. Kinetics of Formation and Dissolution of Weak Polyelectrolyte Multilayers: Role of Salt and Free Polyions, *Langmuir*, **18**, 5607–5612.
- [33] **Dragan, E.S., Schwarz, S.**, 2004. Polyelectrolyte complexes. VI. Polycation structure, polyanion molar mass, and polyion concentration effects on complex nanoparticles based on poly(sodium 2-acrylamido- 2-methylpropanesulfonate), *J. Polym. Sci. A: Polym. Chem.*, **42**, 2495–2505.
- [34] **Thunemann, A. F.; Muller, M.; Dautzenberg, H.; Joanny, J.-F.; Lowen, H.**, 2004. Polyelectrolytes with defined molecular architecture II., *Adv. Polym. Sci.* **166**, 113–171.
- [35] **Seyrek, E.; Dubin, P. L.; Tribet, C.; Gamble, E. A.**, 2003. Ionic Strength Dependence of Protein-Polyelectrolyte Interactions, *Biomacromolecules*, **4**, 273–282
- [36] **Leclercq, L., Boustta, M., Vert, M.**, 2003. A physicochemical approach of polyanion-polycation interactions aimed at better understanding the in vivo behavior of polyelectrolyte-based drug delivery and gene transfection., *J. Drug. Target.*, **11**, 129–138.
- [37] **Etrych, T., Leclercq, Laurent., Boustta, M., Vert, M.**, 2005. Polyelectrolyte complex formation and stability when mixing polyanions and polycations in salted media: A model study related to the case of body fluids., *Eur. Jour. Pharm. Sci.*, **25**, 281–288.
- [38] **Pearson, C., Nagel, J.; Petty, M. C.**, 2001. Metal- Ion Sensing Using Ultrathin Organic Films Prepared by the Layer-by-Layer Adsorption Technique, *J. Phys. D, Appl. Phys.*, **34**, 285–291.
- [39] **Decher, G., and Schmitt, J.**, 1992. Fine - Tuning of the Film Thickness of Ultrathin Multilayer Films Composed of Consecutively Alternating Layers of Anionic and Cationic Polyelectrolytes, *Progr. Colloid Polym. Sci.*, **89**, 160–164.
- [40] **Decher, G.**, 1997. Fuzzy Nanoassemblies: Toward Layered Polymeric Multicomposites., *Science*, **277**, 1232–1237.

- [41] **Decher, G.; Lehr, B.; Lowack, K.; Lvov, Y.; Schmitt, J.**, 1994. New Nanocomposite Films for Biosensors: Layer-by-Layer adsorbed Films of Polyelectrolytes, Proteins or DNA, *Biosens. Bioelectron.*, **9**, 677–684.
- [42] **Decher, G.; Hong, J.-D.; Schmitt, J.**, 1992. Buildup of Ultrathin Multilayer Films by a Self-Assembly Process: III. Consecutively Alternating Adsorption of Anionic and Cationic Polyelectrolytes on Charged Surfaces, *Thin Solid Films*, **210/211**, 831–835.
- [43] **Ono, S. S. and Decher G.**, 2006. Preparation of Ultrathin Self-Standing Polyelectrolyte Multilayer Membranes at Physiological Conditions Using pH-Responsive Film Segments as Sacrificial Layers, *Nano Lett.*, **6(4)**, 592-598.
- [44] **Ramsden, J. J.; Lvov, Y. M.; Decher, G.**, 1995. Determination of optical constant of molecular films assembled via alternate polyion adsorption, *Thin Solid Films*, 254,246-251.
- [45] **M. Eckle and G. Decher.**, 2001. Tuning the Performance of Layer-by-Layer Assembled Organic Light Emitting Diodes by Controlling the Position of Isolating Clay Barrier Sheets, *Nanoletters*, **1**, 45-4.
- [46] **Wong, Y. S.; Pelet, J. M.; Putnam, D.**, 2007. Polymer systems for gene delivery—Past, present, and future, *Prog. Polym. Sci.*, **32**, 799–837.
- [47] **Izquierdo, A.; Ono, S. S.; Voegel, J.-C.; Schaaf, P.; Decher, G.** 2005. Dipping versus Spraying: Exploring the Deposition Conditions for Speeding Up Layer-by-Layer Assembly, *Langmuir*, **21**, 7558-7567.
- [48] **Ariga, K.; Hill, K. P.; Ji, Q.**, 2007. Layer-by-layer assembly as a versatile bottom-up nanofabrication technique for exploratory research and realistic application, *Phys. Chem. Chem. Phys.*, **9**, 2319–2340.
- [49] **Tang, Z.; Wang, Y.; Podsiadlo, P.; Kotov, A. N.**, 2006. Biomedical Applications of Layer-by-Layer Assembly: From Biomimetics to Tissue Engineering, *Adv. Mater.*, **18**, 3203–3224.
- [50] **Zhang, X.; Chen, H.; Zhang, H.**, 2007. Layer-by-layer assembly: from conventional to unconventional methods, *The Royal Society of Chemistry, Chem. Commun.*, 1395–1405
- [51] **Laschewsky, A.; Wischerhoff, E.; Denzinger, E.; Ringsdorf, H.; Delcorte, A.; Bertrand, P.**, 1997. Molecular recognition by hydrogen bonding in polyelectrolyte multilayersP. *Chem.Eur. J.*, **3**, 34–38.
- [52] **Blodgett, K. B., and Langmuir, I.**, 1937. Build-Up Films of Barium Stearate and Their Optical Properties, *Phys. Rev.*, **51**, 964–982.
- [53] **Blodgett, K. B.**, 1934. Monomolecular Films of Fatty Acids on Glass, *J. Am. Chem. Soc.*, **56**, 495.
- [54] **Kuhn, H., and Möbius, D.**, 1971. Systeme aus Monomolekularen Schichten – Zusammenbau und chemisches Verhalten, *Angew. Chem.*, **83**, 672–690.
- [55] **Kuhn, H.**, 1981. Information, electron and energy transfer in surface layers., *Pure and applied Chemistry*, **53**, 2105-2122.

- [56] **Nuzzo, R. G., and Allara, D. L.**, 1983. Adsorption of bifunctional organic disulfides on gold surfaces, *J. Am. Chem. Soc.*, **105**, 4481-4483.
- [57] **Iler, R. K.**, 1966. Multilayers of Colloidal Particles, *J. Colloid Interface Sci.*, **21**, 569–594.
- [58] **Winterton et al.** 1999. *Patent* WO9935520, Coating of polymers.
- [59] **Schlenoff, J. B.; Dubas, S.T.; Farhat, T.**, 2000. Sprayed Polyelectrolyte Multilayers, *Langmuir*, **16**, 9968–9969.
- [60] **Wang, L. Y.; Fu, Y.; Wang, Z. Q.; Fan, Y.; Zhang, X.**, 1999: Investigation into an Alternating Multilayer Film of Poly(4-Vinylpyridine) and Poly(acrylic acid) Based on Hydrogen Bonding, *Langmuir*, **15**, 1360-1363.
- [61] **Sukhishvili, S. A.; and Granick, S.**, 2002. Layered, Erasable Polymer Multilayers Formed by Hydrogen-Bonded Sequential Self-Assembly, *Macromolecules*, **35**, 301-310.
- [62] **Kozlovskaya, V.; Ok, S.; Sousa, A.; Libera, M.; Sukhishvili, S. A.**, 2003. Hydrogen-Bonded Polymer Capsules Formed by Layer-by-Layer Self-Assembly, *Macromolecules*, **36**, 8590-8592.
- [63] **Cho, J. and Caruso, F.**, 2003. Polymeric Multilayer Films Comprising Deconstructible Hydrogen-Bonded Stacks Confined between Electrostatically Assembled Layers, *Macromolecules*, **36**, 2845-2851.
- [64] **Shimazaki, Y.; Mitsuishi, M.; Ito, S.; Yamamoto, M.**, 1997. Preparation of the layer-by-layer deposited ultrathin film based on the charge-transfer interaction, *Langmuir*, **13**, 1385-1387.
- [65] **Pardo-Yissar, V.; Katz, E.; Lioubashevski, O.; Willner, I.**, 2001. Layered Polyelectrolyte Films on Au Electrodes: Characterization of Electron-Transfer Features at the Charged Polymer Interface and Application for Selective Redox Reactions, *Langmuir*, **17**, 1110-1118.
- [66] **Klitzinga, R.V.; Wong, J. E.; Jaeger, W.; Steitz, R.**, 2004. Short range interactions in polyelectrolyte multilayers, *Curr. Op. in Coll. and Inter. Sci.*, 158–162.
- [67] **Blomberg, E.; Poptoshev, E.; Caruso, F.**, 2006. Surface Interactions during Polyelectrolyte Multilayer Build-Up. 2. The Effect of Ionic Strength on the Structure of Preformed Multilayers, *Langmuir*, **22**, 4153-4157.
- [68] **Stockton, W. B. and Rubner, M. F.**, 1997. Molecular-Level Processing of Conjugated Polymers. 4. Layer-by-Layer Manipulation of Polyaniline via Hydrogen-Bonding Interactions, *Macromolecules*, **30**, 2717–2725.
- [69] **Dubas, S.T. and Schlenoff, J.B.**, 1999. Factors Controlling the Growth of Polyelectrolyte Multilayers, *Macromolecules*, **32**, 8153-8160.
- [70] **Dubas, S.T. and Schlenoff, J.B.**, 2001. Swelling and Smoothing of Polyelectrolyte Multilayers by Salt, *Langmuir*, **17**, 7725–772.
- [71] **McAloney, R.A.; Sinyor, M.; Dudnik, V.; Goh M.C.**, 2001. Atomic Force Microscopy Studies of Salt Effects on the Morphology of Polyelectrolyte Multilayer Films, *Langmuir*, **17**, 6655–6663.

- [72] **Voigt, U.; Khrenov, V.; Tauer, K.; Hahn, M.; Jaeger, W.; Klitzing, R. V.**, 2003. The effect of polymer charge density and charge distribution on the formation of multilayers, *J. Phys.: Condens. Matter*, **15**, S213–S218.
- [73] **Ladam, G.; Schaad, P.; Voegel, J.-C.; Schaaf, P.; Decher, G.; Cuisinier, F.**, 2000. In Situ Determination of the Structural Properties of Initially Deposited Polyelectrolyte Multilayers, *Langmuir*, **16**, 1249-1255.
- [74] **Lvov, Y.; Ariga, K.; Onda, M.; Ichinose, I.; Kunitake, T.**, 1999. A careful examination of the adsorption step in the alternate layer-by-layer assembly of linear polyanion and polycation, *Colloids Surf. A*, **146**, 337.
- [75] **Rieglerand, H. and Essler, F.**, 2002. Polyelectrolytes. 2. Intrinsic or Extrinsic Charge Compensation Quantitative Charge Analysis of PAH/PSS Multilayers, *Langmuir*, **18 (17)**, 6694–6698.
- [76] **Ruths, J.; Essler, F.; Decher, G.; Riegler, H.**, 2000. Polyelectrolytes I: Polyanion/Polycation Multilayers at the Air/Monolayer/Water Interface as Elements for Quantitative Polymer Adsorption Studies and Preparation of Hetero-superlattices on Solid Surfaces, *Langmuir*, **16**, 8871-8878.
- [77] **Durstock, M. F.; and Rubner M. F.**, 2001. Dielectric Properties of Polyelectrolyte Multilayers, *Langmuir*, **17 (25)**, 7865–7872.
- [78] **Kharlampieva, E.; and Sukhishvili, S.A.**; 2003. Ionization and pH Stability of Multilayers Formed by Self-Assembly of Weak Polyelectrolytes, *Langmuir*, **19(4)**, 1235–1243.
- [79] **Xie, A. E.; and Granick, S.**; 2002. Local Electrostatics within a Polyelectrolyte Multilayer with Embedded Weak Polyelectrolyte, *Macromolecules*, **35 (5)**, 1805–1813.
- [80] **Hsiao, P.-Y.**, 2006. Chain Morphology, Swelling Exponent, Persistence Length, Like-Charge Attraction, and Charge Distribution around a Chain in Polyelectrolyte Solutions: Effects of Salt Concentration and Ion Size Studied by Molecular Dynamics Simulations, *Macromolecules*, **39 (20)**, 7125–7137.
- [81] **Shklovskii, B. I.; Nguyen, T. T.**, 2001. Adsorption of charged particles on an oppositely charged surface: Oscillating inversion of charge, *Phys. Rev. E* **64**, 041407(1)- 041407(9).
- [82] **Besteman, K.; van Eijk, K.; Lemay, S. G.** 2007. Charge inversion accompanies DNA condensation by multivalent ions, *Nat. Phys.*, **3**, 641-644.
- [83] **Nguyen, T.T. and Shklovskii, B.I.** , 2001. Overcharging of a macroion by an oppositely charged polyelectrolyte, *Physica, A.*, **293**, 324–338.
- [84] **Schlenoff, J. B.; Ly, G.; Li, M.**, 1998. Charge and Mass Balance in Polyelectrolyte Multilayers, *J. Am. Chem. Soc.*, **120 (30)**, 7626–7634.
- [85] **Jomaa, H.W.; Schlenoff, J.B.**, 2005. Salt – Induced Polyelectrolyte Interdiffusion in Multilayered Films: A Neutron Reflectivity Study *Macromolecules*, **38**, 8473-8480.

- [86] **Picart, C.; Mutterer, J.; Richert, L.; Luo, Y.; Prestwich, G. D.; Schaaf, P.; Voegel, J.-C.; Lavalle, P.**, 2002. Molecular basis for the explanation of the exponential growth of polyelectrolyte multilayers, *Proc. Natl. Acad. Sci. U.S.A.*, **99**, 12531-12535.
- [87] **Picart, C.; Lavalle, P.; Hubert, P.; Cuisinier, F. J. G.; Decher, G.; Schaaf, P.; Voegel, J.-C.** 2001. Buildup Mechanism for Poly(L-lysine)/Hyaluronic Acid Films onto a Solid Surface, *Langmuir*, **17**, 7414-7424.
- [88] **Elbert, D. L.; Herbert, C. B.; Hubbell, J. A.**, 1999. Thin polymer layers formed by polyelectrolyte multilayer techniques on biological surfaces, *Langmuir*, **15**, 5355-5362.
- [89] **Boulmedais, F.; Ball, V.; Schwinte, P.; Frisch, B.; Schaaf, P.; Voegel, J. C.** 2003. Buildup of Exponentially Growing Multilayer Polypeptide Films with Internal Secondary Structure, *Langmuir*, **19**, 440-445.
- [90] **Poptoshev, E.; Schoeler, B.; Caruso, F.**, 2004. Influence of Solvent Quality on the Growth of Polyelectrolyte Multilayers, *Langmuir*, **20**, 829-834.
- [91] **Fu, J.; Ji, J.; Shen, L.; Kuller, A.; Rosenhahn, A.; Shen, J.; Grunze, M.**; 2009. pH-Amplified Exponential Growth Multilayers: A Facile Method to Develop Hierarchical Micro- and Nanostructured Surfaces, *Langmuir*, **25**(2), 672-675.
- [92] **Collin, D.; Lavalle, P.; Garza, J. M.; Voegel, J.-C.; Schaaf, P.; Martinoty, P.**, 2004. Mechanical Properties of Cross-Linked Hyaluronic Acid/Poly-(L-lysine) Multilayer Films, *Macromolecules*, **37**, 10195-10198.
- [93] **Richert, L.; Lavalle, P.; Payan, E.; Shu, X. Z.; Prestwich, G. D.; Stoltz, J.-F.; Schaaf, P.; Voegel, J.-C.; Picart, C.**, 2004. Layer by Layer Buildup of Polysaccharide Films: Physical Chemistry and Cellular Adhesion Aspects, *Langmuir*, **20**, 448- 458.
- [94] **Castelnovo, M.; and Joanny, J-F.**, 2000. Formation of Polyelectrolyte Multilayers, *Langmuir*, **16**, 7524-7532.
- [95] **Ball, V.; Winterhalter, V.; Schwinte, P.; Lavalle, P.; Voegel, J.-C.; Schaaf, P.**, 2002. Complexation Mechanism of Bovine Serum Albumin and Poly(allylamine hydrochloride), *J. Phys. Chem. B*, **106**, 2357-2364.
- [96] **Laugel, N.; Betscha, C.; Winterhalter, M.; Voegel, J.-C.; Schaaf, P.; Ball, V.**, 2006. Relationship between the Growth Regime of Polyelectrolyte Multilayers and the Polyanion/Polycation Complexation Enthalpy, *J. Phys. Chem. B*, **110** (39), 19443–19449.
- [97] **Jelesarov, I.; Bosshard, H. R.** 1999. Isothermal titration calorimetry and differential scanning calorimetry as complementary tools to investigate the energetics of biomolecular recognition, *J. Mol. Recognit.*, **12**, 3-18.
- [98] **Godec, A.; Skerjanc, J.** 2005. Enthalpy Changes upon Dilution and Ionization of Poly(L-glutamic acid) in Aqueous Solutions, *J. Phys. Chem. B*, **109**, 13363-13367.

- [99] Winnik, A. M.; Bystryak, M.; Chassenieux, C.; Strashko, V; Macdonald, P. M.; Siddiqui, S., 2000. Study of Interaction of Poly(ethylene imine) with Sodium Dodecyl Sulfate in Aqueous Solution by Light Scattering, Conductometry, NMR, and Microcalorimetry, *Langmuir*, **16**, 4495-4510
- [100] Mezei, A.; and Mszros, R., 2006. Novel Method for the Estimation of the Binding Isotherms of Ionic Surfactants on Oppositely Charged Polyelectrolytes, *Langmuir*, **22**, 7148-7151.
- [101] Rigsbee, D. R.; and Dubin, P. L., 1996. Microcalorimetry of Polyelectrolyte–Micelle Interactions, *Langmuir*, **12**, 1928-1929.
- [102] Picart, C.; Gergely, C.; Arntz, Y.; Voegel, J.-C.; Schaaf, P.; Cuisinier, F. G. J.; Senger, B., 2004. Measurement of film thickness up to several hundreds of nanometers using optical waveguide lightmode spectroscopy, *Biosens. Bioelectron.*, **20**, 553-561.
- [103] Kujawa, P.; Moraille, P.; Sanchez, J.; Badia, A.; Winnik, F. M., 2005. Effect of Molecular Weight on the Exponential Growth and Morphology of Hyaluronan/Chitosan Multilayers: A Surface Plasmon Resonance Spectroscopy and Atomic Force Microscopy Investigation, *J. Am. Chem. Soc.*, **127**, 9224-9234.
- [104] Hubsch, E.; Ball, V.; Senger, B.; Decher, G.; Voegel, J. C.; Schaaf, P., 2004. Controlling the Growth Regime of Polyelectrolyte Multilayer Films: Changing from Exponential to Linear Growth by Adjusting the Composition of Polyelectrolyte Mixtures, *Langmuir*, **20**, 1980-1985.
- [105] Salomaki, M.; Vinokurov, I. A.; Kankare, J., 2005. Effect of Temperature on the Buildup of Polyelectrolyte Multilayers, *Langmuir*, **21**, 11232-11240.
- [106] Porcel, C.; Lavallo, P.; Ball, V.; Decher, G.; Senger, B.; Voegel, J.-C.; Schaaf, P., 2006. From Exponential to Linear Growth in Polyelectrolyte Multilayers, *Langmuir*, **22**, 4376-4383.
- [107] Porcel, C.; Lavallo, P.; Decher, G.; Senger, B.; Voegel, J.-C.; Schaaf, P., 2007. Influence of the Polyelectrolyte Molecular Weight on Exponentially Growing Multilayer Films in the Linear Regime, *Langmuir*, **23**, 1898-1904.
- [108] Michel, M.; Izquierdo, A.; Decher, G.; Voegel, J.-C.; Schaaf, P.; Ball, V., 2005. Layer by Layer Self-Assembled Polyelectrolyte Multilayers with Embedded Phospholipid Vesicles Obtained by Spraying: Integrity of the Vesicles, *Langmuir*, **21**, 7854-7859.
- [109] Lavallo, P., Gergely, C., Cuisinier, F. J. G., Decher, G., Schaaf, P., Voegel, J.-C., Picart, C., 2002. Comparison of the Structure of Polyelectrolyte Multilayer Films Exhibiting a Linear and an Exponential Growth Regime: An in Situ Atomic Force Microscopy Study, *Macromolecules*, **35**, 4458–4465.
- [110] Harold, F. M., 1966. Inorganic Polyphosphates in Biology: Structure, Metabolism, and Function, *Bacteriological Reviews*, **30**(4), 772-794.

- [111] **Thilo, E. and Feldman, W.**, 1959. Condensed phosphates and arsenates. XXIII. The significance of the cation in paper chromatography of condensed phosphates. *Zeitschrift fuer Anorganische und Allgemeine Chemic.*, **298**, 316-337.
- [112] **E. Thilo**, 1965. The Structural Chemistry of Condensed Inorganic Phosphates, *Ange. Chem. Int. Ed. in En.*, **4(12)**, 1061 – 1071.
- [113] **Wazer, V.J.R.**, 1950. Structure and properties of the condensed phosphates. II. A theory of the molecular structure of sodium phosphate glasses, *Jour. of Am. Chem. Soc.*, **72**, 644-647.
- [114] **Kolloff, R. H.**, 1959/ ASTM Bull. No. 237, 74
- [115] **Wazer, V.J.R. and Campanella, D.A.**, 1950. Structure and properties of the condensed phosphates. IV. Complex ion formation in polyphosphate solutions, *Jour. of Am. Chem. Soc.*, **72**, 655-663.
- [116] **McCullough, J. F.; Wazer, V.J.R.; Griffith, E. J.**, 1956. Structure and Properties of the Condensed Phosphates. XI. Hydrolytic Degradation of Graham's Salt, *J. Am. Chem. Soc.*, **78(18)**, 4528–4533.
- [117] **Wazer, V.J.R.; Griffith, E.J.; McCullough, J. F.**; 1954. Analysis of Phosphorus Compounds, *Anal. Chem.*, **26 (11)**, 1755–1759.
- [118] **Griffith, E. J.**, 1956. Analysis of Phosphorus Compounds- Rapid Hydrolysis of Condensed Phosphates in Volumetric Analyses, *Anal. Chem.*, **2 (4)**, 525–526.
- [119] **Wazer, V.J.R.; Griffith, E.J.; McCullough, J. F.**; 1952. The Preparation and Properties of the Twelve-Membered Ring Hexametaphosphate Anion, *Anal. Chem.*, **74**, 4977.
- [120] **Mehrotra, R. C.**, 1975. Synthesis and properties of simple and complex polymetaphosphate glasses of alkali metals, *Pure and Applied Chemistry*, **44(2)**, 201-220.
- [121] **Rashchi, F. and Finch, J. A.**, 2000. Polyphosphates: a review their chemistry and application with particular reference to mineral processing, *Minerals Engineering*, **13**, 1019-1035.
- [122] **Henk-Jan de Jager, H.-J.; Heyns, A. M.**, 1998. Kinetics of Acid-Catalyzed Hydrolysis of a Polyphosphate in Water, *J. Phys. Chem. A*, **102**, 2838-2841.
- [123] **Kulaev, I. S.; Vagabov V. M. ; Kulakovskaya, T. V.**, 2004. The Biochemistry of Inorganic Polyphosphates, 2004 John Wiley & Sons, Cheapter 1, pp:5-7.
- [124] **Strauss, U. P.; Smith, E. H.; Wineman, P. L.**, 1953. Polyphosphates as polyelectrolytes. I. light Scattering and viscosity of sodium polyphosphates in electrolyte solutions, *J. Am. Chem. Soc.*, **75**, 3935-3940.
- [125] **Joseph, J.; and Kim, H. Z.**, 1966. Preparation and analysis by Ion exchange techniques of sodium salts of mandelic acid derivatives, *The Ohio Journal of Science*, **66**, 587-590.

- [126] **Koetz J, Kosmella S In: Radeeva T (ed)**, 2001. Physical Chemistry of Polyelectrolytes, Surfactant Science Series 99, Marcel Dekker, New York.
- [127] **Skoog, D. A.; Holler, F. A.; Crouch, S. R.;** 2006. *Principles of Instrumental Analysis*, 6th Ed., Haurcourt College Publishers.
- [128] **Ladbury, J. E.;** 2004. Application of Isothermal Titration Calorimetry in the Biological Sciences: Things Are Heating Up!, *BioTechniques, Technique Essays*, University College London, **37(6)**, 885-887.
- [129] **Ahn, H. J.; Kang, E. C.; Jang, C. H.; Song, K. W.; Lee, J. O.;** 2000. Complexation behavior of poly(acrylic acid) and poly(ethylene oxide) in water and water-methanol, *J.M.S.—Pure Applied Chem. A*, **37(6)**, pp. 573–590.
- [130] **Vashelani, B. F.; Rajabi, F. H. ; Ahmadi, M. H. ; Nouhi, S,** 2005. Stability constans and thermodynamic parameters of some intramolecular complexes in relation to their specific interaction forces, *Polymer Bulltein*, **55**, 437-445.
- [131] **Brune, D.; Hellborg, R.; Whitlow, H. J.; Hunderi, O.,** 1997. *Surface Characterization: A User's Sourcebook*, Wiley-VCH.
- [132] **Vilalta, A.-C.; Gloystein, K.; Frangis, N.;** 2008. *Principles of Atomic Force Microscopy, Physics of Advanced Materials Winter School Lecture*.
- [133] **Herman B.; and Lemasters, J. J.,** 1993. *Optical Microscopy: Emerging Methods and Applications*, Academic Press, New York.
- [134] **Manning, G. S.,** 1969. Limiting Laws and Counterion Condensation in Polyelectrolyte solutions I. Colligative Properties. *J. Chem. Phys*, **51**, 924-933.
- [135] **Manning, G. S.,** 1974. *Polyelectrolytes*, Ed. E. Selegny, Publishing Co., Dordrecht Holland.
- [136] **Manning, G. S.,** 1979. Counterion Binding In Polyelectrolyte Theory, *Accounts of Chem. Res.*, **12**, 443- 449.
- [137] **Jayaram, B.; DiCapua, F. M.; Beveridge, D. L.,** 1991. A theoretical study of polyelectrolyte effects in protein-DNA interactions: Monte Carlo free energy simulations on the ion atmosphere contribution to the thermodynamics of lambda repressor-operator complex formation, *J. Am. Chem. Soc*, **113**, 5211-5215.
- [138] **Gummel, J.; Boue, F.; Clemens, D.; Cousin, F.,** 2008. Finite size and inner structure controlled by electrostatic screening in globular complexes of proteins and polyelectrolytes, *Soft Matter*, **4**, 1653–1664.
- [139] **Joanny, J. F.; Castelnovo, M.; Netz, R.;** 2000. Adsorption of charged polymers, *J. Phys.: Condens. Matter*, **12**, A1–A7.
- [140] **Hsiao, P.-Y.; Luijten, E.,** 2006. Salt-Induced Collapse and Reexpansion of Highly Charged Flexible Polyelectrolytes, *Phys. ReV. Lett.*, **97**, 148301-148304.

- [141] **Hooper, H. H.; Beltram, S.; Sassi, A. P.; Blaras, H.; Prausnitz, J. M.**, 1990. Monte Carlo simulations of hydrophobic polyelectrolytes. Evidence for a structural transition in response to increasing chain ionization, *J. Chem. Phys.*, **93**, 2715-2724.
- [142] **Hoogeveen, N. G.; Cohen Stuart, M. A.; Fler, G.; Bohmer, M. R.**, 1996. Formation and Stability of Multilayers of Polyelectrolytes, *Langmuir*, **12**, 3675-3681.
- [143] **Caruso, F.; Mohwald, H.**; 1999. Protein Multilayer Formation on Colloids through a Stepwise Self-Assembly Technique, *J. Am. Chem. Soc.* **121**, 6039-6046.
- [144] **Kato, N.; Schuetz, P.; Fery, A.; Caruso, F.**; 2002. Thin Multilayer Films of Weak Polyelectrolytes on Colloid Particles, *Macromolecules*, **35 (26)**, 9780-9787.
- [145] **Sui, Z.; Salloum, D.; Schlenoff, J. B.**; 2003. Effect of Molecular Weight on the Construction of Polyelectrolyte Multilayers: Stripping versus Sticking, *Langmuir*, **19 (6)**, 2491–2495.
- [146] **Johnston, A. P. R.; Read, E. S.; Caruso, F.**, 2005. DNA Multilayer Films on Planar and Colloidal Supports: Sequential Assembly of Like-Charged Polyelectrolytes, *Nano Lett.*, **5**, 953–956.
- [147] **Nguyen, T.T. and Shklovskii, B.I.** , 2001. Complexation of a polyelectrolyte with oppositely charged spherical macroions: giant inversion of charge, *J. Chem. Phys.*, **114**, 5905–5916.
- [148] **Fischer, P.; Laschewsky, A.**, 2000. Layer-by-Layer Adsorption of Identically Charged Polyelectrolytes, *Macromolecules*, **33**, 1100–1102.
- [149] **Adusumilli, M.; Bruening, M.L.**, 2009. Variation of Ion-Exchange Capacity, ζ Potential, and Ion-Transport Selectivities with the Number of Layers in a Multilayer Polyelectrolyte Film, *Langmuir*, **25**, 7478-7485.
- [150] **Soeno, T.; Inokuchi, K.; Shiratori, S.**, 2004. Ultra-water-repellent surface: fabrication of complicated structure of SiO₂ nanoparticles by electrostatic self-assembled films, *Appl. Surf. Sci.*, **237**, 539-543.
- [151] **Jisr, R.M.; Rmaile, H.H.; Schlenoff, J.B.**, 2005. Hydrophobic and Ultrahydrophobic Multilayer Thin Films from Perfluorinated Polyelectrolytes, *Angew. Chem. Int. Ed.*, **44**, 782-785.
- [152] **Zhai, L.; Cebeci, F. C.; Cohen, R. E.; Rubner, M. F.**, 2004. Stable Superhydrophobic Coatings from Polyelectrolyte Multilayers, *Nano Lett.*, **4**, 1349-1353.
- [153] **Smith, A. S.; Mutch, N. J.; Baskar, D.; Rohloff, P.; Docampo, R.; Morrissey, J. H.**, 2006. Polyphosphate modulates blood coagulation and fibrinolysis, *PNAS*, **103(4)**, 903–908.
- [154] **Url-1**< http://www.malvern.com/LabEng/technology/zeta_potential/zetapotentialLDE.htm>, Malvern Innovate solutions in material characterization, accessed at 07.08.2010.

- [155] **Url-2** <<http://www.zebrasc.com/news.asp?pageclass=11301&id=189>>, Zebra (Beijing) Scientific Development Co., Ltd, accessed at 16.08.2010.
- [156] **Url-3** <<http://www.bdbiosciences.com/research/multicolor/spectrumguide/index.jsp>>, Multicolor Flow Cytometry, spectrum Guide, accessed at 15.08.2010.
- [157] **Url-4**<<http://www.ipfdd.de/Ellipsometry.199.0.html>>, Leibniz Institut of Polymer Research, accessed at 16.08.2010.

APPENDICES

APPENDIX A : French Summary

APPENDIX A : French Summary

Comparaison de la formation de complexes de polyélectrolytes en solution et aux interfaces

Résumé de Thèse

Les polyélectrolytes sont des polymères qui contiennent des groupes ioniques dans leurs unités répétitives et de ce fait exhibent des propriétés d'électrolytes [1-6]. Les complexes de polyélectrolytes (PECs) ont formés par interaction entre des polyanions et des polycations conduisant à la libération de petits contre-ions. Les PECs jouent un rôle important dans les technologies environnementales et dans les systèmes biologiques. La recherche sur les principes fondamentaux de la formation des PECs devient de plus en plus importante en raison de leurs nombreuses applications (par exemple dans les industries alimentaires, cosmétiques et pharmaceutiques, fabrication du papier, délivrance de médicament, thérapie génique, propriétés rhéologiques des solutions, films multicouches, etc...) [36, 41, 46, 49, 108,150-153].

La formation de PECs peut avoir lieu en solution ou aux interfaces. Ce dernier phénomène a conduit au développement d'une nouvelle forme de matériaux hybrides nanostructurés sous la forme de films minces [39-45]. Le dépôt de films à base de polymères via un assemblage couche-par couche (LbL) est devenu une méthode populaire de fonctionnalisation de surface en raison de sa simplicité, de son faible coût, du respect de l'environnement et du fait qu'elle ne s'applique pas seulement aux polyélectrolytes de charges opposées mais également à d'autres types de polymères portant des fonctionnalités complémentaires (par exemple, liaisons hydrogènes ou systèmes donneur-accepteur). Par conséquent, de tels films hybrides offrent un grand nombre d'applications potentielles en science des matériaux.

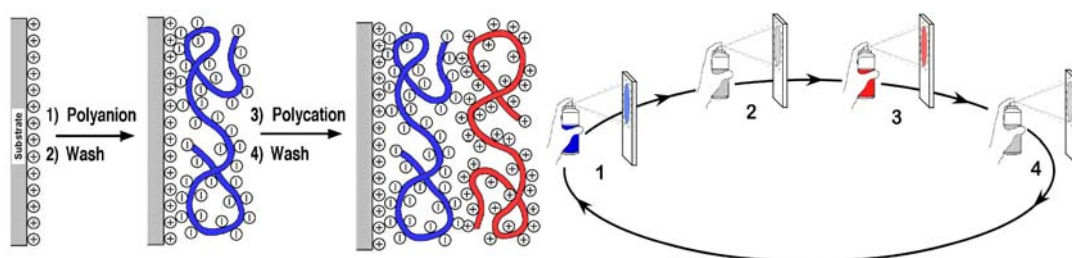


Figure A. 1 : Représentation schématique simplifiée des deux premières étapes d'adsorption illustrant le dépôt d'un film de polyélectrolytes sur un support chargé positivement par pulvérisation. Les contre ions ont été omis pour des raisons de clarté. La conformation des polyélectrolytes est hautement idéalisée et l'interpénétration des couches est montrée afin de mieux représenter l'inversion de la charge de surface après chaque étape d'adsorption. La nomenclature (A/B)_h est utilisée pour décrire la construction d'un film à partir de deux polyélectrolytes (A et B) où h correspond au nombre de cycles de trempage/pulvérisation ou au nombre de paires de couches [1].

Des structures multicouches composées de polyions ou d'autres objets moléculaires ou colloïdaux chargés (ou une combinaison des différents types d'objets) sont fabriquées selon le principe illustré dans la Figure A.1.

Les interactions électrostatiques entre les macromolécules de charges opposées sont la force motrice prédominante dans la formation des PECs. Cependant, les interactions hydrophobes, les forces de Van der Waals et les liaisons hydrogènes peuvent également jouer un rôle, typiquement en augmentant la stabilité des complexes. La formation et les propriétés des PECs dépendent de divers facteurs comprenant la nature et la position des groupes ioniques, la densité et la concentration de charge, la proportion de charges opposées, le poids moléculaire des macromolécules et l'environnement physico-chimique [16-19]. Un aspect important de la description des PECs est leur stoechiométrie, par exemple le rapport molaire des groupes cationiques et anioniques dans le complexe [20-24].

L'objectif de cette étude est de comparer les propriétés d'un PEC classique en solution avec celles d'un PEC formé à une interface (film multicouche) dans des conditions similaires dans le but d'établir les différences fondamentales et les similitudes entre ces deux systèmes. Pour une telle étude, il est avantageux de choisir une paire de polyélectrolytes dont l'interaction peut facilement être contrôlée par des paramètres tels que la concentration, la stoechiométrie, le pH et la force ionique. Ainsi, pour ce travail, le poly(phosphate de sodium) (PSP, $M_w = 2900$ g/mol) et poly(chlorhydrate d'allylamine) (PAH, $M_w = 56000$ g/mol) ont été identifiés comme la paire de polyélectrolytes appropriée pour investiguer la formation de complexes en solution et aux interfaces.

PSP est un polyélectrolyte hydrosoluble et inorganique intéressant avec quelques propriétés uniques [20-24].

La formation de complexes entre PSP et PAH en solution a été étudiée par conductimétrie, viscosimétrie, diffusion dynamique de la lumière, détermination de potentiel zéta et microcalorimétrie en fonction de différents paramètres tels que la concentration, la force ionique et le pH. La formation de complexes PSP/PAH à l'interface a été réalisée principalement par un dépôt LbL par pulvérisation avec des paramètres identiques à ceux utilisés pour les études en solution. Le comportement du complexe à l'interface a été examiné par ellipsométrie, microscopie à force atomique (AFM) et mesures du potentiel zéta.

Tableau A. 1 : Résultats par Conductimétrie.

| Titrant | Solution | Rapport molaire PSP:PAH | |
|--------------------------|--------------------------|-------------------------|-------------------|
| | | Sans Sel | I=0.15 mol/L NaCl |
| 1×10^{-2} M PAH | 1×10^{-2} M PSP | 0.91:1 | 0.77:1 |
| 1×10^{-3} M PAH | 1×10^{-3} M PSP | 1:1.40 | 1:1 |
| 1×10^{-4} M PAH | 1×10^{-4} M PSP | 0.77:1 | 1.25:1 |
| 1×10^{-5} M PAH | 1×10^{-5} M PSP | 1.61:1 | 1.25:1 |
| 1×10^{-2} M PSP | 1×10^{-2} M PAH | 1:1.67 | 1:1 |
| 1×10^{-4} M PSP | 1×10^{-4} M PAH | 1.61:1 | 0.91:1 |

Tableau A. 2 : Résultats par viscosimétrie and conductimétrie.

| Methods | PSP | PAH | Rapport molaire PSP:PAH |
|------------------------------|--------------------------------|--------------------------------|-------------------------|
| Résultats par viscosimétrie | $9.8 \times 10^{-4} \text{ M}$ | $9.8 \times 10^{-4} \text{ M}$ | 1:1 |
| Résultats par conductimétrie | $1 \times 10^{-3} \text{ M}$ | $1 \times 10^{-3} \text{ M}$ | 1:1.47 |

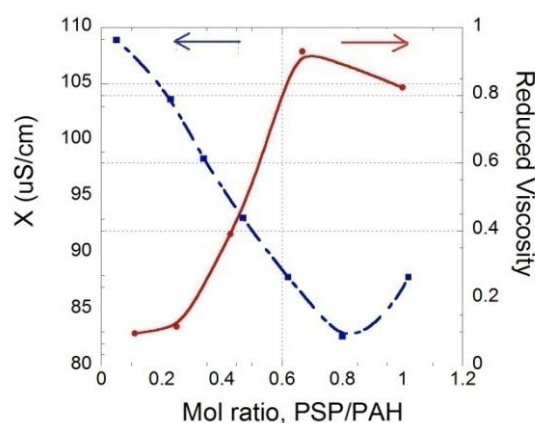


Figure A. 2 : La formation de complexes entre PSP et PAH en solution a été étudiée par conductimétrie et viscosimétrie ($C_{\text{PSP}}=0.01 \text{ g/dl}$, Sans Sel).

Tableau A. 3 : Résultats par surnageant.

| Composition des complexes | Echantillon de contrôle | η_{SP} (surnageant) | η_{SP} (controller) | $\eta_{\text{SP}}(\text{controller}) / \eta_{\text{SP}}$ |
|---|------------------------------------|---------------------------------|---------------------------------|--|
| $1 \times 10^{-4} \text{ M}$ PSP-PAH (rapport molaire 1:1, laisser sédimenter puis ajout de PSP supplémentaire) | $3.3 \times 10^{-3} \text{ M}$ PSP | 0.063 | 0.069 | 1.10 |
| $1 \times 10^{-4} \text{ M}$ PSP-PAH (rapport molaire 1:1, laisser sédimenter puis ajout de PAH supplémentaire) | $3.3 \times 10^{-3} \text{ M}$ PAH | 0.068 | 0.079 | 1.16 |
| $1 \times 10^{-4} \text{ M}$ PSP-PAH (rapport molaire 1.5:1) | $2 \times 10^{-5} \text{ M}$ PSP | 0.102 | 0.110 | 1.08 |
| $1 \times 10^{-4} \text{ M}$ PSP-PAH (rapport molaire 1:1.5) | $2 \times 10^{-5} \text{ M}$ PAH | 0.113 | 0.127 | 1.12 |

Le PSP et le PAH ont été solubilisés dans une solution à 0.15M en NaCl. Le pH de chaque solution a été ajusté à 6.70 qui correspond à la valeur moyenne du pKa de SP et de PAH de telle sorte que le degré de dissociation des deux polyélectrolytes est maintenu identique. La stoechiométrie des complexes PSP/PAH en solution s'est avérée être proche de 1:1 par conductimétrie, viscosimétrie et analyse du liquide surnageant. La légère déviation de la stoechiométrie semble provenir des polyions libres et de l'effet d'écrantage des contre-ions.

Les spectres IR des complexes PSP/PAH obtenus par différentes procédures montrent que les complexes PSP-PAH en solution et sous la forme de solide obtenu par un dépôt LbL sont identiques.

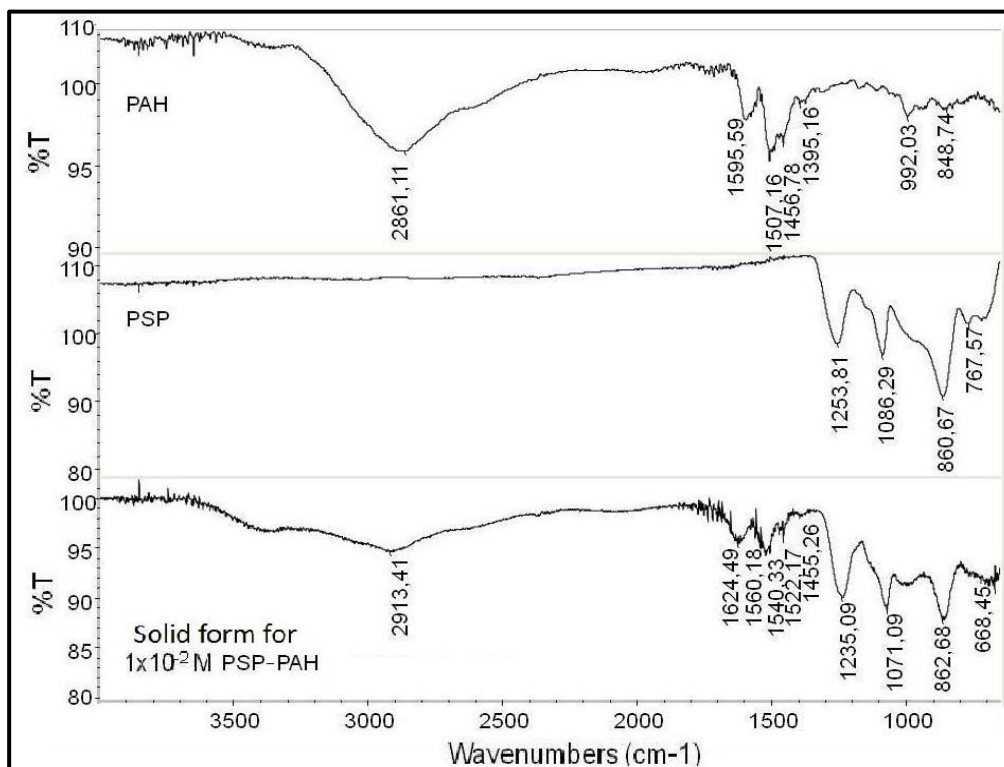


Figure A. 3 : Les spectres IR des complexes PSP/PAH obtenus par différentes procédures.

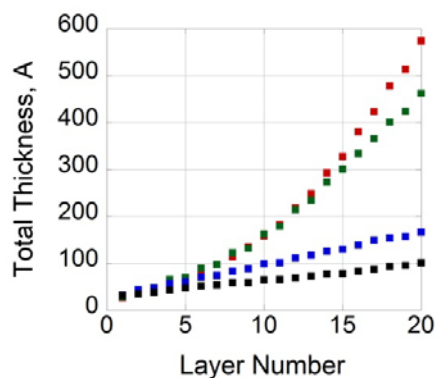


Figure A. 4 : Evolution de l'épaisseur moyenne du film en fonction du nombre de couches par un dépôt LbL par pulvérisation avec des paramètres polyélectrolytes concentration la force ionique, I=0.15M NaCl, et le pH 6.70, Rouge: 1x10⁻²M, Vert: 1x10⁻³M, Bleu: 1x10⁻⁴M, Noir: 1x10⁻⁵M PSP et PAH.

Le résultat des études multicouches a montré que le régime de croissance dépend fortement de la concentration de PSP et PAH. Il a été observé que la croissance de film semble être linéaire aux plus basses concentrations (10⁻⁵ et 10⁻⁴ M) et peut être extrapolée par une croissance superlinéaire à 1x10⁻³ M. La combinaison d'une croissance superlinéaire suivie d'une croissance linéaire a été observée à 10⁻² M.

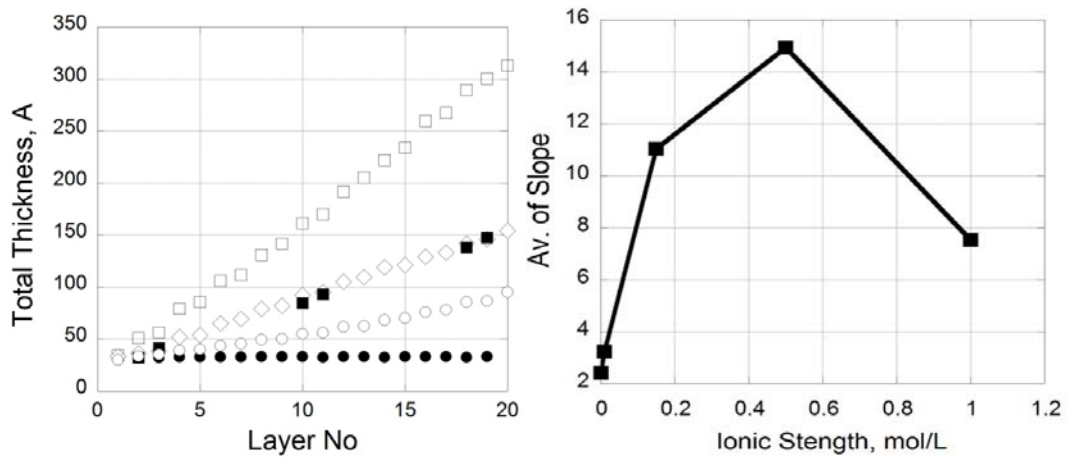


Figure A. 5 : (a gauche) Evolution de l'épaisseur moyenne du film en fonction du nombre de couches à 1×10^{-4} M en présence de, ●: sans sel, ○: $I=0.05$ M NaCl, ■: $I=0.15$ M NaCl, □: $I=0.5$ M NaCl, ◇: $I=1$ M NaCl. (à droite) Evolution de la fonction linéaire de l'inclinaison en présence de 1×10^{-4} M PSP/PAH et pH 6.70 en fonction de la force ionique.

Malgré l'apparition de couleurs d'interférences optiques, les topographies AFM montrent que les dépôts obtenus à 1×10^{-4} M sont de type îlots et que ces îlots augmentent en taille jusqu'à un nombre de couches (k) d'au moins 150 (voir Figure ci-dessous, à gauche). D'autre part, à 10^{-3} M, les dépôts ont une morphologie de films lisses (voir Figure ci-dessous, à droite). L'analyse de la rugosité moyenne (RMS) des dépôts en fonction du nombre d'étapes de dépôt montre un comportement significativement différent. Alors que la rugosité diminue de ~ 5 à ~ 1 nm pour 1×10^{-3} M, elle augmente de ~ 5 à ~ 75 nm pour 1×10^{-4} M.

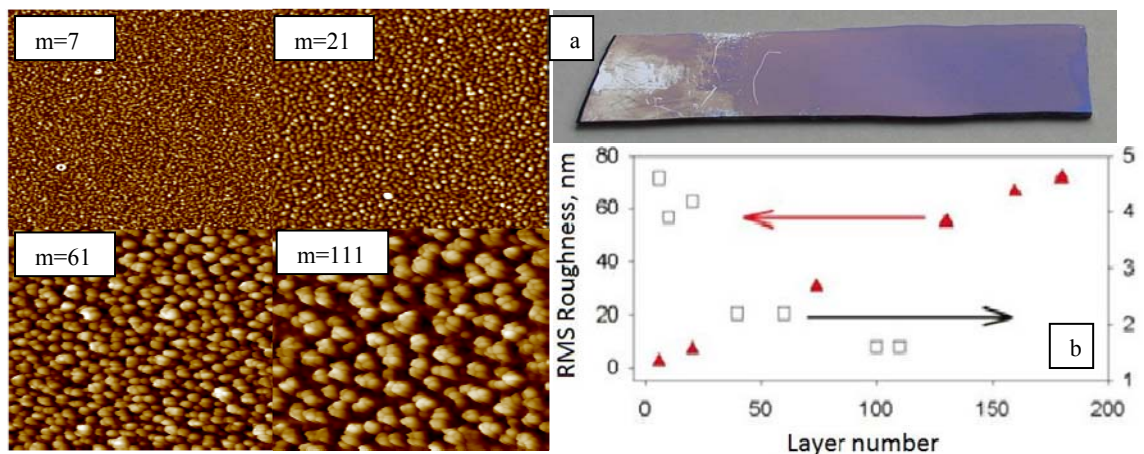


Figure A. 6 : (a gauche) Topographies de surface représentatives ($2 \times 2 \mu\text{m}$) des dépôts par LbL pulvérisation de solutions à 1×10^{-4} M en présence de NaCl 0.15 M à pH 6.7 en fonction du nombre de couches, (à droite) a) Image photographique d'un dépôt obtenu après 150 étapes de dépôt (les marques à gauche de l'échantillon sont dues à la manipulation) b) Evolution de la rugosité moyenne de surface (RMS) (déterminée à partir des topographies AFM) en fonction du nombre de couches m : (▲,axe à gauche) 1×10^{-4} M: (□,axe à droite) 1×10^{-3} M.

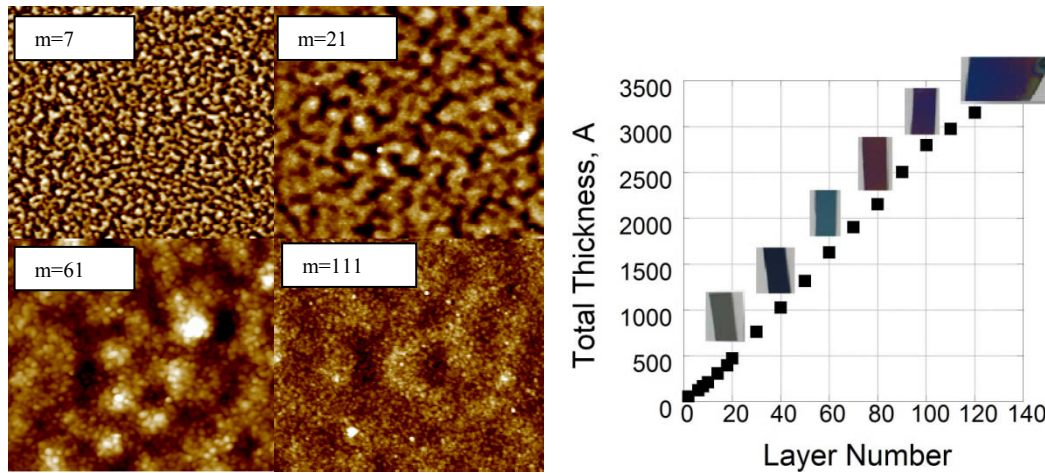


Figure A. 7: (à gauche) Topographies de surface représentatives ($2 \times 2 \mu\text{m}$) des dépôts par LbL pulvérisation de solutions à $1 \times 10^{-3} \text{M}$ en présence de NaCl 0.15 M à pH 6.7 en fonction du nombre de couches, (à droite) a) Image photographique d'un dépôt obtenu après 30, 40, 60, 80 100 et 120 étapes de dépôt.

La microcalorimétrie a montré que la complexation de PSP-PAH est très lente. Tout en étant dynamique, l'effet de l'addition de PSP et de PAH au complexe PSP/PAH à l'équilibre est négligeable en termes de propriétés thermodynamiques. Ce résultat est également en bon accord avec des études de diffusion dynamique de la lumière. Des études de conductimétrie, de viscosimétrie et de diffusion dynamique de la lumière réalisées en fonction du temps ont montré que les cinétiques de la complexation de PSP/PAH en solution et aux interfaces sont du même ordre de grandeur.

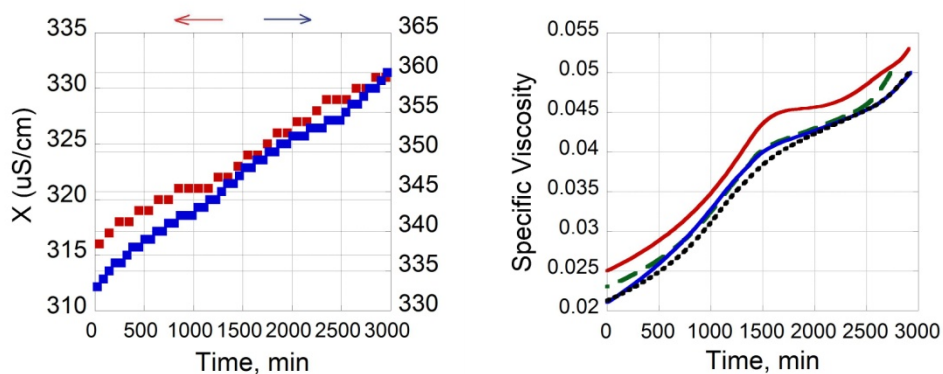


Figure A. 8 : Des études de conductimétrie et viscosimétrie par formation des complexes PSP/PAH en solutions en mélangeant PSP et PAH dans un rapport molaire 1:1 réalisées en fonction du temps en présence de NaCl 0.15 M à pH 6.7. Rouge: $1 \times 10^{-2} \text{M}$, Vert: $1 \times 10^{-3} \text{M}$, Bleu: $1 \times 10^{-4} \text{M}$, Noir: $1 \times 10^{-5} \text{M}$ PSP et PAH.

Les complexes formés en solution en mélangeant PSP et PAH dans un rapport molaire 1:1 dans les mêmes conditions montrent une lente augmentation de leur taille (jusqu'à $2,5 \mu\text{m}$ 24h après le mélange PSP avec PAH) et une inversion de leur potentiel zéta (ζ) (passage d'une valeur positive à une valeur négative d'environ -20 mV).

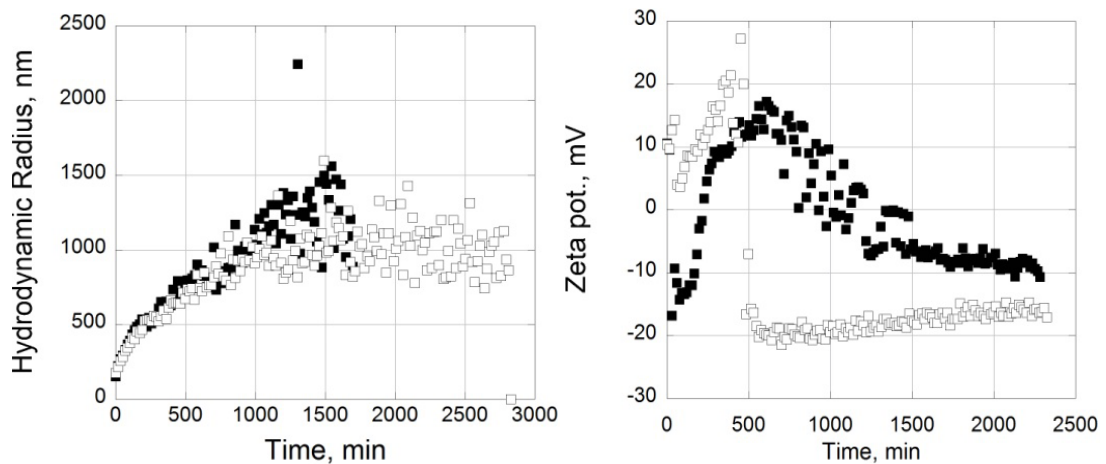


Figure A. 9 : Formation des complexes PSP/PAH en solutions en mélangeant PSP et PAH dans un rapport molaire 1:1 à 1×10^{-4} M en présence de NaCl 0,15 M et à un pH de 6.7 (a gauche) Evolution du hydrodynamic radius, (à droite) Evolution du potentiel ζ , ■: PSP ajouter, □:PAH ajouter.

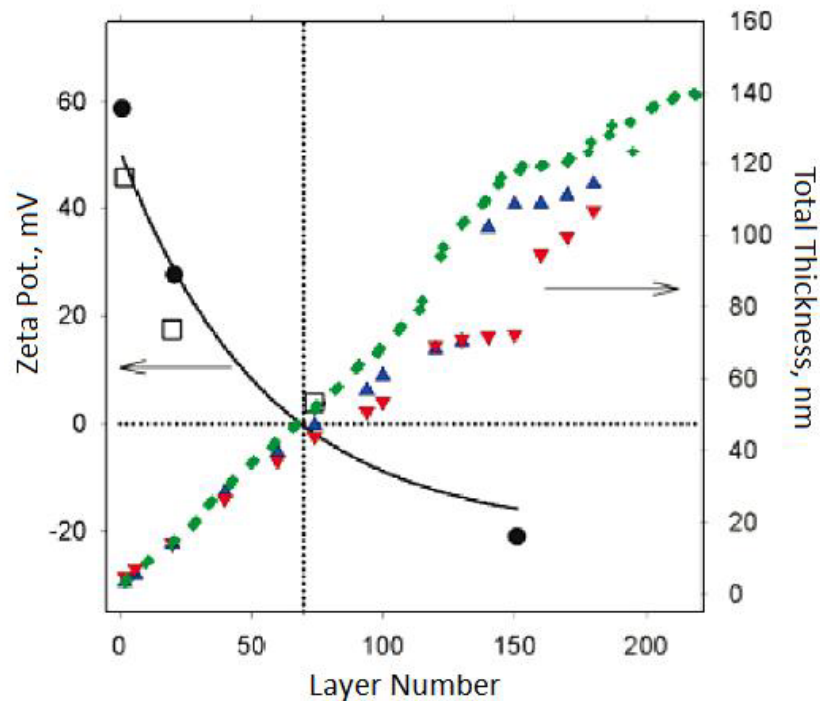


Figure A. 10 : Evolution du potentiel ζ macroscopique (les barres d'erreur correspondant à la déviation standard sur 5 mesures sont plus petites que les symbols) des dépôts obtenus par pulvérisation alternée de PSP et PAH dans des conditions identiques aux expériences en solution (courbe de droite) sur une plaque de verre recouverte de PEI en fonction du nombre de couches (m): aux chiffres pairs de m correspondent à un dépôt avec une dernière couche pulvérisée de PSP (négative) ; aux chiffres impairs de m correspondent à un dépôt avec une dernière couche pulvérisée de PAH (positive). La ligne horizontale en pointillé correspond à $\zeta=0$ mV et la ligne verticale au nombre de couches (m). A gauche, axe des ordonnées de droite: Evolution de l'épaisseur moyenne du film en fonction de k . Les différents symbols correspondent à différentes expériences.

Une autre observation non courante est liée au potentiel ζ dont le signe est normalement censé correspondre au signe de la charge du polyélectrolyte de la dernière couche adsorbée [73, 109]. De plus, il a été rapporté dans la littérature que même des films à croissance superlinéaire, exhibant une croissance de type îlot pour un faible nombre de couches ($k < 15$), montrent une alternance de signe pour le potentiel ζ [93]. Cependant, il a été observé que le potentiel ζ n'alterne pas entre des valeurs positives et négatives lors du dépôt de PSP et PAH. Aussi longtemps que le potentiel ζ est positif (i.e., pour $k=75$), le potentiel ζ diminue continuellement avec une l'augmentation de k . Lorsque le potentiel zéta approche zéro, une instabilité se produit par rapport à la croissance régulière du film précédent. Certains échantillons montrent temporairement une croissance légèrement sublinéaire alors que d'autres échantillons montrent une croissance légèrement superlinéaire. Après que ζ est atteint une valeur plateau d'environ -20 mV (après 150-200 étapes de dépôts), la croissance du film continue avec approximativement la même pente que celle observée pour un faible nombre de couches.

De façon intéressante, la croissance de la taille des complexes et l'altération du potentiel ζ se produisent dans la même gamme en solution et à l'interface dans lequel le processus de complexation peut même être interrompu par séchage et les étapes piégées cinétiquement peuvent être étudiées.

Les deux polyélectrolytes utilisés, PSP et PAH, ont été soigneusement caractérisés. Il a été démontré qu'une augmentation de la concentration de PSP et de PAH permet une transition progressive d'une croissance linéaire à une croissance superlinéaire.

Nous avons trouvé que le dépôt de PSP/PAH est un exemple intéressant de croissance de film dans lequel la rugosité à l'échelle nanométrique augmente linéairement avec l'épaisseur du film alors que l'homogénéité macroscopique du film est remarquable. Il est très surprenant que les chaînes de PAH peuvent s'adsorbées à la surface avec un potentiel ζ macroscopiquement positif et que la formation des complexes de polyélectrolytes à l'interface conduit au développement d'îlots avec une polydispersité faible et avec des tailles croissantes de plus de 300 nm sans coalescence vers un film continu.

Ces résultats indiquent également que des interactions autres qu'électrostatiques semblent contribuer à la construction du film multicouche de telle sorte à ce que des changements structuraux dynamiques se produisent dans les complexes de polyélectrolytes sur la surface.

La formation de complexes entre PSP et PAH en solution est en effet dynamique. L'ordre d'addition polycation/polyanion lors de la formation du complexe et l'effet de l'addition de PSP et PAH sur le complexe sont négligeables en terme de propriétés thermodynamiques. Il est intéressant d'observer que la taille des complexes croît dans la même gamme en solution et à l'interface.

Ces découvertes nous ont conduit à proposer un modèle dans lequel le dépôt se construit par aggrégation progressive de PSP et PAH accompagnée par leur diffusion latérale pour former les complexes.

La présente étude nous a permis de découvrir un nouveau régime de croissance de films par simple dépôt de solutions aqueuses par pulvérisation: une croissance par dépôts d'îlots qui ne coalescent pas jusqu'à 150 étapes de dépôts.

Dans cette étude, des motifs de multicouches de polyélectrolytes ont été obtenus et décrit pour la première fois. Les dimensions des motifs nanométriques sont fonction

du nombre de cycles de dépôt. L'augmentation progressive de la taille des grains et l'existence apparente de différentes échelles de rugosité pourraient avoir des applications très intéressantes telles que des revêtements superhydrophobes complémentaires à ceux qui ont été conçus en utilisant l'approche LbL traditionnelle [36, 41, 46, 49, 108,150-153].

CURRICULUM VITAE



Candidate's full name: Nejlâ Çini

Place and date of birth: Istanbul / 1977

Permanent Address: Istanbul Technical University, Faculty of Science and Letters, Department of Chemistry. Analytical Chemistry Department.

Universities and Colleges attended:

2003 – Present Ph. D. Student, in the Chemistry Programme at the Institute of Science and Technology, Technical University of Istanbul, Istanbul, Turkey

and 2007-Present

CNRS-UPR 022, Institute Charles Sadron, Louis Pasteur University, Strasbourg, France

1999 – 2003 Ms. Sci., Technical University of Istanbul, Chemistry Programme at the Institute of Science and Technology (*Title of Thesis: "Chemometric Analysis of SEM-EDAX, Porosity, and Soluble Salts Data For Archaeo-Ceramics", May, 2003*)

1994 – 1999 Bachelor of Science (BS), Marmara University, Atatürk Education Faculty, Chemistry Department (English Programme), Istanbul.

Publications:

"Step-by-Step Assembly of Self-Patterning Polyelectrolyte Films Violating (Almost) All Rules of Layer-by-Layer Deposition", N. Cini, T. Tulun, G. Decher, V. Ball, J. Am. Chem. Soc. **2010**, 132, 8264–8265.

